Spectroscopic Study of the Conformational Changes Involved in the Activation of Calcium/Calmodulin-Dependent Protein Kinase II

By

Francisco Guillermo Rodríguez Mena

Dissertation

Submitted to the Faculty of the

Graduate School of Vanderbilt University

in partial fulfillment of the requirements

for the degree of

DOCTOR OF PHILOSOPHY

in

Chemistry

August, 2016

Nashville, Tennessee

Approved:

Hassane Mchaourab, Ph.D

Jens Meiler, Ph.D

Roger Colbran, Ph.D

Michael P. Stone, Ph.D

Acknowledgements

I am indebted to Dr. Laurel Hoffman, who pioneered the study of CaMKII in the Mchaourab laboratory and whose findings gave form to the R3 equilibrium hypothesis on which my investigation rests. Moreover, her stocks, constructs, and protocols provided an invaluable starting point for learning and carrying out experiments. I am grateful to past and current members of the Mchaourab laboratory, the Center for Structural Biology, and the Department of Chemistry at Vanderbilt University for all the help and resources throughout my stay in the graduate program. Special gratitude is shown for Guangyong Yang for teaching me protein expression and purification, Dr. Hanane Koteiche for instruction in molecular biology techniques, Dr. Richard Stein for his help with DEER data collection and fitting, Dr. Soumya Ganguly and Dr. Markus Voehler for essential counsel and pivotal experimental setup of Methyl-TROSY and triple resonance experiments during the early stages of the NMR study, and Dr. Dungeng Peng for support in analyzing assignment data, use of truncated constructs, and backbone relaxation experiments that allowed me to carry the NMR project forward. I would very much like to thank the members of my committee: Dr. Roger Colbran, Dr. Mike Stone and Dr. Jens Meiler for their insight. Most of all, I am particularly beholden to my advisor, Dr. Hassane Mchaourab, for his perspicacity, for giving me the opportunity to partake in scientific research, for providing such an interestingly unique experience in my professional development, and for his charisma, stories and life lessons. Finally, I would like to thank my undergraduate advisors, Dr. Judith Brusslan and Dr. Tom Maricich at CSULB, and Dr. Andrius Baskys at the Long Beach VA for introducing me to research and sparking my curiosity.

TABLE OF CONTENTS

LIST OF TABLES

LIST OF FIGURES

Figure Page

Chapter I: Background and Introduction

Ca^{2+} Signaling, Calmodulin, and CaMKII Activation:

Calcium (Ca^{2+}) signaling underlies diverse biological mechanisms including excitation-contraction coupling in cardiac cells (Zhang et al., 2004), apoptosis (Orrenius et al., 2003), and neuronal synaptic plasticity (Pi et al., 2010). At basal conditions, the intracellular calcium concentration in most cell types is in the nanomolar range due to the combined effect of pumps that drive the net flux of the cation either to the outside of the cell or into the endoplasmic reticulum and mitochondria (Clapham, 2007). In addition, various proteins found in different subcellular compartments and the cytosol function as buffers through Ca^{2+} binding and release (Schwaller et al., 2010). Stimuli (first messengers) transiently alter the activities of these pumps or channels either by making them leakier for Ca^{2+} entry, decreasing its efflux, or promoting the release of internal Ca^{2+} stores (Berridge et al., 2000). The resulting intracellular Ca^{2+} spikes are detected by intermediary messengers such as calmodulin (CaM), a small (17kDa) acidic protein containing two lobes at the N- and C- termini (nCaM and cCaM), with two EF hand motifs per lobe(Burger et al., 1983; Ogawa and Tanokura, 1983; Chin and Means, 2000; Grabarek, 2011). Each EF hand is capable of binding one Ca^{2+} through coordination with a median dissociation concentration ≈ 1.4μM (the four Ca^{2+} binding sites have different dissociation constants, and the affinity is one order of magnitude greater for cCaM) (Olwin et al., 1984; Vetter and Leclerc, 2003). Calcium-bound calmodulin (Ca^{2+}/CaM) subsequently undergoes changes in conformation that modify the flexibility of the lobes, more prominently of cCaM (Tripathi and Portman, 2009) and the linker between them, making otherwise inaccessible hydrophobic residues available for binding specific

targets (Johnson, 2006) (such as myosin light-chain kinase, caldesmon, eukaryotic elongation factor-2 kinase, and phosphodiesterase type-1). This conformational change allows Ca^{2+}/CaM to wrap around the recognition motif on the target protein, which is usually either an α-helical or unstructured element. Initially, Ca^{2+}/CaM anchors the target at one of its lobes, more commonly cCaM. This is followed by contacts with nCaM and the rapprochement of the target to the binding pocket on Ca^{2+}/CaM. Finally, new contacts between the target and Ca^{2+}/CaM are established. The CaM-binding motif on the target assumes an α-helical structure in many, but not all, complexes. Many CaM targets cannot by themselves bind Ca^{2+}, but through interaction with CaM, their activity becomes Ca^{2+}-dependent. Thus, Ca^{2+}/CaM functions as a modular agent in calcium signal transduction (Wayman et al., 2011).

Among CaM's targets is the ubiquitously expressed Calcium/Calmodulin-dependent protein kinase II (CaMKII), a serine/threonine-specific kinase that phosphorylates over forty known peptide or protein substrates. The enzyme responds not only to the amplitude of the Ca^{2+} signal, but also to the frequency of repeated Ca^{2+} transients (De Koninck and Schulman 1998; Fujii et al., 2013). There are four human CaMKII genes (α, β, δ and γ) and about thirty splice variants (Tombes et al., 2003). The α and β isoforms are predominantly found in the forebrain, where they make up to 2% of total protein (Bennett et al., 1986; Lin et al., 1987). On the other hand, the δ and γ isoforms are expressed in most tissue types, though in much smaller amounts, but are abundant in heart and smooth muscle cells (reviewed in Griffith et al., 2003). The CaMKII polypeptide consists of a catalytic or kinase domain at the N-terminus, a regulatory domain, a linker which varies in length among the various isoforms, and an association domain at the C-terminus (Hudmon and Schulman, 2002). The catalytic domain is bi-lobate: its N-terminal lobe, involved in

ATP binding, possesses a mainly β-stranded structure, which is connected to the C-terminal lobe via a hinge region where the catalytic cleft lies at the intersection between the lobes. The CaMKII holoenzyme exists in a dodecameric structure of two hexameric rings stacked together with the catalytic domains pointing radially outward from the center of the rings (Kolodziej et al., 2000). Homo-oligomeric as well as hetero-oligomeric enzymes are known, with the most common ratio being 3:1 α:β in the forebrain and 1:3 in the cerebellum (Miller and Kennedy, 1985). Holoenzymes containing the various subunit compositions and splice variants exhibit distinct Ca^{2+} frequency responses, which refers to the acquisition of Ca^{2+}-independent activity when stimulated by high frequency Ca^{2+} pulses (Brocke et al., 1999; Bayer, De Koninck, and Schulman, 2002). Isolated association domains of the holoenzyme have been crystallized, which assemble into 14-subunit oligomers of two heptameric rings (Hoelz et al., 2003; Rosenberg et al., 2006), suggesting the hexameric arrangement is adopted in the native protein to resolve the strain imposed on the ring by the catalytic domains. This explanation is supported by the change from a 12- to 14-mer assembly by proteolytic cleavage of the catalytic domains (Rellos et al., 2010).

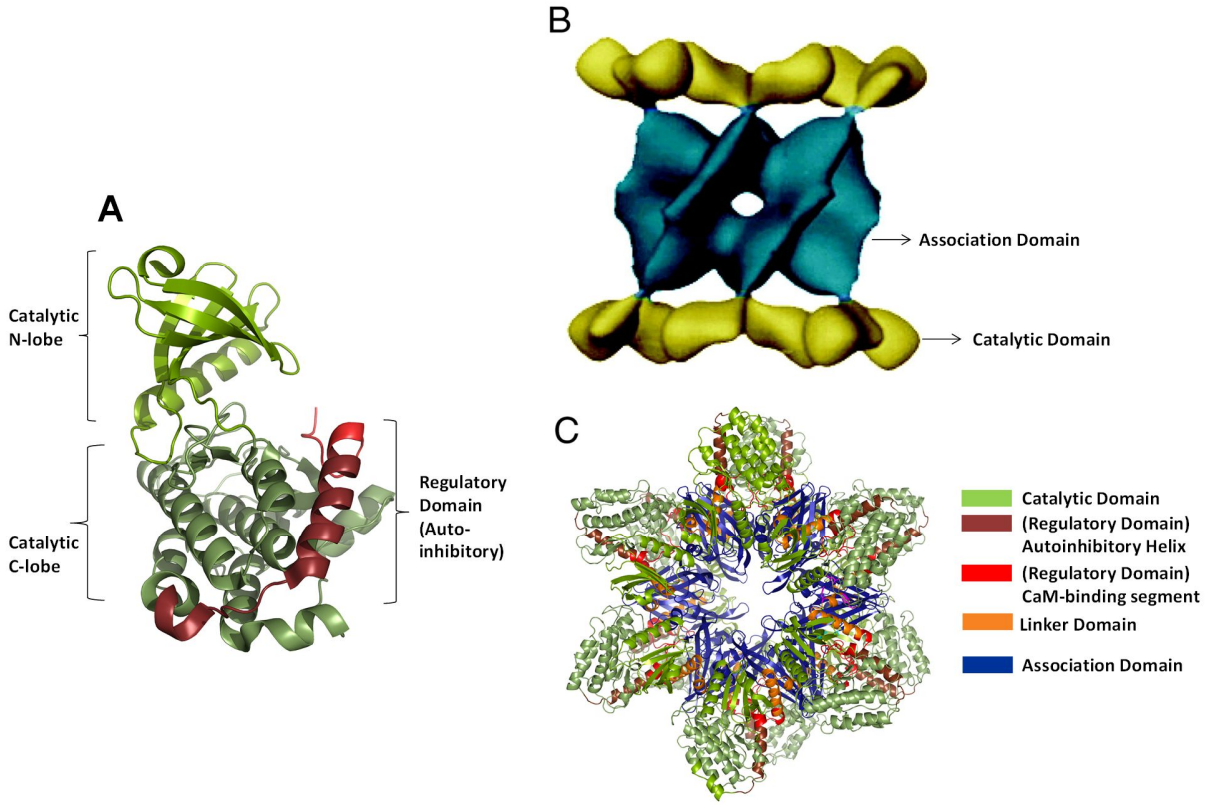

Figure 1.1: Structure of CaMKII. A. The Kinase monomer (PDB 2VN9 chain A)[(Rellos et al., 2010)] consists of the N-lobe (light green), involved in ATP binding, the C-lobe (olive) which allows for substrate peptide anchoring and presentation, and the regulatory domain (red), which acts as an auto-inhibitory region in the basal state. B) Electron microscopy structure of the holoenzyme, showing a dodecamer formed from two hexameric rings[(Kolodziej et al., 2000).] Subunits are held together by the association domains (teal), with the catalytic domains pointing outward (yellow). C) Crystal structure of the CaMKII holoenzyme showing the different domains (PDB 3SOA)[(Chao et al., 2011)].

In its basal or apo state (absence of Ca^{2+} signals), CaMKII remains in an inactive conformation with the regulatory domain acting as an inhibitor bound to the catalytic domain through hydrophobic interactions, thereby blocking access of substrates to the kinase (Kanaseki, et al., 1991; Rosenberg et al., 2005). Binding of Ca^{2+}/CaM to the regulatory domain disrupts the interaction between the regulatory and catalytic domains, leading to activation of CaMKII (Rellos et al., 2010, Chin and Means, 2002). In this fashion, CaMKII translates changes in Ca^{2+} concentration into downstream cell signaling pathways to phosphorylate target proteins. Distinct from other Ca^{2+}/CaM-dependent protein kinases, CaMKII can attain Ca^{2+}/CaM-independent activity through a process of *trans*-autophosphorylation. This entails the **inter**subunit transfer of

the γ-phosphate from ATP onto T286 (Mukherji and Soderling, 1994; Lai et al., 1987), a residue in the regulatory domain that is buried in contact with the kinase domain in the apo state. Ca^{2+}/CaM binding exposes T286, making it accessible to the kinase domain of an adjacent subunit (Rosenberg et al., 2006; Rellos et al., 2010; Lai et al., 1986; Lu et al., 2003). Autophosphorylation prevents the T286-bearing helix (hereafter R1) from re-establishing contacts with the kinase. T286 phosphorylation also decreases the dissociation of Ca^{2+}/CaM by 1000-fold (K_D lowered to 10^{-2}nM from 45nM) thus trapping CaM and keeping the enzyme in an active state (Meyer et al., 1992; Waxham et al., 1998). By contrast, **intra**subunit phosphorylation of T305/T306 within the CaM binding subdomain prevents CaM binding, rendering the enzyme Ca^{2+}-unresponsive (Mukherji and Soderling, 1994; Colbran and Soderling, 1990; Colbran, 1993). Following an initial activation by Ca^{2+}/CaM, some proteins that resemble the regulatory domain sequence are also able to bind to the docking site on the catalytic domain where T286 is normally buried. An example of this is the NR2B subunit of the NMDA receptor, which locks the kinase in its autonomously-active state (Bayer et al., 2001). If the subunit is phosphorylated at T286 and T305/T306, it becomes completely Ca^{2+}-independent and retains autonomy. Moreover, phosphatases, including PP1 (in specialized compartments of postsynaptic neurons), PP2A (in the cytosol), and PP2C (Fukunaga et al., 1992) return the autonomously-active enzyme to the apo state following the decay of the Ca^{2+} signal and also serve to maintain a balanced pool of the non- and phosphorylated conformations at resting conditions (Strack et al., 1997).

Roles of CaMKII in Biological Processes

CaMKII in Synaptic Function

Long Term Potentiation (LTP) is a long lasting strengthening of synaptic transmission wherein a brief stimulus strengthens communication between neurons. Glutamate released from a presynaptic terminal into the synaptic cleft binds to postsynaptic AMPA receptors (AMPAR) causing Na^+ influx. Periods of intensive synaptic stimulation activate AMPARs to depolarize the postsynaptic neuron and facilitate NMDA receptor (NMDAR) activation. NMDARs also bind glutamate but Mg^{2+} blocks these channels at resting membrane potential. which is relieved by the depolarization to allow Ca^{2+} influx and the activation of CaM and CaMKII (Hudmon and Schulman, 2002). CaMKII phosphorylates AMPAR at S831 of its GluA1 subunit, causing increased conductance by making the receptor more efficient at coupling glutamate binding with channel opening (Kristensen et al., 2011). The increased postsynaptic depolarization enhances the likelihood that a postsynaptic action potential (AP) will be initiated, resulting in a signal being transmitted down the axon. A study in which CaMKII was labeled with two fluorophores, mEGFP and REACh, and transfected into hippocampal CA1 neurons showed that activation of CaMKII by photoactivation of "caged" glutamate – glutamate bound to a photolabile group - is associated with LTP (Lee et al., 2009). The conformational change associated with CaMKII activation was tracked by changes in Förster resonance energy transfer (FRET). Glutamate uncaging in the extracellular space of single dendrites resulted in changes in spine volume and morphology that were correlated with CaMKII accumulation only in the activated dendrites. Inhibition of CaMKII or NMDAR blockage abolished the change, while transfection of T286A mutant CaMKII resulted

in smaller changes in morphology. Moreover, CaMKII is not only involved but also necessary for long-term memory, and prolongation of CaMKII activity through autonomy is critical for LTP. Mice bearing a T286A mutation that prevents persistent activity after CaM dissociation, showed impairments in LTP and failed at hippocampus-dependent spatial learning tasks (Giese et al., 1998).

CaMKII has also been involved in long-term depression (LTD), a persistent reduction in synaptic strength – the opposite of LTP. A FRET imaging study (Aow et al., 2015) found that ligand binding to the PhosphoCaMKII-NMDAR complex during LTD increases T286 dephosphorylation and reduces the interaction between CaMKII and NMDAR. The same study found ligand binding to alter the location of PP1 associated with NMDAR, suggesting CaMKII dephosphorylation within the complex is an NMDA-driven PP1 reaction. A further role for CaMKII in LTD involves AMPAR phosphorylation at S567 of GluA1 (Coultrap et al., 2014). This results in decreased trafficking of AMPARs to the PSD and synaptic membrane, thereby decreasing sensitivity to the stimulus.

CaMKII in Heart Function

Novel mechanisms that maintain CaMKII activation after initial Ca^{2+}/CaM binding have been discovered within the past ten years. These mechanisms depend on post-translational modification of regulatory domain residues, which are presumed to disrupt the interaction between the R1 segment and the catalytic domain. Their dysregulation appears to be relevant in heart disease (reviewed in Erickson, 2014). It should be noted that these modifications also occur in neuronal isoforms α and β, though this section will focus on the δ isoform that is prevalent in the heart, and on effects related to its activation.

CaMKII Oxidation

Elevated aldosterone or angiotensin-II, seen in heart failure (Swedberg et al., 1990) or diabetes (Luo et al, 2013) result in increased levels of reactive oxygen species that generate autonomous CaMKII activity through oxidation of the Met281/Met282 pair (Erickson et al., 2008), a process that requires sarcoplasmic reticulum (SR) function (Wagner et al., 2011). Oxidized CaMKII has been implicated in Na^+ and Ca^{2+} overload (Wagner et al., 2011), myocardial rupture (He et al., 2011, Velez Rueda et al., 2012), cardiac hypertrophy and apoptosis (Swaminathan et al., 2011, Velez Rueda et al., 2012), and atrial fibrillation (Purohit et al., 2013). It is possible that acute and/or chronic β-adrenergic stimulation, which increases reactive oxygen species in mitochondria (Andersson et al., 2011, Bovo et al., 2012), also leads to CaMKII activation through this pathway, though it has not been shown. CaMKII oxidation and related apoptotic effects on myocytes seem to be reversed in mice by methionine sulfoxide reductase (MsrA) activity, which reduces and inactivates CaMKII (Erickson et al., 2008), as determined from $MsrA^{-/-}$ mutants.

CaMKII O-Glycosylation

The addition of O-linked N-acetylglucosamine to Ser280 in the presence of Ca^{2+}/CaM is glucose-dependent and renders CaMKII autonomously active (Erickson et al., 2013). The reaction is catalyzed by O-GlcNAc transferase from a glucose metabolite substrate and is reversed by O-GlcNAcase. CaMKII and O-GlcNac are both involved in glucose induced SR Ca^{2+} leak in hyperglycemia, suggesting that activation of CaMKII through this pathway is related to cardiac pathologies of diabetic origin (Erickson et al., 2013).

CaMKII S-Nitrosylation from β-adrenergic stimulation

In heart disease, increased β-adrenergic signaling leads to CaMKII activation, which has been implicated in abnormal heart remodeling in mice (Zhang et al., 2005). CaMKIIδ deletion mutant mice were protected against the development of heart failure that is induced by chronic administration of the β-adrenergic agonist isopreterenol (Grimm et al., 2015). In myocytes isolated from WT mice, SR Ca^{2+} leak induced by isopreterenol was also found to involve CaMKIIδ phosphorylation of RyR2 at Ser2814. By contrast, the CaMKIIδ deletion mutant showed reduced SR Ca^{2+} leak (Grimm et al., 2015). These results suggested a link between elevated β-adrenergic signaling, CaMKII activation, and SR Ca^{2+} instability in heart failure. Isopreterenol treatment also led to fibrosis (excessive formation of connective tissue) in the hearts of WT mice but not in CaMKIIδ deletion mutants. The mRNAs of collagen type I and III, which are produced at increased levels during the development of fibrosis, were upregulated following chronic β-adrenergic stimulation by isopreterenol in hearts from WT mice only (Grimm et al., 2015). Additionally, inhibition of NO synthase-1 and CaMKII abolishes Ca^{2+}-independent, isopreterenol-induced SR Ca^{2+} leak (Curran et al., 2014), relating nitric oxide to β-adrenergic activation of CaMKII. More specifically, stimulation of the β-adrenergic receptor results in increased nitric oxide production and subsequently CaMKII S-nitrosylation (Gutierrez et al., 2013, Curran et al., 2014) - the transfer of NO onto the thiol group of a cysteine residue. The site of modification was determined from treatment of Camui, a FRET-based CaMKII sensor, with the NO donor GSNO. Following Ca^{2+}/CaM activation, S-nitrosylation of Cys290 generates autonomously active CaMKII (Erickson et al., 2015), however, S-nitrosylation of Cys273 prior to Ca^{2+}/CaM activation inhibits the enzyme, showing that NO may have opposing effects on CaMKII activity depending on the timing and

conditions present during increased NO production in the heart. The structural mechanism underlying CaMKII inhibition by Cys273 S-nitrosylation is presently unclear and an avenue of further research. In cardiac myocytes, NO release following β-adrenergic stimulation is correlated with increased SR Ca^{2+} leak (Curran et al., 2014) again highlighting a possible connection to irregular Ca^{2+} handling and abnormal electrical signals in heart disease.

CaMKII Structure

There is significant sequence conservation for the catalytic and association domains across all four human CaMKII isoforms (95 and 80%, respectively, Chao et al., 2011)[65]. However, the length of the linker between the regulatory and association domains is most variable across isoforms and splice variants. The catalytic and regulatory domains were initially crystallized independently from the association domain by use of truncated constructs. Several crystal structures of truncated catalytic domains have been reported, summarized in Table 1.1.

PDB	Notes		Citation
2BDW	C.elegans CaMKII		Rosenberg et al., 2005
2VZ6	Human CaMKIIα bound to Indirubin-E804		Rellos et al., 2010
3BHH	Human CaMKIIβ bound to 5CP		Rellos et al., 2010
2VN9	Human CaMKIIδ bound to GVD		Rellos et al., 2010
2WEL	Human CaMKIIδ in complex with Ca^{2+}/CaM		Rellos et al., 2010
2V70	Human CaMKIIγ bound to Bisindoylemaleimide-IX		Rellos et al., 2010
3KK8	C. elegans CaMKII enzyme-substrate complex		Chao et al., 2010
3KK9	C. elegans CaMKII enzyme-substrate complex		Chao et al., 2010
3KL8	C. elegans CaMKII bound to peptide inhibitor CaMKIINtide		Chao et al., 2010

Table 1.1: Crystal Structures of truncated CaMKII including the catalytic domain.

A common finding revealed by the truncated kinase crystal structures involved the conformation of a region in the C-lobe termed the activation loop. Unlike other eukaryotic protein kinases that

need to be phosphorylated at this loop to adopt an active conformation, this region is already positioned as in the active structures of other kinases. This corroborated previous findings that CaMKII is constitutively active in constructs that only comprised the catalytic domain (Zou and Cline, 1996; Shoju et al., 2005) which does not bear any phosphorylation sites at this loop. However, discrepancies regarding the functional unit (monomer or dimer) and the structure of the Ca^{2+}/CaM-binding region are of note when comparing these structures.

The *C. elegans* CaMKII catalytic domain crystallized as an antiparallel dimer held together by a coiled-coil interface of entirely helical regulatory domains (PDB 2BDW). By contrast, dimerization of catalytic domains has been detected by analytical ultracentrifugation in the truncated human constructs (Rellos et al., 2010) and in the holoenzyme in cells by FRET (Thaler et al., 2009). The findings in solution also stood in opposition to human catalytic domain crystal structures bound to different active site inhibitors where such dimer interface was not observed (PDB 2VN9, 2VZ6, 2V70, 3BHH). Unlike the *C. elegans* crystal, the Ca^{2+}/CaM-binding region was unstructured and made contacts with the catalytic domain in crystal 2VN9 (much of the C-terminus of the regulatory region was not resolved in the other structures). In this same study, a truncated human CaMKIIδ monomeric construct bound to Ca^{2+}/CaM was also crystallized (PDB 2WEL). Additionally, in opposition to the autoinhibited structures, the R1 region containing T286 was unfolded and bound to another kinase active site in the CaMKII enzyme-substrate complex crystals (PDB 3KK8, 3KK9).

Properties of the Regulatory Domain

Three structurally-relevant components have been identified in the regulatory domain: the pseudo-substrate sequence that bears T286 (R1); the clamp lodging the helix to the catalytic domain in the apo state (R2); and the region containing the Ca^{2+}/CaM recognition motif (R3) (Rosenberg et al., 2005; Chao et al., 2011).

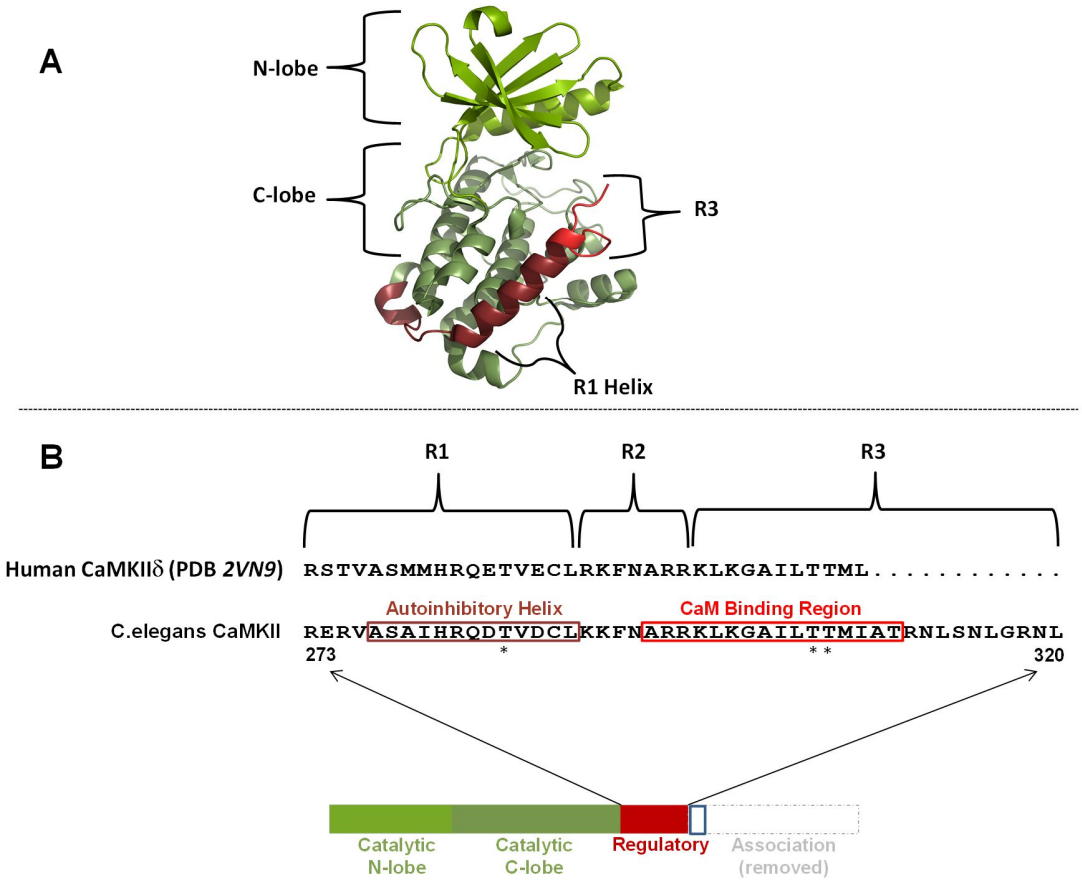

Figure 1.2: CaMKII Polypeptide and Subdivisions of the Regulatory Domain. The CaMKII sequence comprises a catalytic domain that confers kinase activity (light green and olive); a regulatory domain that inhibits the kinase in the apo state (red); a linker that varies in length across isoforms (blue); and an association domain that assembles the holoenzyme (dashed). The regulatory domain contains the helix surrounding autophosphorylation site Thr286 ("R1"), the clamp that contacts the catalytic domain ("R2") and the dynamic region with the CaM-binding segment ("R3"). The construct used for these studies (residues 1-340) lacks the association domain to afford monomeric protein, in order to simplify interpretation of the data.

The lack of data on the dynamics of the regulatory domain as well as the antiparallel coiled-coil interaction observed in the *C.elegans* structure led to conflicting explanations about the nature of the region and the mechanism of enzyme activation. The question remained whether the observed interface was responsible for partially blocking nucleotide binding site, in which case binding of CaM would lead to activation by disrupting the coiled-coil. Alternatively, unknown regulatory-catalytic domain interactions altered by changes in domain flexibility due to CaM and ATP could not be ruled out for relief of inhibition because the new interface only partially blocked the catalytic cleft. This conundrum called for a thorough investigation of regulatory domain dynamics in solution, as well as further evidence on the nature of domain interactions.

Previous studies on the *C. elegans* homologue (unc-43) lacking the association domain have led to a model of autoinhibition that has the R3 segment in an equilibrium between a docked and undocked conformation relative to the ATP-binding site and the R1 segment docked against the T286 recognition site (T-site) of the catalytic domain in the apo state (Hoffman et al., 2011). The backbone mobility of the regulatory domain was postulated to permit the interconversion between discrete conformations that allow for binding of Ca^{2+}/CaM and ATP. Nucleotide binding was thought to shift the R3 equilibrium towards the undocked, flexible conformation. However, binding of Ca^{2+}/CaM prior to nucleotide would disrupt the equilibrium, leading to an ordering of R3 and relief of its blockage of the catalytic site. This finding was consistent with fluorescence studies that showed that Ca^{2+}/CaM can adopt either an extended or a compact conformation when bound to CaMKIIα, and that ATP favored the compact conformation (Török et al., 2001) and stabilized the Ca^{2+}/CaM-CaMKII complex (Tzortzopoulos and Török, 2004) as well as crystal structures of Ca^{2+}/CaM bound to a peptide derived from the regulatory domain of CaMKII, in

which the R3 region was ordered and engulfed by Ca^{2+}/CaM (PDB 1CDM Meador et al., 1993; 3GP2 Ng et al., 2010).

Ca^{2+}/CaM was also found to increase the backbone mobility of the R1 helix and increase the separation between R1 residues four positions apart in sequence. This was interpreted as the unfolding of the R1 segment to expose T286 for autophosphorylation. This was in agreement with biochemical data showing enhanced affinity for nucleotide after Ca^{2+}/CaM binding, as well as the crystal structure of Ca^{2+}/CaM bound to CaMKII (PDB 2WEL - Rellos et al., 2010). The model based on these findings (Hoffman et al., 2011) also helps to explain the apparent cooperativity (Hill coefficients >2) between holoenzyme subunits in CaMKII (Chao et al., 2010) wherein the R1 region of one kinase is displaced to occupy the active site of the adjacent subunit, thereby dislodging the neighboring R3 region and allowing Ca^{2+}/CaM binding to the "phosphorylating" subunit. Following the expansion of R1 and autophosphorylation, and the eventual dissociation of Ca^{2+}/CaM, the R3 equilibrium would be restored, while preventing the docking of the R1 helix until T286 is dephosphorylated. The research plan proposed herein is based upon this model and presents an avenue for its elaboration.

CHAPTER II: Study of CaMKII by Double Electron-Electron Resonance

Motivation and Aim

Biochemical findings have provided clues that the regulatory region might restrict access to both the nucleotide and peptide binding sites on CaMKII. Peptides derived from the regulatory domain (spanning R1 through R3) inhibited the enzyme competitively with respect to substrate peptide (Payne et al., 1988) or to ATP (Colbran et al., 1989) depending on peptide length, assay stoichiometry, and autophosphorylation state of the enzyme (Kelly et al., 1988). Additionally, it has been well established that CaM binding increases affinity for ATP by an order of magnitude (King et al., 1988; Shields et al., 1984), suggesting that binding of CaM to R3 partially enhances access to the ATP binding site on the kinase. Along with site-specific evidence from EPR studies of the regulatory domain (Hoffman et al., 2011), these findings support a synergism between CaM and ATP binding in activating holoenzyme subunits in the basal state.

CaMKII crystal structures do not report a consistent secondary structure of the R3 region. R3 appeared unstructured in monomeric constructs of different human CaMKII isoforms (Rellos et al., 2010). By contrast in an earlier *C. elegans* CaMKII crystal structure, this region formed an antiparallel coiled-coil dimer interface with another monomer (Rosenberg et al., 2005). In the full-length human holoenzyme crystal, R3 makes contacts not with the active site but with the association domain at a previously unidentified interface (Chao et al., 2011). Furthermore, interpretation of these diverging findings is obfuscated by the presence of active site inhibitors in most of these crystal structures.

The R3 segment of the regulatory domain, including the CaM binding region, was reported to be in equilibrium between two conformations: one is structured and docked near the active site while the other is dynamic, unstructured and undocked from the enzyme (Hoffman et al., 2011). This insight came from analysis of the mobility of spin labels introduced along the regulatory domain of a monomeric construct of *C. elegans* CaMKII. Conformational heterogeneity was evident in the EPR spectral lineshape of the R3 segment, with a predominantly buried population of the spin label alongside a minor, mobile population in the absence of nucleotide. ATP binding increases the mobile population which was interpreted as the undocked conformation. This spectroscopic data was suggested to reflect a dynamic R3 region in equilibrium between docked and solvent-exposed conformations. The shift in equilibrium of R3 in the ATP-bound state could thereby facilitate CaM binding due to exposure of R3 to the solvent. Whereas the aforementioned EPR study provided evidence that R3 exists as an ensemble of populations with vastly different dynamics in solution, it did not quantify the scale of the movement of the regulatory domain following ATP and CaM binding and possible conformational changes within the catalytic domain were not investigated. Specifically, the question of whether CaM and/or ATP binding induce reorientation of the N-terminal lobe relative to the C-terminal lobe is relevant to the activation mechanism of the kinase in order to better understand how changes in the regulatory domain affect catalytic domain conformation. To address these aspects of CaMKII mechanism, spin label pairs were placed at representative positions in the regulatory domain and in the kinase core for distance measurements by Double Electron-Electron Resonance (DEER) spectroscopy. Distances were measured between the regulatory domain and kinase core, and within the kinase core in the apo state (absence of substrates), in the presence of nucleotide

(ATP), or CaM-bound conditions. The findings that follow demonstrate a change in the R3 dynamic equilibrium from a short to an extended conformation as a consequence of ATP binding. Moreover, it is found that upon CaM binding, R3 is disengaged away from the kinase. The following results are in agreement with an alternative docking interface for R3 in the C-lobe following the shift in the R3 equilibrium post ATP-binding. Furthermore, shorter distances are found between the catalytic lobes after addition of ATP, in concordance with a closed kinase conformation; finally, movement of R1 is found upon Ca^{2+}/CaM binding.

Experimental Design

Protein Expression and Purification

Cysteine-less *C.elegans* CaMKII isoform d construct encoding residues 1-340 used previously (Hoffman et al., 2011) was the template for generating double cysteine mutants with a modified Quikchange protocol. The CaMKII 1-340 plasmid was expressed in *E.coli* strain BL21(DE3)pLysS in LB medium. Protein production was induced by addition of 0.4mM IPTG at $O.D._{600nm}$ = 1.2, and the culture was grown for 18hr at 18^{o}C. Cells were resuspended in 50mM HEPES, 150mM NaCl, 10mM imidazole, 10% (v/v) glycerol, 1mM PMSF, 2mM TCEP, pH 8. After sonication and separation of the soluble fraction, the filtered lysate was loaded onto a Cobalt column. The protein was eluted with 50mM HEPES, 150mM NaCl, 250mM imidazole, 10% (v/v) glycerol, pH 7.5. Labeling with 40X MTSSL was carried out at 4^{o}C in a centrifugal concentrator, and further incubated at 4^{o}C for 12-16hr. The protein was further purified by size exclusion chromatography on a Superdex-75 column (GE). Unbound MTSSL was removed by washing in a centrifugal concentrator. The final buffer for DEER experiments was 50mM HEPES, 100mM NaCl, 2.5mM

EDTA, 0.02% NaN3 and 30% (w/v) glycerol, with final CaMKII 60-180μM. 500X MgATP and 3X CaM/20mM $CaCl_2$ were used. All EPR and NMR experiments were carried out at physiological pH of 7.4 on a D135N background that abolishes the catalytic activity of the kinase but does not affect the structure, to prevent a heterogeneous mixture of apo and autophosphorylated CaMKII, unless otherwise stated.

Methods

Electron paramagnetic resonance (EPR) is a technique that allows for the detection of electronic transitions of species possessing unpaired electrons. An oscillating magnetic field in the microwave frequency generates a transition between energy levels of spin states. In the context of proteins without any paramagnetic centers, cysteine residues capable of being specifically labeled with an EPR-active probe such as (1-Oxyl-2,2,5,5-tetramethylpyrroline-3-methyl) methanethiosulfonate spin label (MTSSL) are incorporated at the site of interest through mutagenesis.

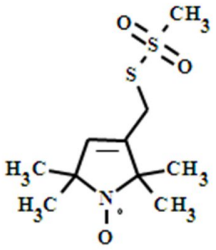

Figure 2.1: Structure of MTSSL. The four methyl groups attached to the ring stabilize the unpaired electron.

The probe reacts with the nucleophilic thiol group on the cysteine side-chain forming a disulfide linkage. Typically, this requires prior removal of native cysteines and their replacement with residues found in homologues or with a small, non-reactive residue such as alanine or valine,

substitutions that often leave protein structure and function uncompromised. An advantage of this method is that the probe can be placed at a specific location within the protein; the disadvantage is that the throughput is extremely slow.

Origin of EPR signal

The intrinsic angular momentum (spin) and charge of the electron confer the particle a permanent magnetic moment. The dynamics related to the electron spin transitions form the basis of the spectroscopic utility of EPR.

When subjected to an external magnetic field in the z-direction, the magnetic moment will interact with the field with energy

$$H = -U_z H_o \text{ (Eq. 1)}$$

,with U_z being the magnetic moment of the electron. The relation can be rewritten in terms of the electron spin quantum operator,

$$H = gBH_oS_z \text{ (Eq. 2)}$$

where H_o is the applied magnetic field, g is a dimensionless constant specific to the chemical environment of the unpaired electron species, B is the electron Bohr magneton, and S_z is the spin operator with eigenvalues M_s +- ½. Therefore, two energy levels exist: $-1/2gBH_o$ (α) and $+1/2gBH_o$ (β). Paired electrons in the same orbital have opposite spin quantum numbers, and are EPR silent because there is no net interaction with the field since both electron spins would be flipped in opposite directions, hence the need for an unpaired electron for EPR.

The EPR signal arises from the net absorption of the slightly more populated α state promoted to the β state, which occurs when the incident radiation matches the energy difference between the levels:

$$\Delta E = h\upsilon = gBH_o \quad \text{(Eq. 3)}$$

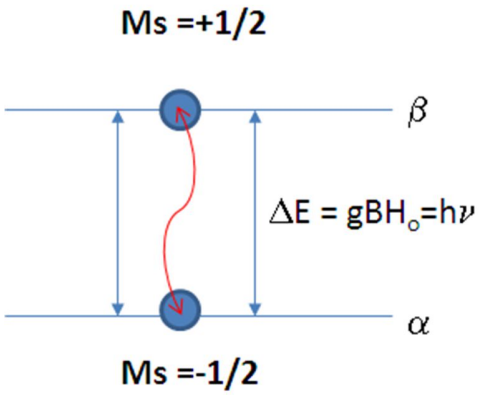

Figure 2.2: Origin of EPR signal. Shown is the energy difference between two spin states for an unpaired electron subjected to an external magnetic field.

Where h is the Planck constant and n is the frequency of electromagnetic radiation. From relation (3), the separation between energy levels is directly related to the strength of the magnetic field. It can be gleaned that when $H_o = 0$, there is no energy difference between the α and β levels. The applied magnetic field breaks the degeneracy of the two levels; due to the negative charge of the particle, an electron in the α level will be aligned with the magnetic field, and so becomes the lower energy state. In the EPR experiment, the transition is usually accomplished by keeping the frequency constant while varying the field strength.

The distribution of spins in the α and β states at thermal equilibrium is described by the Boltzmann distribution and is obtained from the relation:

$$N_\alpha/N_\beta = e^{(\Delta E/\kappa T)} \text{ (Eq. 4)}$$

Thus, there is both a temperature as well as magnetic field strength dependence on the proportion of spins in each state. The EPR signal is the average from the spin transition occurring in the ensemble of molecules in solution. At thermal equilibrium, there is a slight excess of electrons in the α state according to the Boltzmann distribution. This results in net magnetization M_o as spins precess about the z axis, parallel to the applied field. For a magnetic field strength of 3400 Gauss, the transition will occur with radiation of 9.5GHz, a frequency in the microwave region termed X-band, commonly used in continuous wave (CW) EPR described below.

Relaxation Processes

In the absence of an external magnetic field, the bulk magnetization M is zero because the spin states α and β are equal in energy. After the field is applied, the spins will generate a bulk magnetization M_z. Because the equilibrium of the ensemble of spins is in the z axis, the spins are perturbed and detected on the x-y or transverse plane. A 90^o ($\pi/2$) pulse rotates M on the x-y plane, causing the ensemble to reach coherence. Once the pulse is no longer applied, relaxation mechanisms return the ensemble to equilibrium, allowing for signal detection. The net magnetization in the direction of B_o is restored by the processes of T1 and T2 relaxation. T1 describes spin-lattice relaxation, or the loss of pulse energy to the surroundings that leads to recovery of magnetization along the z axis. Energy conversion into vibrational and rotational processes of the lattice molecules contributes to the T1 mechanism. It is because of T1 relaxation that the α and β states do not become equally populated, which would preclude net transitions and hence the signal. T2 describes spin-spin relaxation, or how quickly spin flips cause loss of

coherence along the x-y plane. Collisions between vicinal spins and dipolar interactions are responsible for T2 relaxation.

Additionally, the M_x and M_y components of the M vector induce a torque on the ensemble of spins. This makes the net magnetization vector precess about the z-axis. This causes the x and y components of the magnetization to cancel out, with the net magnetization vector to align with the field. The precession frequency is referred to as the Larmor frequency, and the behavior of M_x and M_y as a function of time is given by the Bloch relations:

$$dM_x/dT = gH_oM_y - M_x/T_2 \text{ (Eq. 5)}$$

$$dM_y/dT = gH_oM_x - M_y/T_2 \text{ (Eq. 6)}$$

Hyperfine Splitting

Because the unpaired electron in a nitroxide spin label resides in the N-O bond near the N nucleus, its interaction with the ^{14}N nuclear spin (I= 1, $m_ℓ$ = -1,0,+1) splits the resonance into three signals. This hyperfine coupling between the two electron spin states and the three nitrogen nuclear spin states occurs within the context of the selection rules $\Delta M_s=1$, $\Delta I =0$, hence, only electronic spin transitions take place.

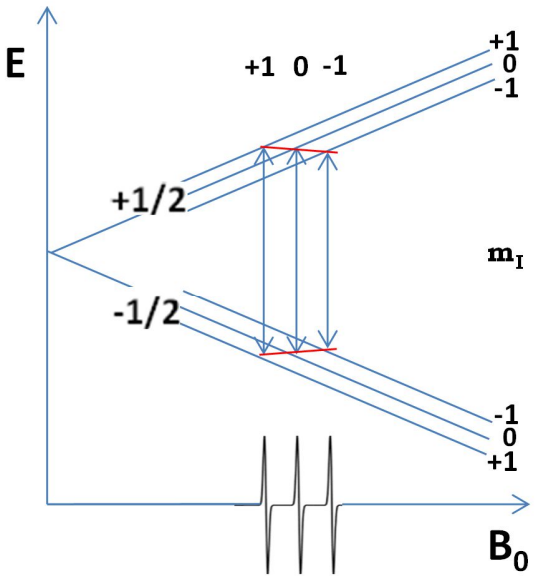

Figure 2.3: Contributions from hyperfine splitting to the EPR spectrum of a nitroxide.

The EPR spectrum of a nitroxide spin label therefore shows three absorbance lines separated by the hyperfine coupling constant A_0. The constant describes the interaction between the unpaired electron and the neighboring ^{14}N nucleus. In the case of isotropic interactions of the electron, the splitting results in degenerate energy levels. Such is not the case for a fixed radical, for instance a nitroxide attached to a protein, which will experience orientation-dependent interactions with respect to the applied magnetic field.

Another correction to the energy term comes from spin-orbit coupling, which is possible due to perturbations in the orbital angular momentum caused by its interaction with the external magnetic field. Due to these local perturbations, the g and A_o tensors become anisotropic, i.e. dependent on the orientation of the nitroxide with respect to the effective magnetic field.

In the continuous wave (CW) EPR experiment, the sample is subjected to a continuous microwave irradiation as the magnetic field is swept in the perpendicular axis. The mobility of the probe,

which is reflective of the environment surrounding its site of attachment, can be inferred from the spectral lineshape. A free nitroxide averages out components in all directions and the three peaks in the spectrum are equal. MTSSL bound to an unfolded region is able to rotate rapidly about the bonds connecting it to the protein backbone (Hubbell et al., 1996) and manifests as a sharp peak spectrum. The other motional extreme is an immobilized probe, such as a nitroxide in a crystal lattice will resolve all anisotropic components, giving rise to broadened peaks. Likewise, a nitroxide buried within the hydrophobic core of the protein will resolve immobile components in the spectrum. Loop regions and surface residues, with mobilities intermediate between these two extremes, also cause the probe to reorient itself with distinct rotational correlation times, which relate to how fast the nitroxide probe tumbles in solution. MTSSL can isomerize mainly from rotation about the Cγ-Cε and Cε-S bonds with the protein placing steric constraints on the rotamers possible depending on the environment at the site of attachment. Thus, inspection of CW EPR spectra of singly-labeled mutants can provide information regarding the extent of solvent exposure and local mobility of the labeled residue and its environment (Mchaourab et al., 1996).

Double Electron-Electron Resonance

Distances 20-50Å can be measured with the pulsed EPR technique Double Electron-Electron Resonance (DEER). Instead of a constant irradiation, two microwave frequencies, termed observe and pump, are applied in a pulsated sequence. The first (90^{o}) pulse at the observe frequency tips the magnetization of a population of spins into X-Y plane; due to magnetic inhomogeneities from the environment, such as dipole-dipole interactions, the spins precess with different frequencies

and generate a free induction decay (FID). After a time τ1, a 180° pulse is applied, which changes the orientation of the spins in the opposite direction and causes them to rephase, generating an echo.

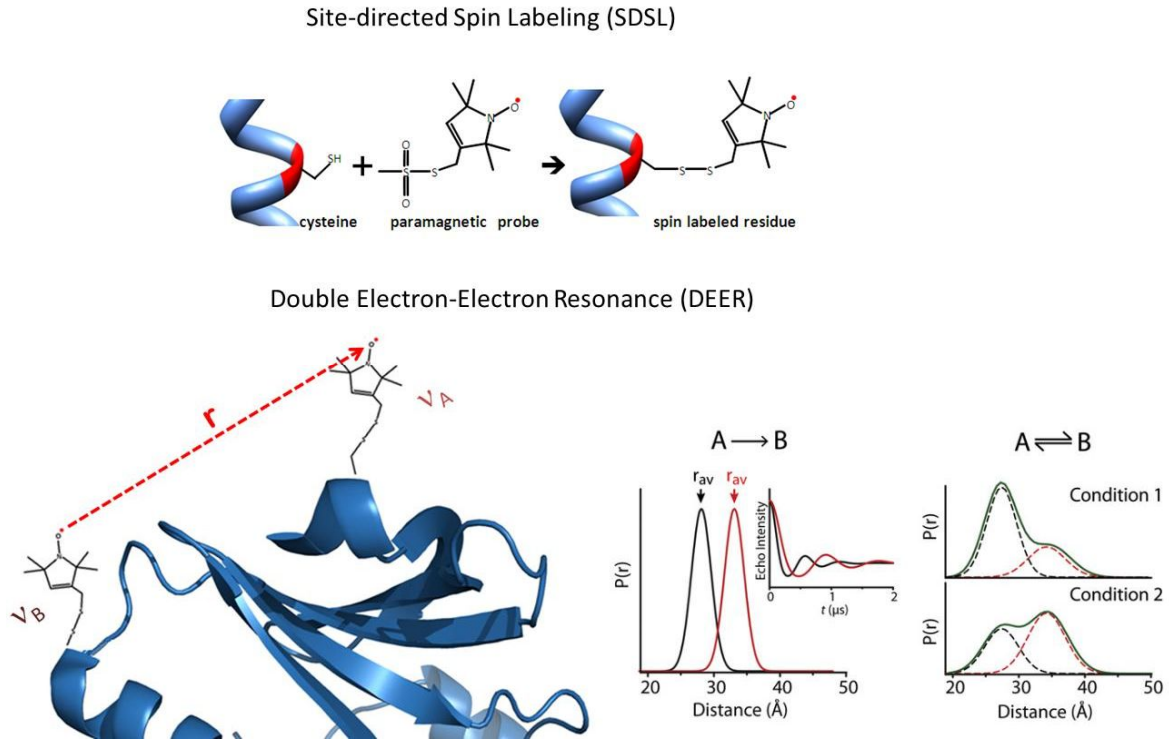

Figure 2.4: Site-Directed Spin Labeling and Electron Paramagnetic Resonance: *Left Panel:* Site-directed spin labeling (SDSL) refers to the introduction of cysteine residues at the site of interest through mutagenesis and attachment of the paramagnetic probe MTSSL through disulfide linkage. *Right Panel:* Placement of two MTSSL probes allows for distances between 20-50Å to be measured with the pulsed EPR technique Double Electron-Electron Resonance (DEER), which reports changes in average distance as well as changes in distributions (bottom left, reproduced with permission from Cell Pres, 19(11). 1549-61.

As the observe frequency spins refocus, a 180° pulse is applied at the pump frequency, flipping the magnetization of a separate population of spins. Dipolar coupling between the observe and pump populations occurs only if they are within proximal distance of each other. Finally, a 180° pulse is applied at the observe frequency to refocus the signal. The different magnetic environment experienced by the observe spins after the pump frequency pulse will be manifested on the refocused echo. Changing the time of the pump pulse allows for a modulation

of the echo intensity, so that the contribution of coupling on the refocused echo can be inferred. The signal will oscillate with a periodicity related to the intensity of the coupling, which in turn depends on the distance between the spin labels (Tsvetkov et al., 2008). A distance distribution derived from the DEER data fit provides information different distances between the labels arising from discrete conformational states.

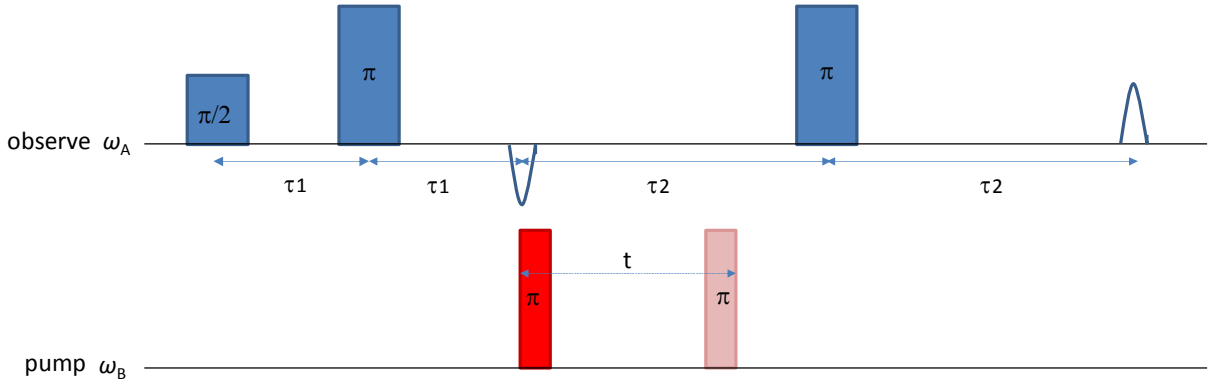

Figure 2.5: Four-pulse DEER experiment. The π pulse at the pump frequency inverts spins B, inverting the local field that B spins exert on A spins. The time t is varied and the effect of the coupling on the refocused echo can be detected. Adapted from Annu. Rev. Phys. Chem. 2012. 63:419–46.

For the data in the following section, CW EPR was carried out at 25°C on a Bruker EMX spectrometer with modulation amplitude of 1.5G, center field of 3520G, sweep width of 120G, and power of 10.02mW. Four-pulse DEER was carried out at 83K on a Bruker 580 pulsed EPR spectrometer at Q-band (34 GHz).

Results and Discussion

Effect of ATP and Ca^{2+}/CaM on R3 Subdomain of the Regulatory Domain

The R3 subdomain (residues 296-310) contains the CaM-binding motif. DEER was carried out between mutants labeled at R3 and either the kinase domain or R1 (refer to Figure 1.2). It was hypothesized that if R3 exists in a dynamic equilibrium, heterogeneous distance distributions would be present in the apo and +ATP conditions. Moreover, the distributions would look fairly similar in terms of the average distances, but the ratios among the different distance peaks would be altered by nucleotide in favor of longer components. Exemplifying the dynamic nature of CaMKII, most of these mutants have a sharp, short distance peak (e.g. 33-307; 65-307; 79-307; 85-307; 125-307) as well as one or more longer distance peaks that tend to be broader, suggesting the longer component encompasses conformations with increased disorder at the R3 tail. It was found that the shorter distances predominate in the apo condition, whereas MgATP reverses this trend. It is worth noting that for most of these mutants, the average distances remain unchanged between apo and MgATP conditions, and the effect of nucleotide seems to be mostly on the proportion of the populations. This is consistent with a change in a dynamic equilibrium from the R3 tail docked to the kinase and a flexible R3 exposed to the solvent. Measurements for pair 17-307 show a deviation from this trend, with broad, overlapping distances in both the apo and MgATP conditions. The distribution even becomes somewhat tighter, though still broad with addition of nucleotide. A plausible explanation is that because site 17 lies in the middle of the β-strand 1, involved in anchoring of the alpha and beta phosphates of ATP (Hanks and Hunter, 1995), the changes reflect both N-lobe rotation and the tightening of the β-cap, as well as the change in the R3 equilibrium. Nonetheless, it can still be gleaned that there

are shorter components in the apo condition, consistent with the postulated shift in R3 toward longer (solvent-exposed) conformations. By contrast, with respect to Ca^{2+}/CaM, the echo decays look flat and the oscillations from the components seen in the apo and MgATP conditions are majorly or completely suppressed. This can be seen in the distributions, which are mostly composed of distances longer than those of the other two conditions. For some mutants (26-307; 79-307; 85-307) the distance gets longer than >50Å. Whereas the formation of Ca^{2+}/CaM/CaMKII heterodimers previously reported cannot be excluded, CaM:CaMKII was kept at a low 3:1 excess and the samples were frozen immediately after mixing to minimize aggregation (K_D of CaMKII-CaM dimers = 50 μM, Rellos et al., 2010). The effect of Ca^{2+} was not studied since saturating Ca^{2+} was used. The results in the +CaM condition are interpreted as a sequestration of the R3 tail by Ca^{2+}/CaM away from the catalytic lobes of the kinase. Notably, the CW EPR spectrum does not always show changes amongst the conditions in spite of differences in DEER. This lends credence to the proposed shift in the R3 equilibrium by ATP being due to conformational changes of the protein as opposed to changes in spin label rotamers.

DEER pairs were then made between the N-lobe and N-terminal and C-terminal ends of R3, represented by sites 300 and 315. The rationale for these experiments was to test whether the dynamic equilibrium extended throughout the ends of the R3 subdomain. Distance measurements for pairs 45-300 and 65-300 do not show changes between the apo and ATP conditions. The N-terminal end of R3 may therefore be stably held in contact with the kinase lobe in the ATP-bound state. For measurements to site 315, the distributions appear broader, reflecting increasing disorder at the top of the R3 tail. However, there were also no major changes between the apo and ATP conditions. It is possible that the C-terminal end of R3, which is

adjacent to a linker of variable length between isoforms, is disordered and exposed to the solvent to the extent that it does not participate in the R3 equilibrium. This is consistent with CW EPR spectra of mutants labeled at site 315, which show a highly mobile component reflective of a flexible region. Ca^{2+}/CaM seems to have the same effect at sites 300 and 315 as it does at site 307 in the middle of the CaM-binding segment, which implies CaM binding sequesters the whole R3 region away from the kinase lobes.

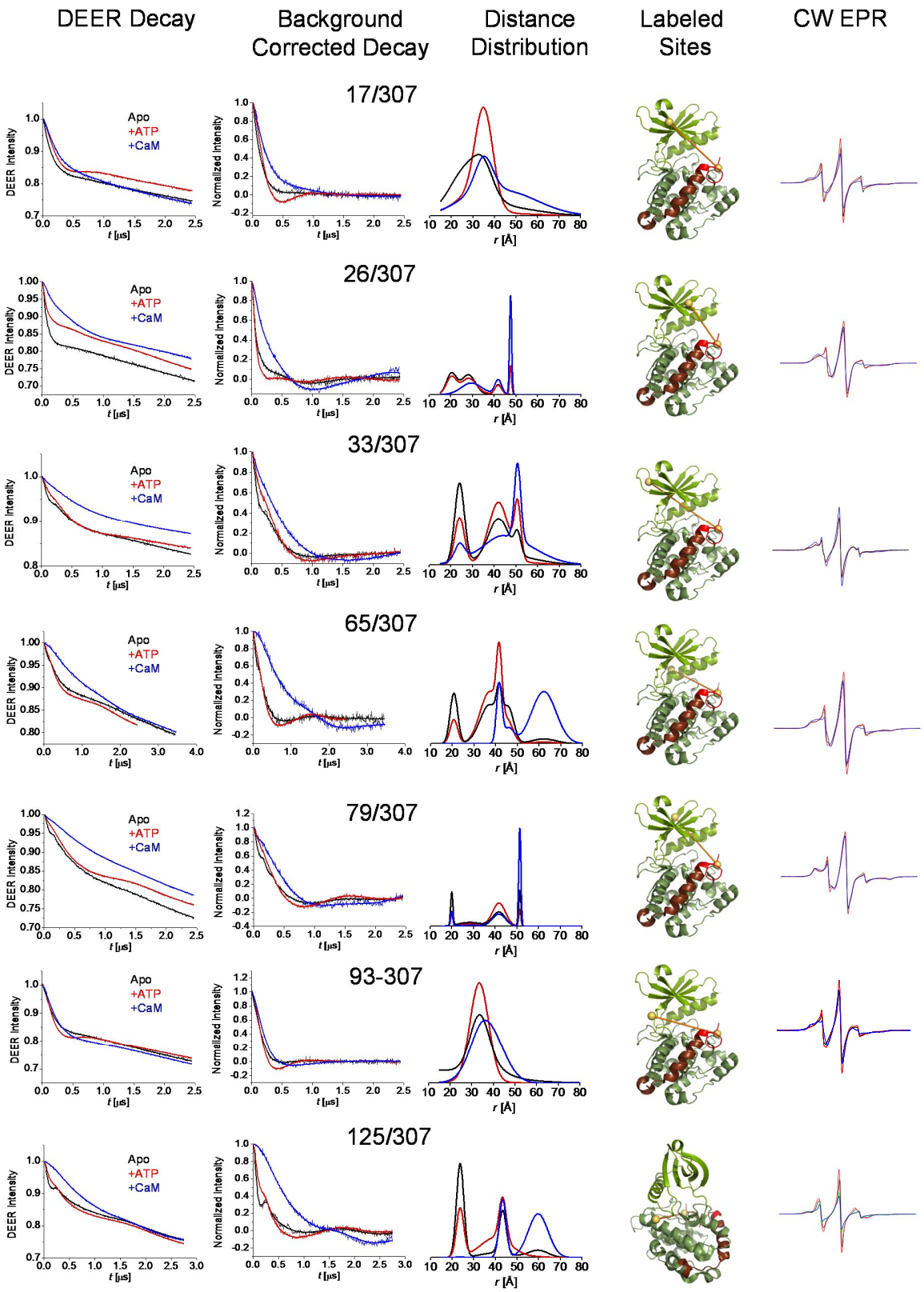

Figure 2.6: The R3 region containing the CaM binding element (site 307) shows heterogeneous distributions with

short (<30Å) and long distance populations in the apo state; these populations are present in the ATP condition but in different proportions. The CaM condition gives the longest components, with decays showing high heterogeneity.

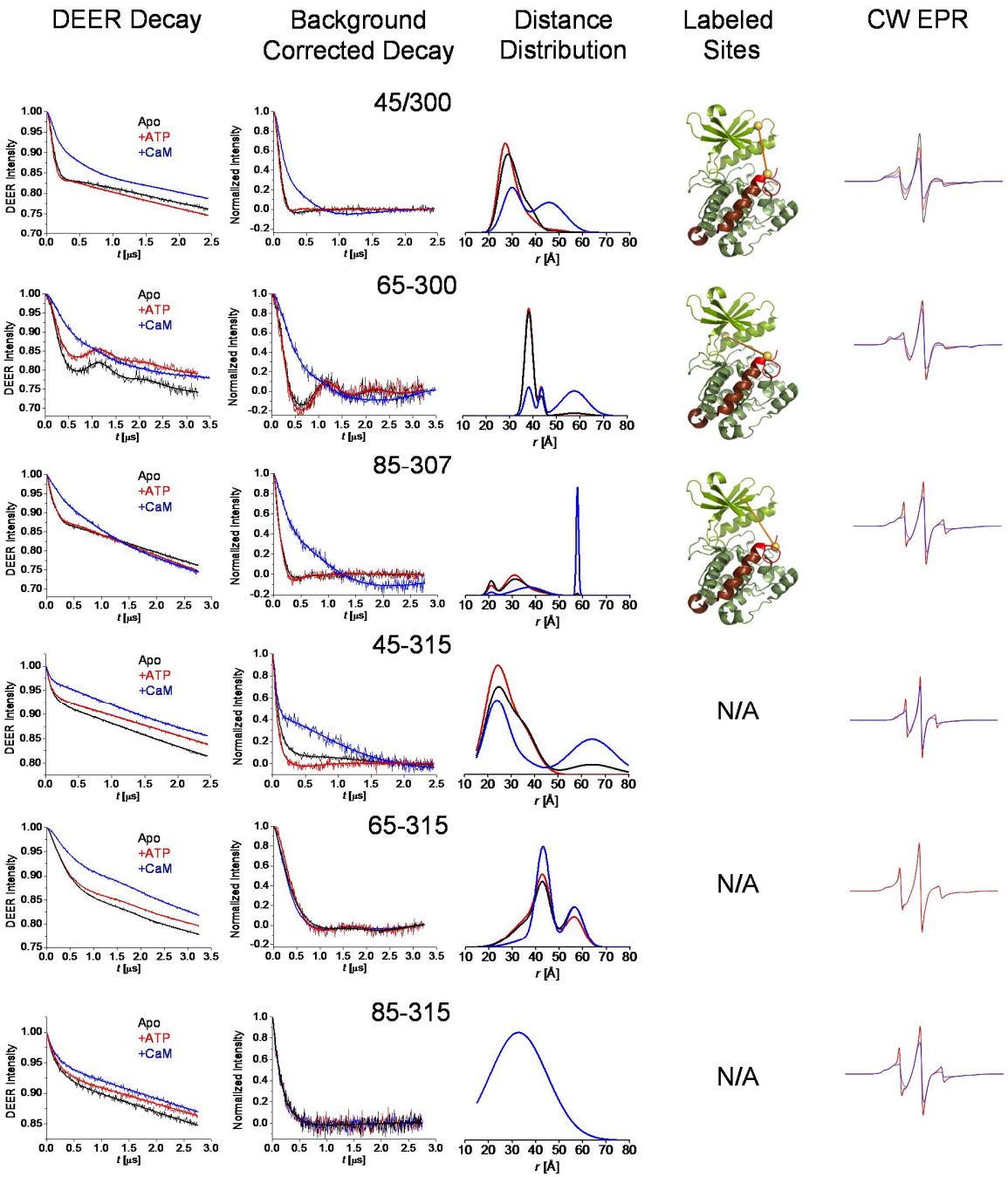

Figure 2.7: Distances measurements to the N- and C- terminus of the R3 region. Measurements to site 300 at the N-terminus of R3 (45-300: 65-300) show distributions largely unchanged between the apo and ATP states. The CW spectra also show a mobile component that is nonetheless more restricted than that of site 307 in the middle of R3 (compare 65-300, 65-307). The C-terminus of R3 (65-315, 85-315) also does not appear to be modulated by ATP, although inspection of the broad distances in the distribution and the CW EPR spectra indicates this is likely due to the increased disorder of the C-terminus compared to both the middle (307) and N-terminus (300) of the R3 region.

ATP causes R3 to Become Closer to a Region of the Catalytic C-lobe

The CaM binding motif within R3 contains residues T305/T306, which can be autophosphorylated to prevent binding of CaM and keep the subunit in an autoinhibited state. Pairs were made between R3 and two C-lobe regions associated with tethering the R3 segment: the peptide positioning loop (site 170), and helix-G (site 227). It was hypothesized that the change in the R3 equilibrium would bring R3 closer to these regions in the ATP state, so that the tail can be presented for autophosphorylation. Accordingly, unlike most other pairs to site 307 shown previously, MgATP favors shorter components in the distributions for mutants 170-307 and 227-307. Meanwhile, Ca^{2+}/CaM shows the same effect as other distance pairs to site 307, increasing the separation between R3 and the catalytic domain.

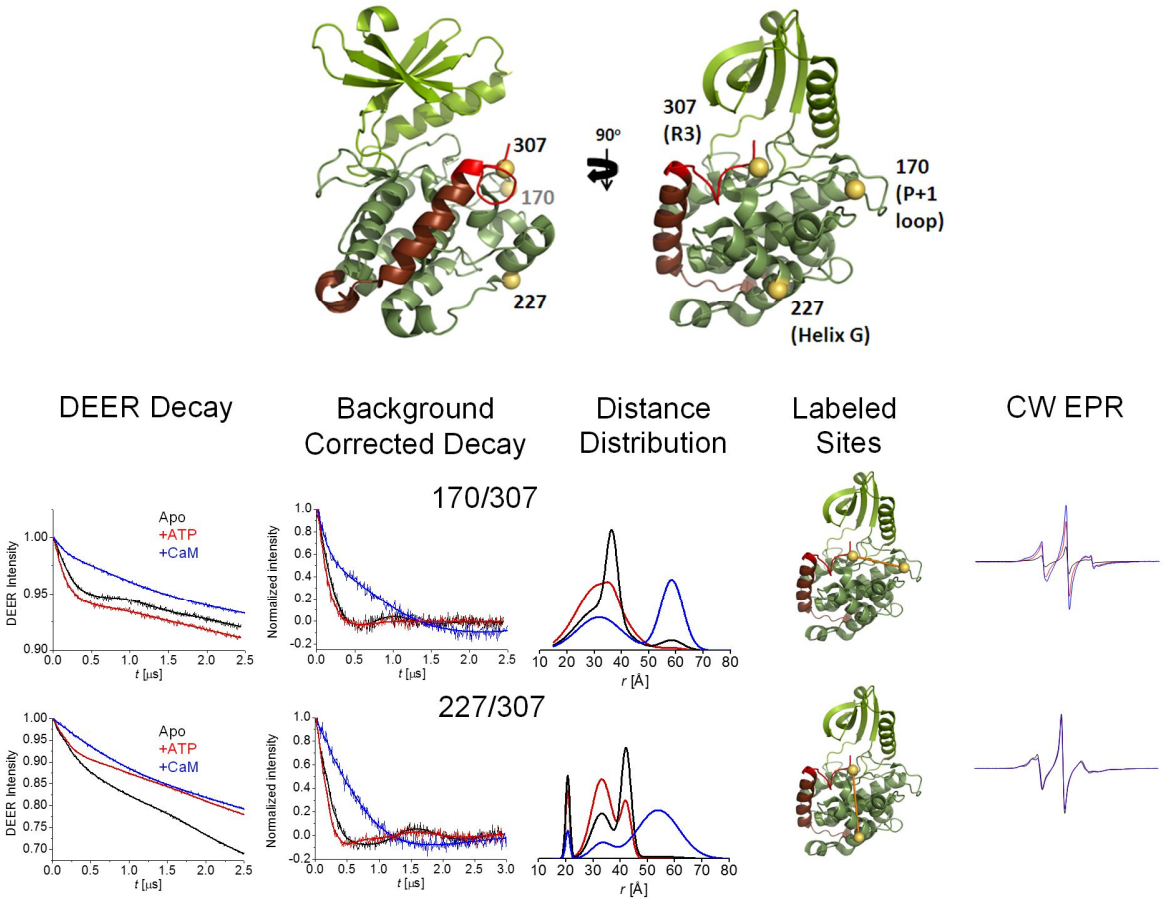

Figure 2.8: The change in the R3 equilibrium may allow R3 to bind the C-lobe. Addition of ATP shortens the distance between the R3 segment and two regions in the C-lobe: the P+1 loop (170), involved in positioning of substrate peptide, and helix-G (227).

Effect of ATP on Catalytic Domain

It was hypothesized that the change in the R3 equilibrium brought about by MgATP could be coupled to conformational changes in the catalytic lobes of the kinase. Comparison of crystal structures of active and inactive eukaryotic protein kinases, notably PKA (Akamine et al., 2003; Zheng et al., 1993; Johnson et al., 2001), has identified a rotation of the N-lobe toward the C-lobe as a hallmark of the transition to the active state. In keeping with this observation, DEER pairs were measured at different sites within the catalytic lobes and between the lobes and the regulatory domain. Small (~5Å) changes were found for pairs between the β-sheet cap of the N-

lobe and helix E of the C-lobe (12-125; 33-125) which suggest that the kinase domain adopts a compact conformation upon MgATP binding. Larger changes were found when probing the outer end of the N-lobe cap (site 17, pair 17-288), consistent with movement of the lobe. By contrast, measurements to site 51 in helix-C of the N-lobe report a broad distance with an average change (<5Å) with nucleotide. Helix-C bears nucleotide anchoring residues and is rotated in the active conformation of other protein kinases. The absence of changes in mobility or distance when probing this structure suggests that it may already be in the proper orientation to coordinate MgATP. Additionally, the broad distance distributions suggest that the N-terminus of helix-C may be dynamic, as has been inferred previously by alignment of monomeric crystal structures (Rellos et al., 2010).

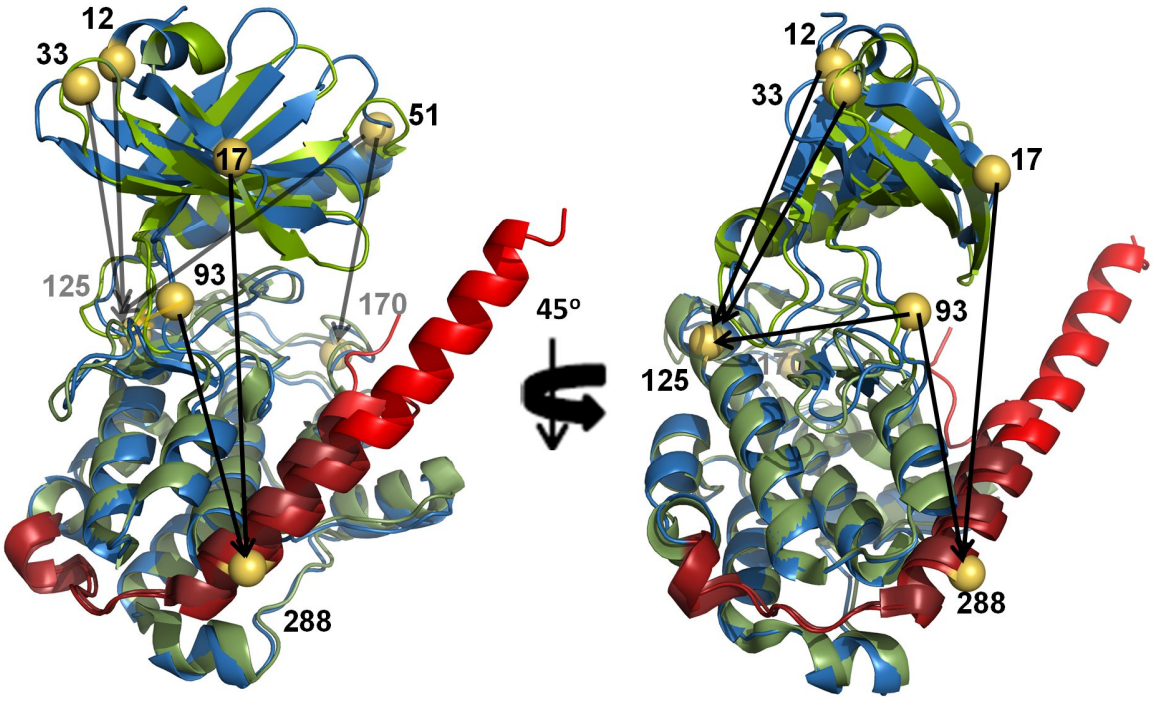

Figure 2.9: Labeling pairs chosen to study movement of the kinase N-lobe due to ATP. Superimposition of crystal structures of truncated apo *C. elegans* CaMKII (PDB 2BDW chain A, blue) and truncated CaMKII bound to inhibitor (PDB 2VN9 chain A, green) showing the rotation of the N-lobe.the R1 and R3 regions are depicted (dark and bright red). To test the hypothesis that ATP binding rearranges the catalytic N-lobe to adopt a closed kinase conformation,

distances were measured between the N-lobe and C-lobe (12-125; 33-125, 51-170; 93-125) and between the N-lobe and R1 (17-288; 93-288). DEER data is reproduced below.

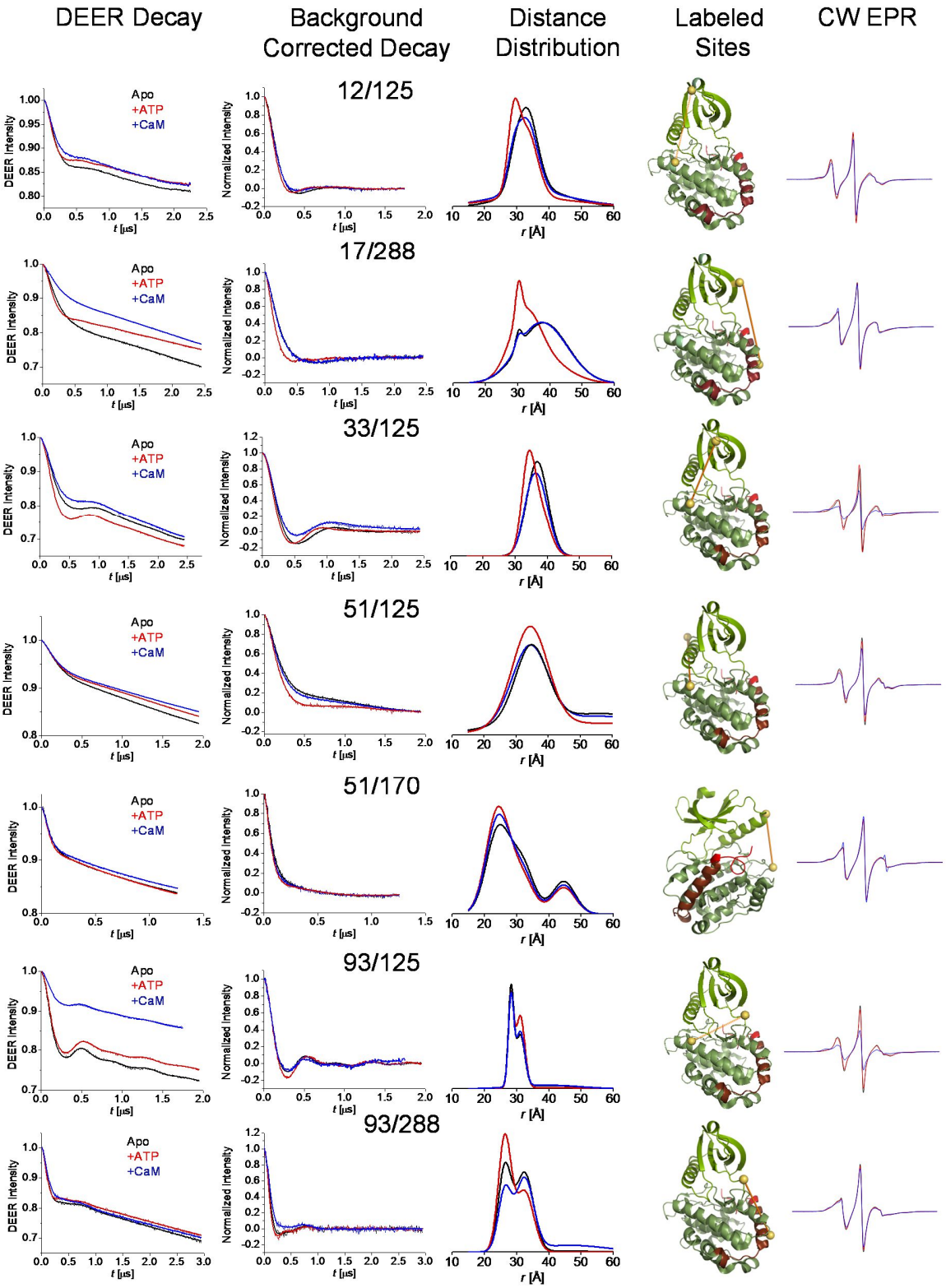

Measurements between the C-lobe and R1 show small or no changes in the distance distribution between apo and +MgATP. This is consistent with what is known about eukaryotic protein kinases where the C-lobe remains largely static in the interdomain rotation induced by nucleotide (143-227; 143-288). However, more pairs may be needed between the lobes and within the C-lobe to address this conclusively.

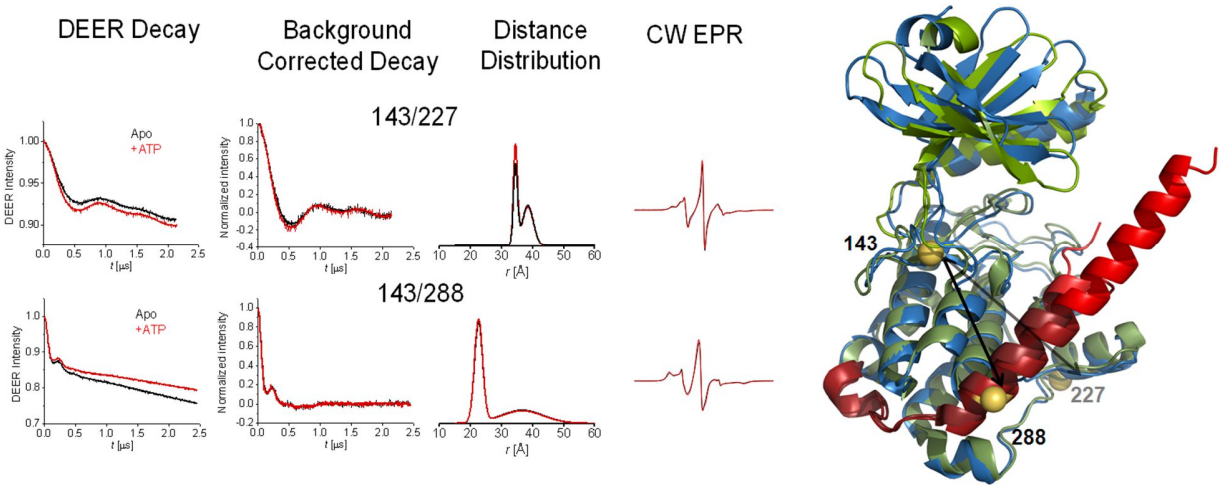

Figure 2.10: Effect of ATP on the C-lobe. Measurements within the C-lobe (143-227) or between the C-lobe and R1 (143-288) do not show a change in the distance between apo and ATP conditions.

CaM Disrupts Interaction Between Autoinhibitory Helix and Substrate Binding Pocket

The conformational changes at R3 due to CaM-binding are thought to propagate down to the R1 helix, causing it to dissociate from the catalytic domain to make the substrate binding sites accessible. Distances were measured between the catalytic domain and the R1 autoinhibitory helix to assess the effect of CaM binding. No changes in the distribution were observed for site 285 at the bottom of the helix, but the mobility of the label is affected by CaM (CW spectra). Distance distributions for pairs to site 288 become broader and longer in the +CaM condition (Figure 2.11). For instance, the raw DEER decays for mutants 111-288 and 143-288 show less

defined oscillations upon CaM binding indicating a loss of structure of R1. However, compared to R3, the effect of CaM on R1 is more attenuated.

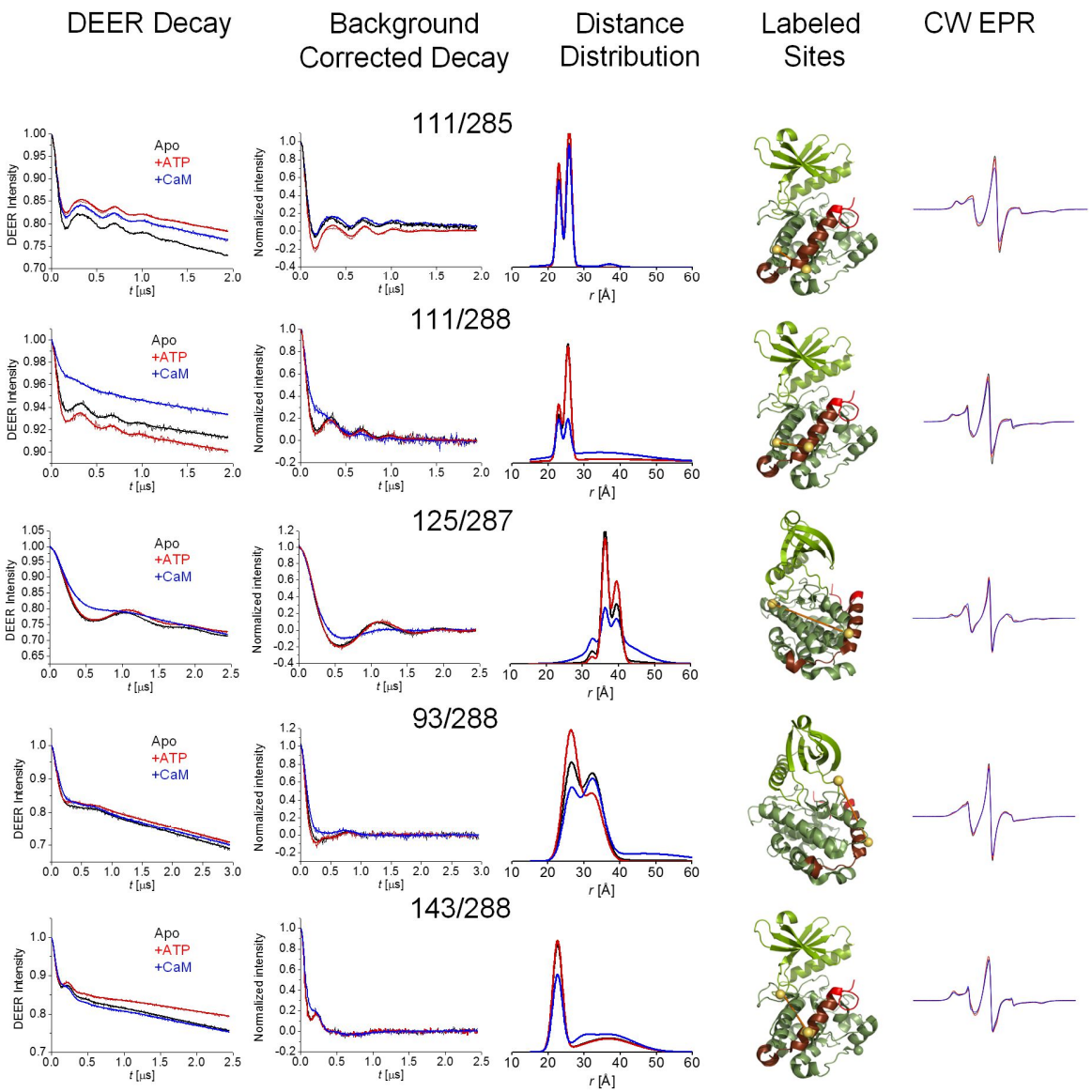

Figure 2.11: CaM causes re-structuring of autoinhibitory helix. Distance measurements between the R1 region, which comprises the auto-inhibitory helix that blocks the substrate-binding site of the kinase, and residues from the catalytic domain are shown. Site 288 is at the base of the regulatory helix and exposed to the surface. Whereas no change is observed from apo after addition of ATP (except for pair 93-288, see text), CaM shifts the distance distributions to longer distances, in agreement with a dislodgement of the auto-inhibitory helix. The effect is not as pronounced when site 285 is probed , which lies at the bottom of the R1 region, suggesting the N-terminal end of the auto-inhibitory helix functions as a pivot for the dislodgement.

While Ca^{2+}/CaM-induced displacement of the R1 helix is the canonical mechanism that confers CaMKII activity, the precise structural changes underlying the relief of autoinhibition remain largely undefined. It has been proposed that CaM distally affects the secondary structure of R1 to suppress inhibition, in accordance with a crystal structure of CaMKII bound to Ca^{2+}/CaM (Rellos et al., 2010). Scanning spin label mobility of the regulatory domain provided evidence in solution of a disordering of the R1 region in the Ca^{2+}/CaM-bound state, which was interpreted as an unfolding of the helix into a long loop exposed to the solvent (Hoffman et al., 2011). By comparison, non-canonical mechanisms that maintain CaMKII activity, such as the oxidation of the Met280/Met281 pair in the mouse isoform beta (Erickson et al., 2008), O-GlcNAc modification at Ser280 (Erickson et al., 2013), or S-nitrosylation at Cys290, also require prior activation by Ca^{2+}/CaM, presumably because disruption of the interaction between R1 and the kinase is necessary to expose these residues for modification. The results of the present study show no change in distance with Ca^{2+}/CaM at the N-terminus of the R1. By contrast, longer distances are obtained in the +CaM state farther up the helix (Figure 2.11).

Further confirmation that Ca^{2+}/CaM affects both R1 and R3 comes from mutant labeled at both subdomains of the regulatory domain (287-307). Unlike distances between the catalytic lobes and R3, the +CaM distances are intermediate to those in apo and +ATP conditions, which can be explained by Ca^{2+}/CaM disengaging both subdomains, whereas ATP is mainly affecting R3 relative to both R1 and the kinase (Figure 2.12).

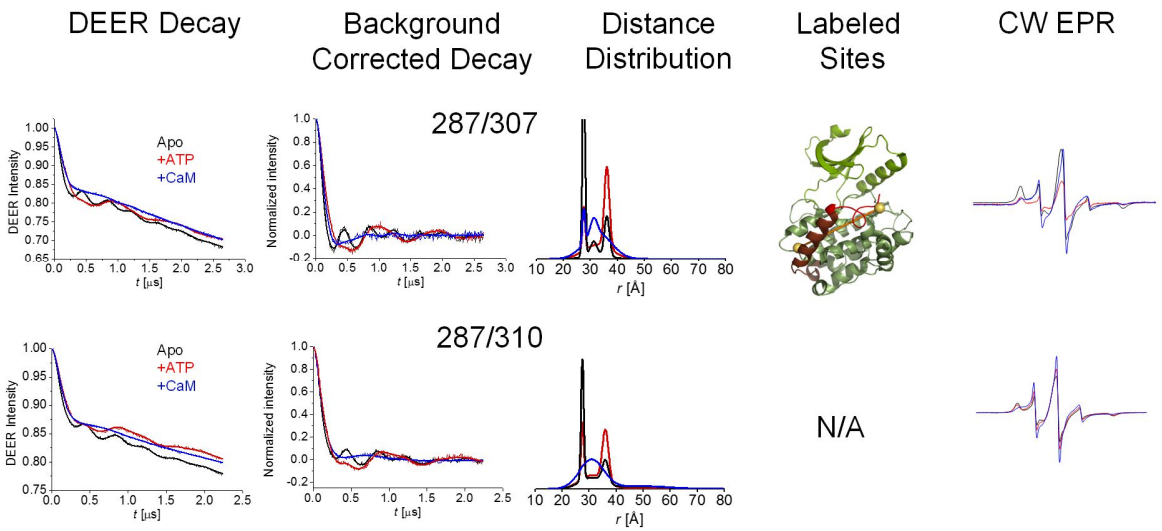

Figure 2.12: Effect of ATP and CaM on DEER mutants labeled at both R1(287) and R3(307 or 310). The conformational heterogeneity of the regulatory domain can be seen from the multiple peaks in the distance distribution. ATP changes the distributions in favor of the conformations that give rise to the components of longer distances. CaM gives broader distributions with distances intermediate between those in the apo and ATP conditions, which is interpreted as being indicative of a dual restructuring of the R1 and R3 regions, by disengaging contacts between R1 and the kinase C-lobe, and by sequestering R3 away from the kinase.

Taken together, this suggests that the base of R1 serves as a pivot for the movement of the regulatory domain away from the kinase upon CaM binding. However, samples were frozen immediately after mixing to minimize the formation of CaMKII/Ca^{2+}/CaM dimers, so we cannot exclude the possibility that Ca^{2+}/CaM may cause a farther expansion of R1 with longer incubation times. The requirement for CaM dislodging of the R1 autoinhibitory helix from the C-lobe falls in line with a sequential mechanism of activation where the substrate pocket is exposed to the solvent for the subsequent binding of peptides.

Concerted Effect of Ca^{2+}/CaM and Substrate Peptide on C-lobe Conformation

Displacement of the R1 segment enables substrate binding by relieving the blockage of the peptide binding pockets in the C-lobe. Measurements within the hydrophobic core of the C-lobe in the presence of substrate peptides show distance changes when both Ca^{2+}/CaM and peptide are added to the protein (Figure 2.13). These changes are reported when probing the P+1 loop, involved in substrate positioning (site 170), and β-sheet 6 of the activation segment (143), which is C-terminal to the catalytic loop involved in phosphotransfer. Similar results were obtained with peptide derived from the inhibitor protein CaMKIIN (not shown). Additionally, measurements between the P+1 loop (170) and Helix-G (227), associated with substrate-binding (Kornev et al., 2008), show a minor, longer component that becomes more populated with Ca^{2+}/CaM and peptide. Addition of peptide alone or Ca^{2+}/CaM alone showed no change in the distributions for pairs 143-170 and 170-227 (not shown). It was also found that Ca^{2+}/CaM affected the distributions for pair 111-170 highlighting a role of Ca^{2+}/CaM in positioning the C-lobe for peptide binding. Site 111 resides on Helix-E, a conserved structure in the hydrophobic core of protein kinases (Hanks and Hunter, 1995) associated with a hydrogen-bonding network across different subfamilies (Kornev et al., 2008). Meanwhile, distribution changes for mutant 143-227 appear to be subtler.

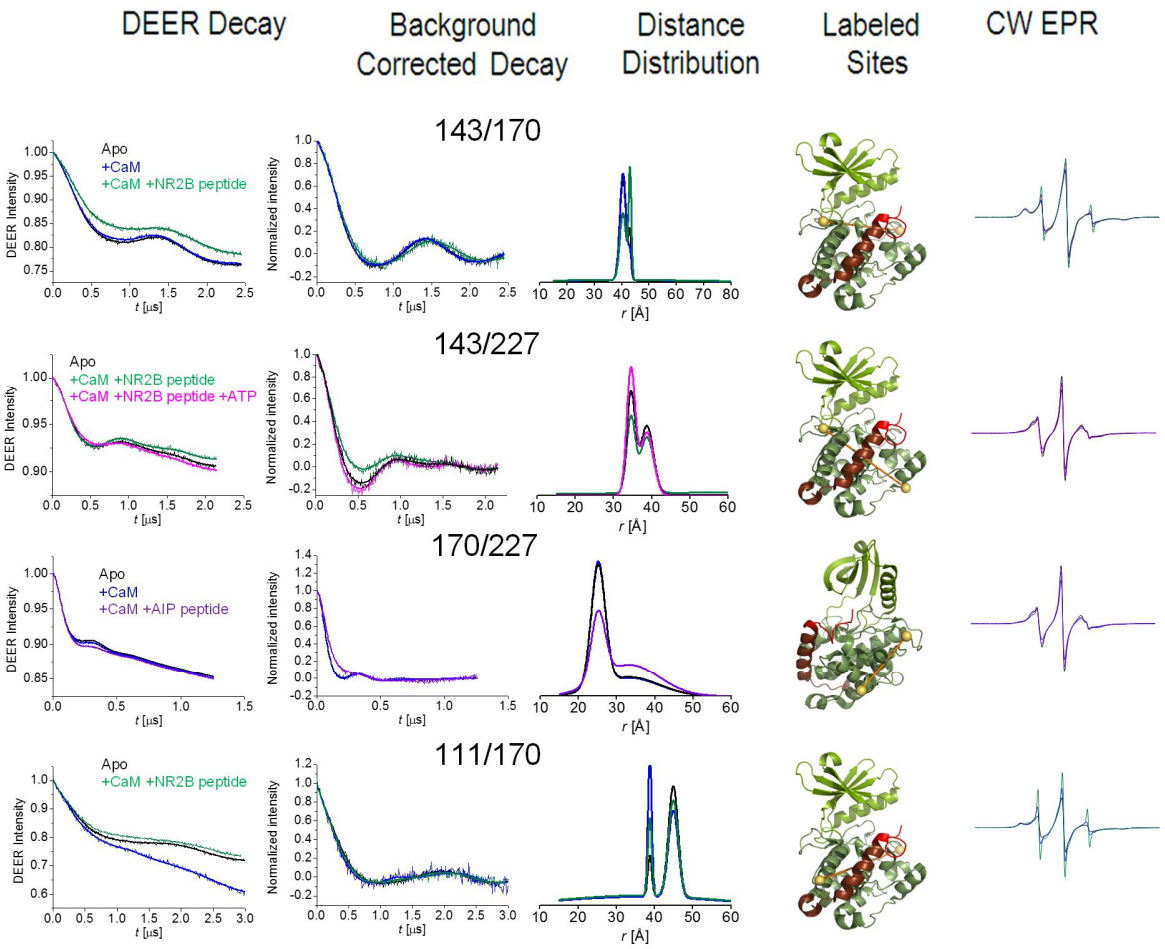

Figure 2.13: Rearrangement of the C-lobe due to the concerted effect of Ca^{2+}/CaM and peptide. CaM dislodgement of R1 can also be inferred from changes in distance to site 170 in the peptide positioning loop that are observed when both CaM and peptide substrate are present. Measurements between sites 143 and 227 report no distance changes between the apo and +CaM/+peptide conditions, discarding a global effect of the mixed CaM/peptide sample on C-lobe conformation.

Measurements were also made between the C-lobe and R1 (Figure 2.14). A broadening of the distance distribution for pairs 111-285, 125-287, and 143-288 is suggestive of competition between the R1 helix and peptide for the pocket where R1 is lodged to the C-lobe (previously termed the T-site). This appears as broadening of the distribution for the mutants 111-285 and 125-287, and as an enhancement of an intermediate component in the case of 143-288. From CW EPR spectra of these mutants, it appears that Ca^{2+}/CaM increases rigidity, whereas the

peptide restores or even makes these regions more flexible, possibly reflecting dynamics of peptide anchoring.

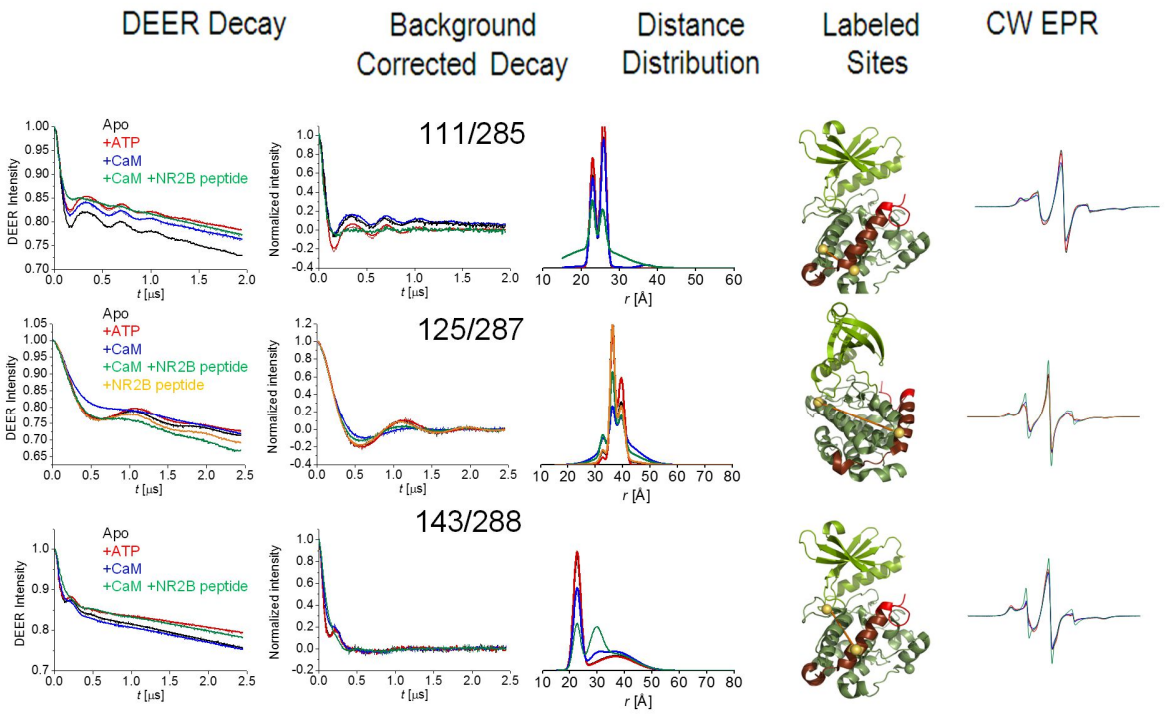

Figure 2.14: Increase in heterogeneity in the R1 region due to the concerted effect of Ca^{2+}/CaM and peptide. Measurements to the R1 helix, represented by sites 285, 287, and 288, show the appearance of more populations with the addition when both CaM and peptide are present compared to the other conditions. Addition of peptide alone does not change the distribution compared to apo (pair 125-287).

Conclusion from DEER Data

Comparison of distances between apo and +ATP conditions for pairs to the R3 subdomain show that most peaks appear at the same distance in the presence of nucleotide, however, the longer distances make up the predominant component (Figure 2.6, black and red traces). This finding is interpreted as further evidence that the change in label mobility due to ATP for site 307 in the R3 region (Hoffman et al, 2011) is due not merely to a change in conformation of the spin label, but an actual shift in the position of the equilibrium in favor of the longer (flexible) population.

In agreement with the role of CaM in binding to R3 to activate CaMKII, R3 moves farther from sites labeled on the catalytic domain in the +CaM state (Figures 2.6 and 2.7, blue trace), which can be explained as a sequestering of the R3 tail by CaM. Similar changes were not observed for distance measurements between the kinase lobes in the same conditions (Figure 2.9), suggesting the changes were due solely to the interaction of CaM with the R3 subdomain.

Within the context of the holoenzyme, it has been postulated that the R3 segment may modulate the cooperative activation of adjacent subunits (Chao et al., 2010) and it is speculated that the R3 equilibrium may contribute to a parallel regulatory switch that controls intrasubunit activity. The crystal structure of the full-length human CaMKII holoenzyme has R3 bound to the association domain instead of the catalytic domain. It is conceivable that the dynamic nature of R3, as well as the subunit exchange in the holoenzyme (Stratton et al., 2013) allow the regulatory domain to adopt these conformational extremes at different time points throughout the lifetime of the oligomer. The sequestration of R3 away from the kinase by CaM falls in line with the increased affinity for ATP following Ca^{2+}/CaM activation of the CaMKII holoenzyme.

Chapter III: Study of CaMKII by Nuclear Magnetic Resonance

Introduction

NMR is well suited for studying conformational dynamics in proteins because it allows for the detection of lowly populated states, changes in the position of equilibria due to binding events, and collective protein motion. Assignment experiments can identify different resonances arising from the same residue in different chemical environments, reflecting discrete conformational states. With such knowledge, it is in principle possible to obtain residue-specific information about backbone motion, unfolding, and even the exchange rate of a conformational interconversion. Isotopic labeling is in many cases sufficient to gain insight into these parameters, posing an advantage over methods that require the attachment of artificial probes. In practice, solubility concerns, protein size, sensitivity issues, and broadening from the exchange process itself can complicate the analysis. This can be of particular concern in the case of oligomers and macromolecular complexes, for which it is usually necessary to truncate the protein into fragments containing the region of interest. Keeping in mind the breadth of knowledge that can be acquired from NMR studies of proteins in solution, it was decided to to exploit this technique to study the Ser/Thr protein kinase CaMKII in a monomeric form. The native enzyme is dodecameric with a bi-annular arrangement of two hexameric rings stacked together. CaMKII overexpression has been linked to arrhythmias and the development of CaMKII-specific inhibitors remains an avenue of exploration. For these reasons, an understanding of the dynamics involved in the activation of the kinase is of therapeutic significance. CW EPR and DEER data of the regulatory domain of CaMKII, specifically of the R3 subdomain containing the calmodulin-binding motif, have uncovered dynamic features pointing to an ATP-modulated

"Supported in part by grants for NMR instrumentation from the NSF (0922862), NIH (S10 RR025677) and Vanderbilt University matching funds".

equilibrium of the R3 tail. This equilibrium is thought to encompass conformations where R3 is docked to the kinase as well as solvent-exposed, undocked R3 conformations. EPR studies, however, require prior removal of native cysteines and the introduction of spin labels, which may alter the rate of the equilibrium. Here, NMR methods are employed to study the effect of ATP on assigned R3 residues and derive backbone N-H motion parameters from T1 and T2 relaxation experiments and heteronuclear NOE. A truncated, monomeric CaMKII construct containing the entire R3 region (CaMKII 1-318) bearing a D135N inactivating mutation was used. To date, the author is not aware of an NMR-based study of recombinant CaMKII containing the catalytic and regulatory domains in the literature.

Rationale and Overview (Choice of Technique)

From EPR data of the regulatory domain shown by mobility studies (Hoffman et al., 2011) and in the previous chapter, it was thought that the R3 region becomes more flexible with ATP binding. The R3 subdomain within the regulatory domain of CaMKII is thought to participate in autoinhibition by partially blocking the kinase active site. The displacement of the R3 region, reflective of a shift in a dynamic equilibrium, would also result in a change in the chemical environment surrounding the residues undergoing conformational changes. For this reason, a technique that was able to give insight on the flexibility of specific, native residues in a protein was preferable. NMR T1 and T2 measurements of R3 residues in the apo and ATP conditions would consolidate EPR data suggesting that R3 is majorly undocked from the kinase domain in the presence of nucleotide. The objective of this study was to identify the docking residues of the R3 region by NMR and the effect ATP has on the region.

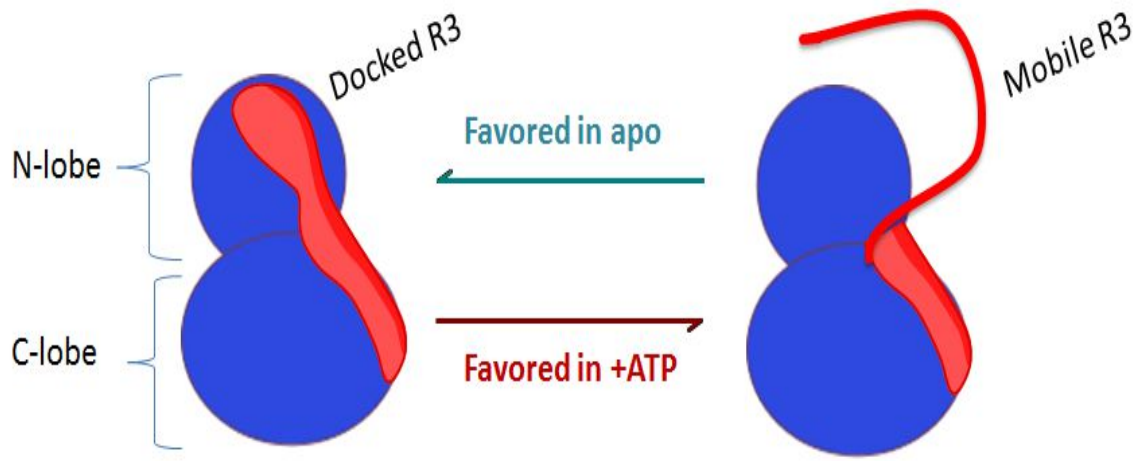

Figure 3.1: illustration of the R3 equilibrium.

Study Design: Assignment of NMR Resonances of Monomeric CaMKII for the Quantification of Dynamic Parameters of R3 Residues. The concept of the investigation was to employ NMR to detect residues of the R3 subdomain undergoing local environment changes upon nucleotide binding due to conformational transitions. The size of the monomeric constructs used (42-38KDa) prevented the use of standard acquisition techniques due to signal loss. TROSY NMR (Pervushin et al., 1997) would be used to acquire the backbone amide (2D ^{1}H-^{15}N) spectrum of CaMKII 1-318 (Figure 11), which would serve as a skeleton for tracking conformational changes on a per-residue. Specifically, 3D NMR experiments based on magnetization transfer between NMR-active nuclei (^{1}H, ^{13}C, ^{15}N) were used to "walk" along the protein backbone and map the order of residues observed back to the 2D ^{1}H-^{15}N TROSY spectrum. The strategy, summarized in Figure 3.3, involved the use of complementary experiments for identifying specific atoms (e.g. Cα vs Cβ vs CO), thus allowing the order of the backbone resonances to be established.

Following identification of the R3 resonances from the assignment experiments, the idea was to use the appearance of the R3 resonances in the NMR spectrum as an indication of the exchange timescale between the two populations. A hypothetical example is provided (Figure 3.2).

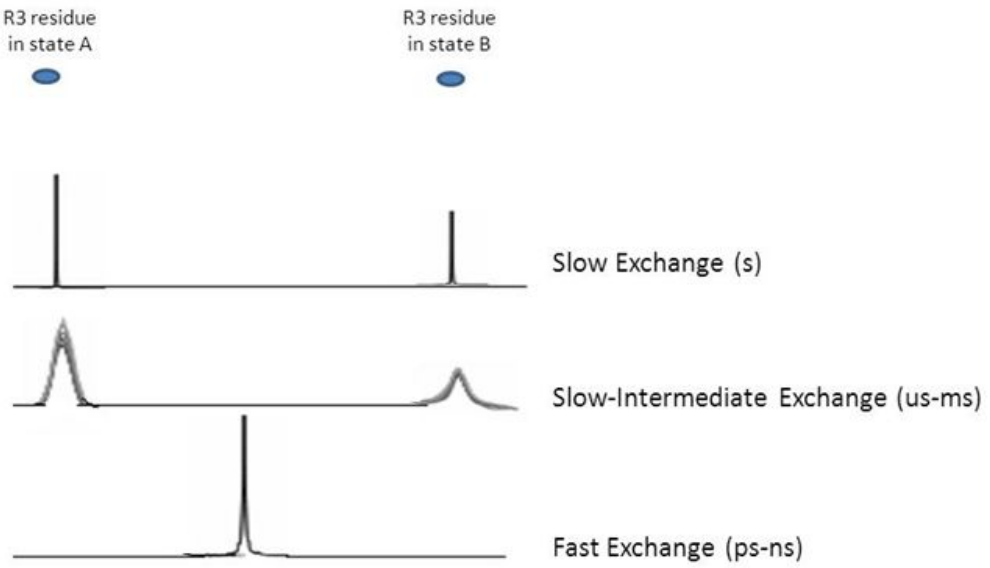

Figure 3.2: Exchange Timescale Affects Spectrum Appearance. After the R3 resonances have been assigned to specific residues, cues can be gathered about the exchange rate. If two or more resonances are assigned to the same R3 residue, this would indicate the equilibrium is undergoing slow exchange (>μs timescale). On the other hand, fast exchange (<ps timescale) would lead to averaging of the signals, such that only one resonance would be observed for an R3 residue.

Because the order of the exchange process would not be known beforehand, and inspection of the spectrum would not give a conclusive estimation of the timescale, experiments that measure dynamics on different timeframes would be employed. If R3 motion was thought to be in the fast exchange limit (ps-ns scale), dynamics would be indirectly probed by measuring relaxation parameters T1 and T2, as well as the heteronuclear Overhauser Effect (hnNOE) across the amide N-H bond. T1 and T2 describe the longitudinal (recovery of net magnetization) and transverse (loss of x,y coherence) components of nuclear spin relaxation, while the hnNOE is a through space

coupling between different nuclei (^{1}H-^{15}N) that is affected by the orientation of the bond vector and the distance between the spins. Because backbone dynamics affect these three parameters, they serve as indicators of local mobility (Jarymowycz and Stone, 2006). However, if R3 were in a slow timescale ZZ-Exchange (ms-s) or CPMG relaxation dispersion experiments (μs-ms) would be used to extract the rate of exchange between two populations in the by applying a series of spin-echo pulses of different duration that affect R_{ex}, the contribution to spin relaxation from the exchange between the two populations (reviewed in Kleckner and Foster, 2010).

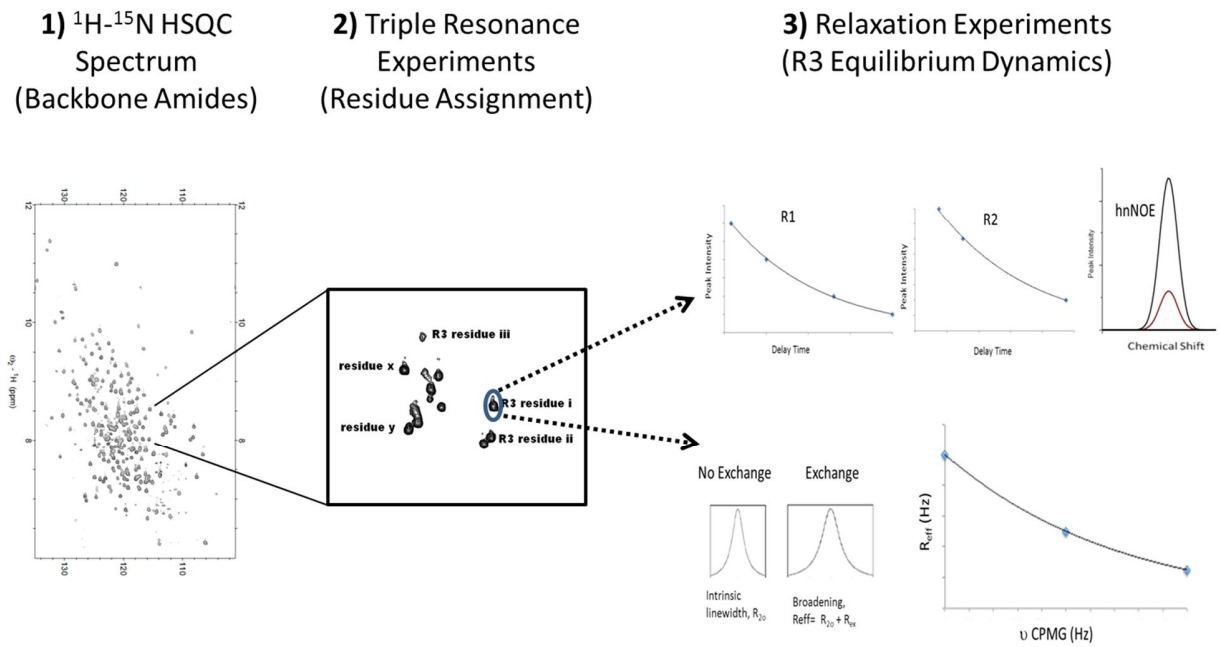

Figure 3.3: NMR Strategy for Characterizing R3 Equilibrium Dynamics. Measurement of the timescale of the R3 dynamic equilibrium will be accomplished by 1) obtaining a fingerprint ^{1}H-^{15}N TROSY spectrum of the backbone amides; 2) linking the TROSY signals to specific residues through triple resonance experiments, from which the R3 residues can be selected; and 3) measuring backbone amide relaxation parameters (fast exchange, top right) or CPMG or ZZ-exchange experiments that extract the contribution of the dynamic equilibrium to R3 peak broadening (slow exchange, bottom right). Partially adapted from Biochim Biophys Acta. 1814(8):942-68.

Transverse Relaxation Enhanced Spectroscopy (TROSY)

Larger proteins in solution tumble more slowly, causing nuclear relaxation which results in signal broadening. Additionally, the increased number of signals makes it difficult to resolve different resonances due to overlap. Improvements in resolution and sensitivity can be achieved by increasing field strength and protein concentration, but due to instrumental limitations and sample solubility issues the gains achieved by these means alone are generally insufficient for obtaining informative spectra for proteins >40kDa. Two mechanisms govern transverse relaxation for larger proteins at high field strengths: dipole-dipole (DD) relaxation, which describes the interaction between spins close in space, and chemical shift anisotropy (CSA), which refers to the non-spherical electronic environment around the nucleus. In a conventional backbone amide spectrum, called HSQC, each H-N gives rise to four components due to the two relaxation mechanisms being able to interact destructively or constructively. The peak observed in the HSQC spectrum is broadened because it is the decoupled average of the four correlations. The TROSY pulse sequence selects for the slowest relaxing component, at which the DD and CSA mechanisms are almost equal (Pervushin et al., 1997). This results in a sharp signal in the spectrum, thereby enhancing sensitivity and resolution at the expense of the total signal. Typically, deuteration is also employed to obtain high quality spectra for larger proteins. Deuteration reduces signal losses due to lower DD-induced relaxation between deuterons and neighboring nuclei. With total deuteration, remaining protons are mostly limited to the amide H-N, which additionally reduces signal broadening by removing coupling to non-amide backbone protons.

TROSY has been extended to selectively labeled ^{1}H-^{13}C $^{13}CH_3$ groups of Ile, Leu/Val, Ala and Met on totally deuterated proteins (Korzhnev et al., 2004). Methyl-TROSY makes use of a heteronuclear multiple quantum coherence (HMQC) acquisition, in which transverse ^{1}H magnetization is allowed to evolve creating a subset of spins with anti-phase magnetization. A $\pi/2$ pulse applied to the anti-phase magnetization induces slowly relaxing zero- and double-quantum coherences in ^{13}C, so termed because spin flips for ^{1}H and ^{13}C nuclei occur as a coupled entity. Finally, after evolution of the zero- and double-quantum coherences, the magnetization is converted to ^{13}C single-quantum coherence by a π pulse and transferred back to ^{1}H by a $\pi/2$ pulse for detection (Kay, 2011). Deuteration achieves the dual role of isolating the $^{13}CH_3$ group and, as mentioned previously for H-N spectra, of reducing ^{1}H-^{1}H relaxation to increase sensitivity. Methyl-TROSY of labeled Met was employed to study the effect of ATP on the R3 region of CaMKII as will be discussed further.

Nuclear Spin Relaxation Measurements

In order to obtain an NMR signal, a radiofrequency excitation is applied to perturb the Boltzmann distribution of nuclear spin states at thermal equilibrium. Neighboring nuclei and electron currents generate magnetic fields that cause spins to relax, restoring the Boltzmann distribution. Additionally, spins lose coherence due to Larmor frequency oscillating fields. The CSA and DD mechanisms are responsible for these changes in the local magnetic field because they depend on the orientation of the H-N bond relative to the applied field, and in the case of DD on the separation between the nuclei as well. Relaxation processes are influenced by protein motion because the orientation of the bond vector is affected by tumbling and by backbone dynamics in

the ps-ns timescale. Thus, measurement of the T1 and T2 relaxation times serve as reporters of internal dynamics that take place within this timeframe. The T1 and T2 measurements are performed by making a series of experiments with different relaxation delays so that the magnetization is retained on the ^{15}N nucleus for different time periods in each measurement. The decay of magnetization can then be extracted from a fit of the data (Kleckner and Foster, 2012).

Results and Discussion

Sample Optimization

Initial efforts were aimed at optimizing sample conditions. First, a construct of residues 1-340 was purified off Ni-NTA affinity chromatography and size exclusion chromatography, but a contaminant of lower molecular weight corresponding to CaMKII truncated at residue 318 (in the regulatory domain) could not be removed. From previous studies of the regulatory domain of CaMKII (Hoffman et al., 2011) it was known that local mobility of the regulatory region is not altered by the presence of the contaminant, so it was decided to use the preparation for pilot experiments and means to achieve greater purity would be explored at later stages. Other constructs used for this purpose will be discussed further and are listed in Appendix I. The first experiment on the 1-340 construct consisted of acquiring a backbone amide spectrum of unformly ^{1}H-^{15}N labeled protein. TROSY, an acquisition method that increases sensitivity and resolution for larger proteins, was used due to the size of 1-340 (42kDa) nearing the upper limit of a standard H-N spectrum. The spectra in apo and ATP conditions were recorded at 40^{o}C, 250μM protein, and field strength of 600MHz. The ATP sample contained 10 molar equivalents

of MgATP (2.7mM). Both spectra displayed a wide spread in both ^{1}H and ^{15}N dimensions, suggesting the protein was folded. The conformational change caused by nucleotide addition is evident from the shift in position of various resonances throughout the spectrum. Comparison of a ^{1}H spectrum at 25°C and 40°C showed better defined peaks at the higher temperature (not shown). For this reason, the TROSY experiments were set up at 40°C; however, this resulted in both the apo and ATP samples precipitating by the end of the run.

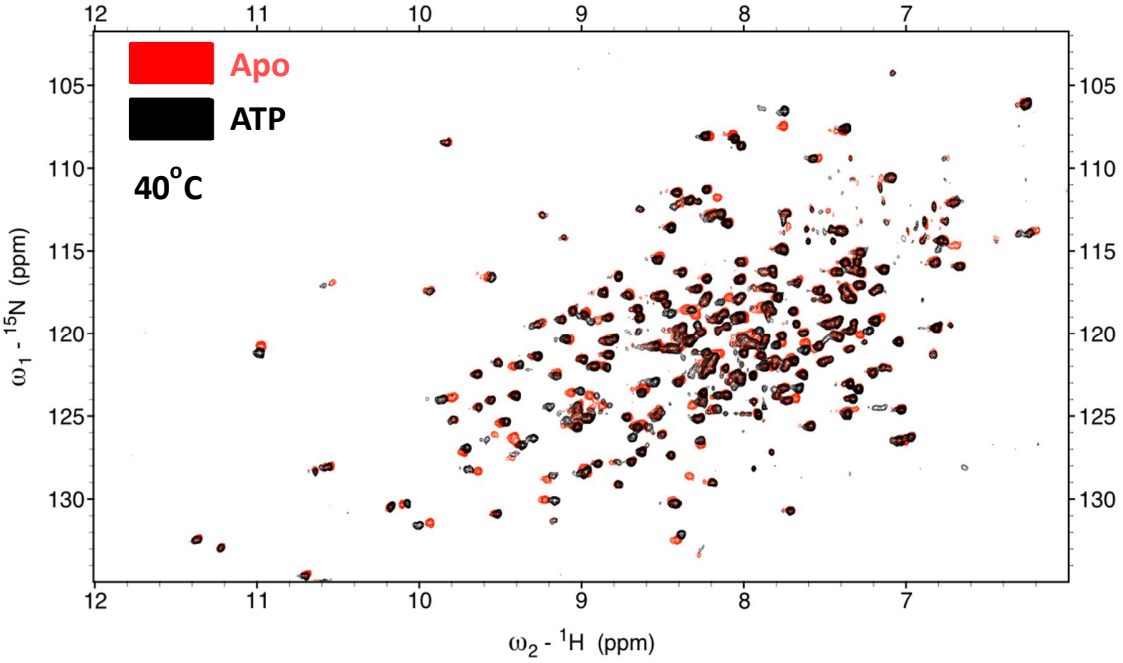

Figure 3.4: ^{1}H-^{15}N TROSY spectrum of CaMKII 1-340 in apo (red) and ATP conditions. The buffer was 50mM HEPES, 100mM NaCl, 2.5mM EDTA, 1mM DTT, 0.02% NaN3, 5% D_2O, pH 7.4. CaMKII was 250μM; MgATP was 2.7mM (10X over protein).

As part of optimization of conditions, the effect of pH on the signal of the spectrum was next investigated. It was thought that lowering the pH might help reduce bleaching of amide protons and thus increase the sharpness and number of signals. Whereas the gel filtration chromatogram at pH 6.4 did not suggest the protein was aggregating (Figure 3.5, panel A), the spectrum did not align well with that of the pH 7.4 sample (Figure 3.5, panel B).

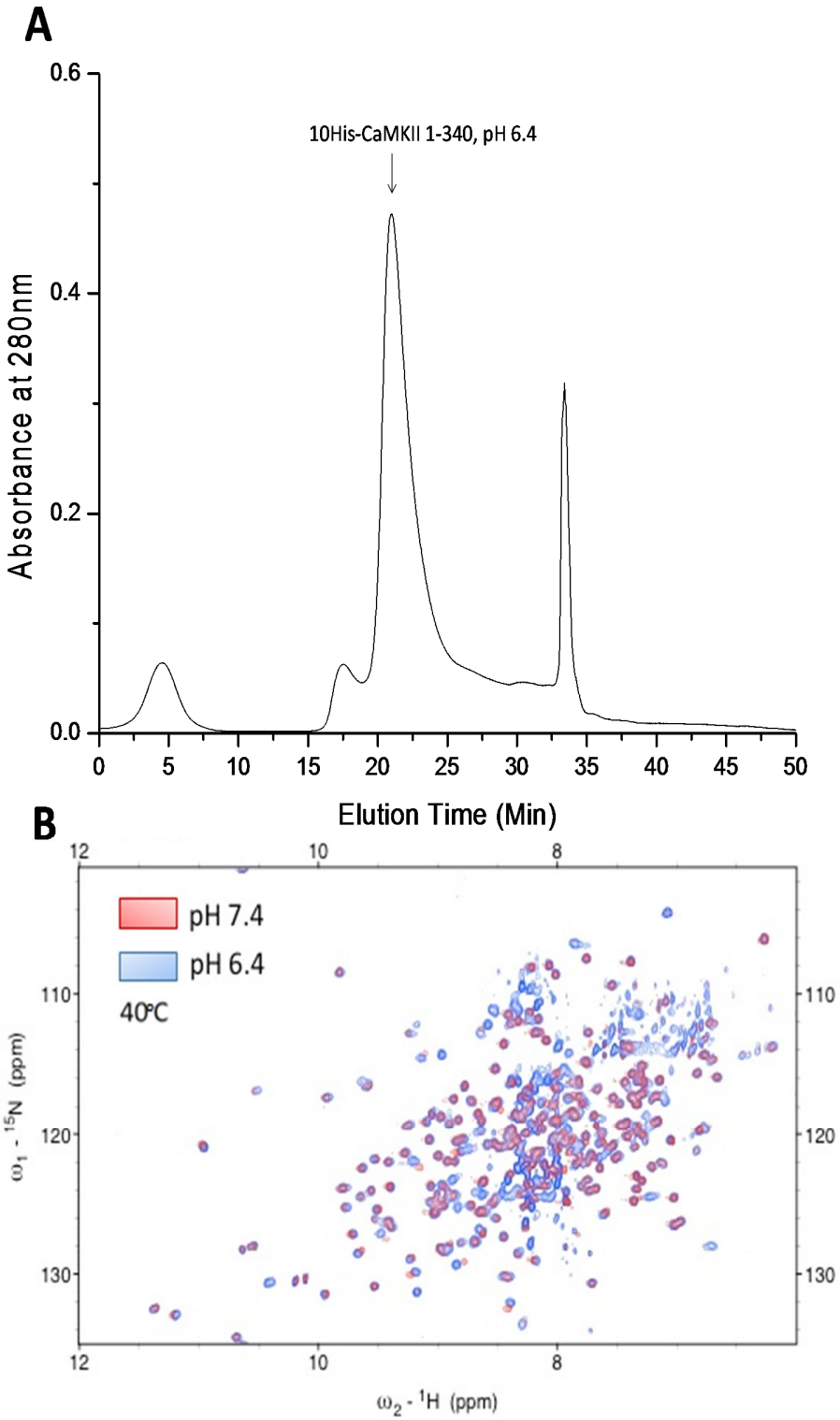

Figure 3.5: A: Gel filtration chromatogram for CaMKII 1-340 at pH 6.4 in buffer containing 50mM HEPES, 50mM NaCl, 1 mM DTT, 2.5mM EDTA, 0.02% NaN_3, 5% D_2O. Flow rate was 0.5mL/min on a Superdex-75 column (25mL column volume) B: ^{1}H-^{15}N Spectrum of apo CaMKII 1-340 at pH 7.4 and 6.4.

Increasing the contour levels between the spectra at the two pH values, it can be seen that there is a cluster of highly intense resonances in the region around (8ppm, 124ppm) in the lower pH spectrum, indicative of flexible residues (Figure 3.6). Some of these could be due to protonation of the His tag and possibly to perturbation of the flexibility of the R3 subdomain. SDS-PAGE does not support the formation of degradation products as a source of the sharp resonances at pH 6.4 that are not present in the pH 7.4 sample.

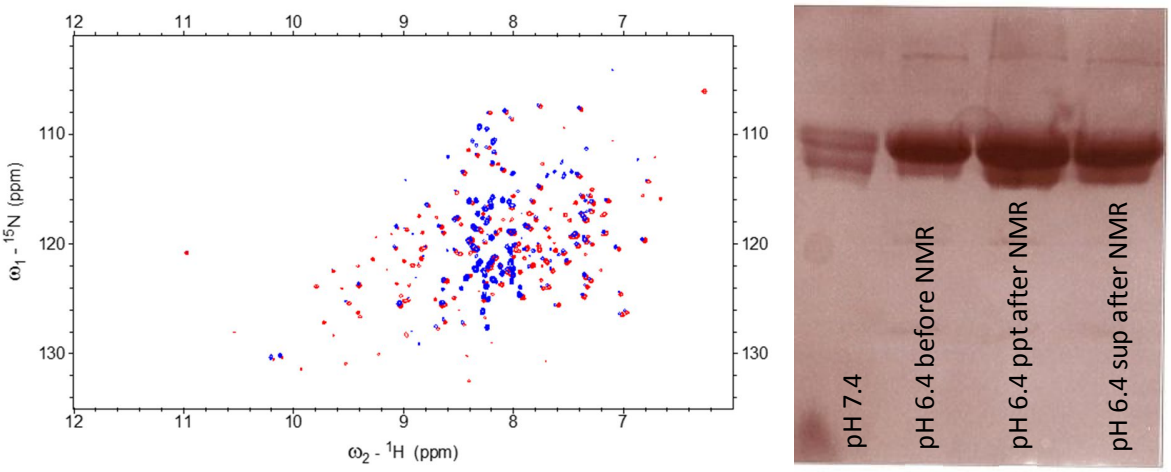

Figure 3.6: ^{1}H-^{15}N Spectrum of apo CaMKII 1-340 at pH 7.4 (red) and 6.4 (high countour level).

The effect of temperature was also tested on a sample at pH 6.4 with the idea being that higher temperature would give better quality spectra from sharper signals. Following the acquisition of the spectrum at 25°C, the temperature was raised to 40°C and a second spectrum was taken (Figure 3.7). There was improvement from reduced broadening especially in the region 8-9ppm, 117-125ppm (^{1}H, ^{15}N) where most of the resonances for this construct appear. However, the higher temperature led to substantial precipitation and so it was decided to use 25°C or lower for future experiments, where possible.

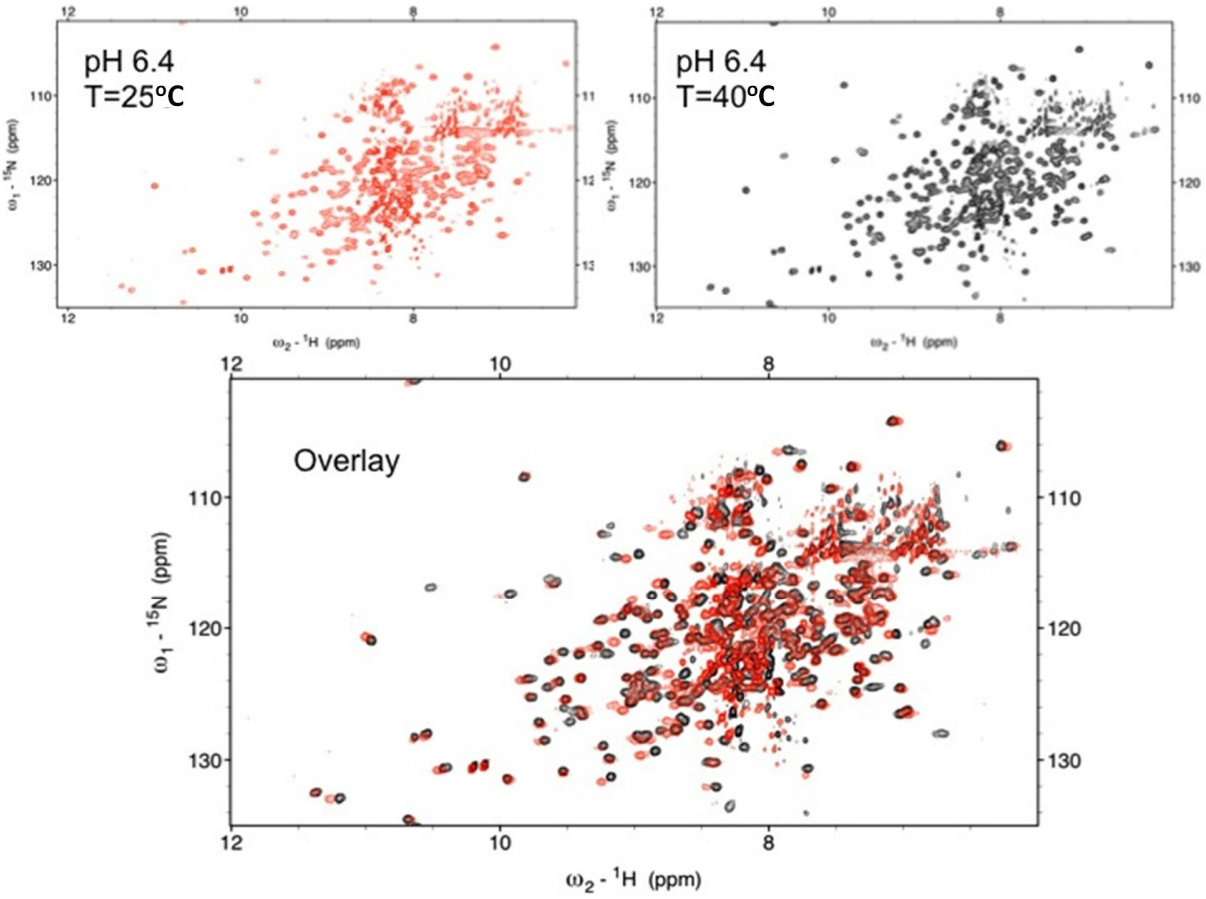

Figure 3.7: ^{1}H-^{15}N Spectrum of apo CaMKII 1-340 at pH 6.4 at 25°C and 40°C.

Because of the instability of the protein and changes in the spectrum at the lower pH, it was decided to keep a pH of 7.4 for future NMR experiments, as well as cleave the His tag. Thrombin cleavage of the tag proved unsuccessful or led to protein aggregation, so it was necessary to change the construct to one bearing a 3C protease cleavage site for removal of the His tag at 4°C under reducing conditions (10mM DTT). This construct is named 6His-1-340 in Appendix I.

Use of Truncated Constructs

In the next set of experiments, a construct lacking the entire regulatory domain (residues 1-277) was expressed in parallel with the 1-340 construct. The His-tags were cleaved from both constructs during purification. The rationale for comparing truncates of different length was that superimposition of the spectra could allow for identification of the resonances belonging to the regulatory domain, and so to R3. However, it was found that the two spectra did not overlap very well, in addition to the shorter construct precipitating throughout the course of the run. This makes it difficult to draw any conclusions other than that the shorter construct exists in a different conformation. It is known that a construct of CaMKII 1-290 is constitutively active (Tavalin, 2008, Petit et al, 1994 Science. 1994 Dec 16;266(5192):1881-5., supporting the idea of a change in catalytic domain conformation due to removal of the regulatory domain.

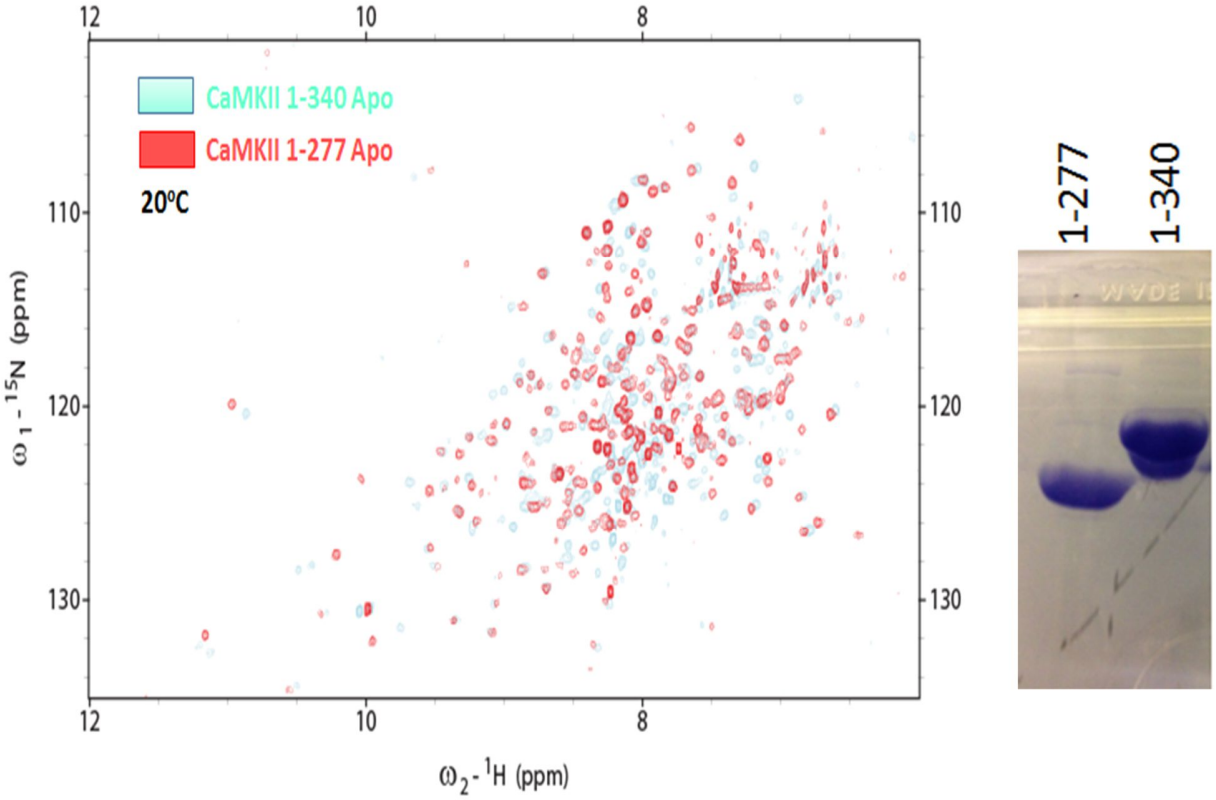

Figure 3.8: ^{1}H-^{15}N Spectrum of apo CaMKII 1-277 overlaid onto 1-340 at pH 7.4.

The spectrum of 1-277 did not change as markedly upon addition of MgATP as it did for the construct with the regulatory domain. It is conceivable that without the entire regulatory region, the kinase lobes may adopt a compact orientation relative to each other, at least partially explaining the differences between the constructs and the reduced changes with MgATP for the shorter construct. Use of 1-277 was abandoned.

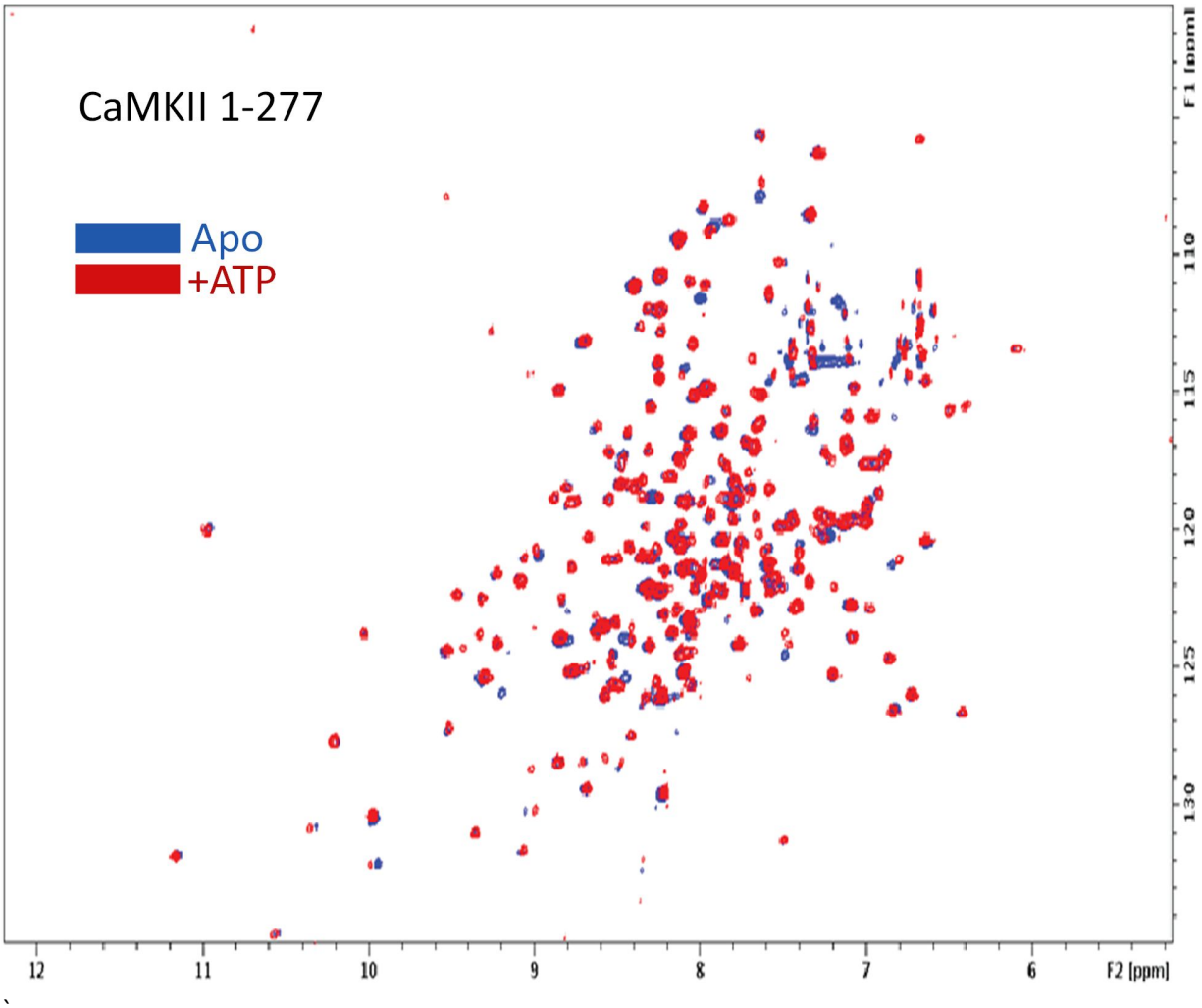

Figure 3.9: Overlay of the ^{1}H-^{15}N TROSY spectrq of the CaMKII 1-277 protein in apo and ATP conditions.

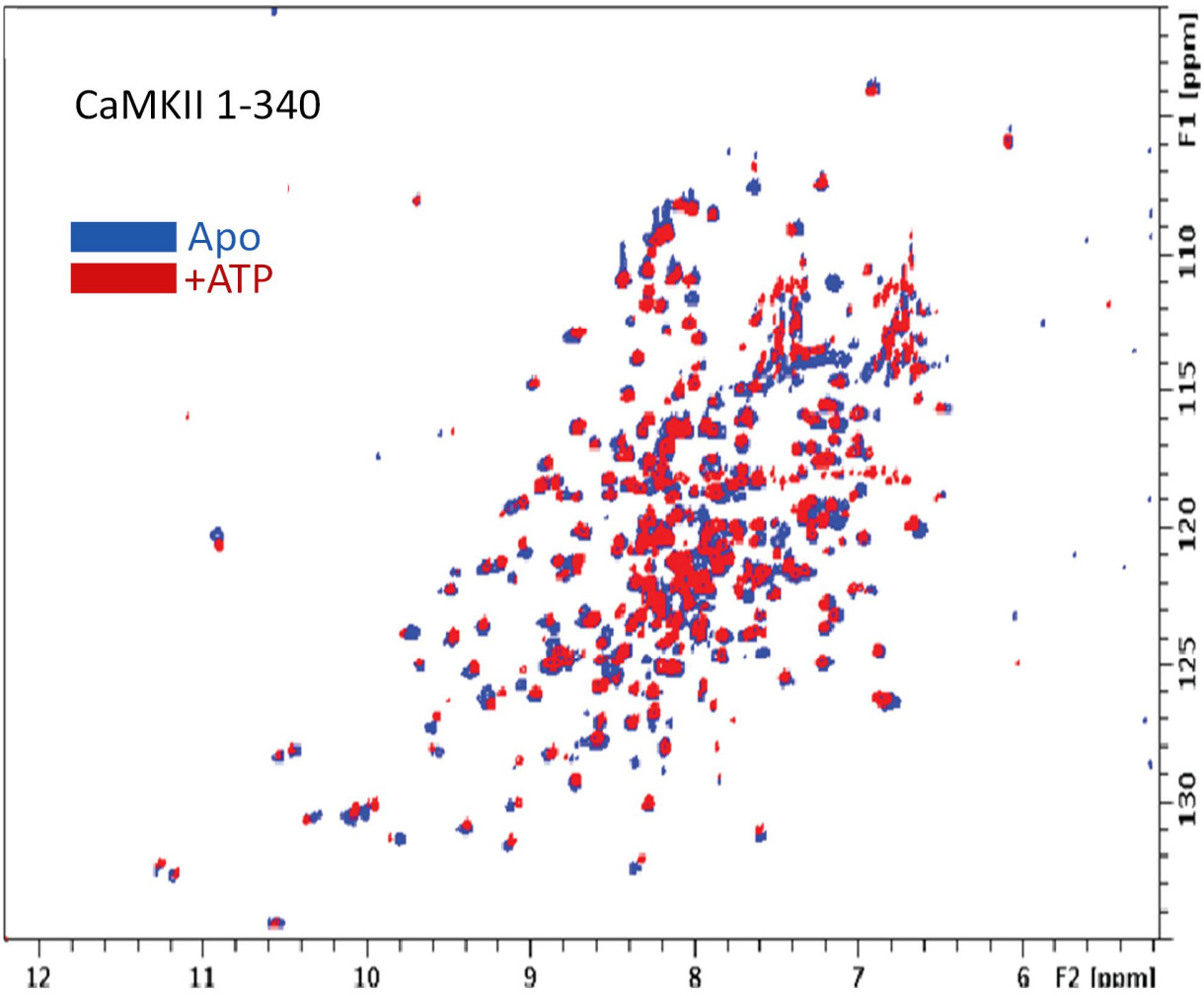

Figure 3.10: Overlay of the ^{1}H-^{15}N TROSY spectra of the CaMKII 1-340 protein in apo and ATP conditions.

From this point forward, it was decided that the inability to separate the truncation product from the 1-340 protein as well as its instability at the conditions required for NMR called for the use of a shorter construct for future experiments. The 1-318 construct was chosen because it afforded a single band on SDS-PAGE, the His tag could easily be cleaved with 3C protease, it retained the R3 region, and it was purified in sufficient yield (3mg per liter of culture). The buffer was also changed from HEPES to potassium phosphate with 10mM DTT to reduce cysteine oxidation, both of which further increased sample stability.

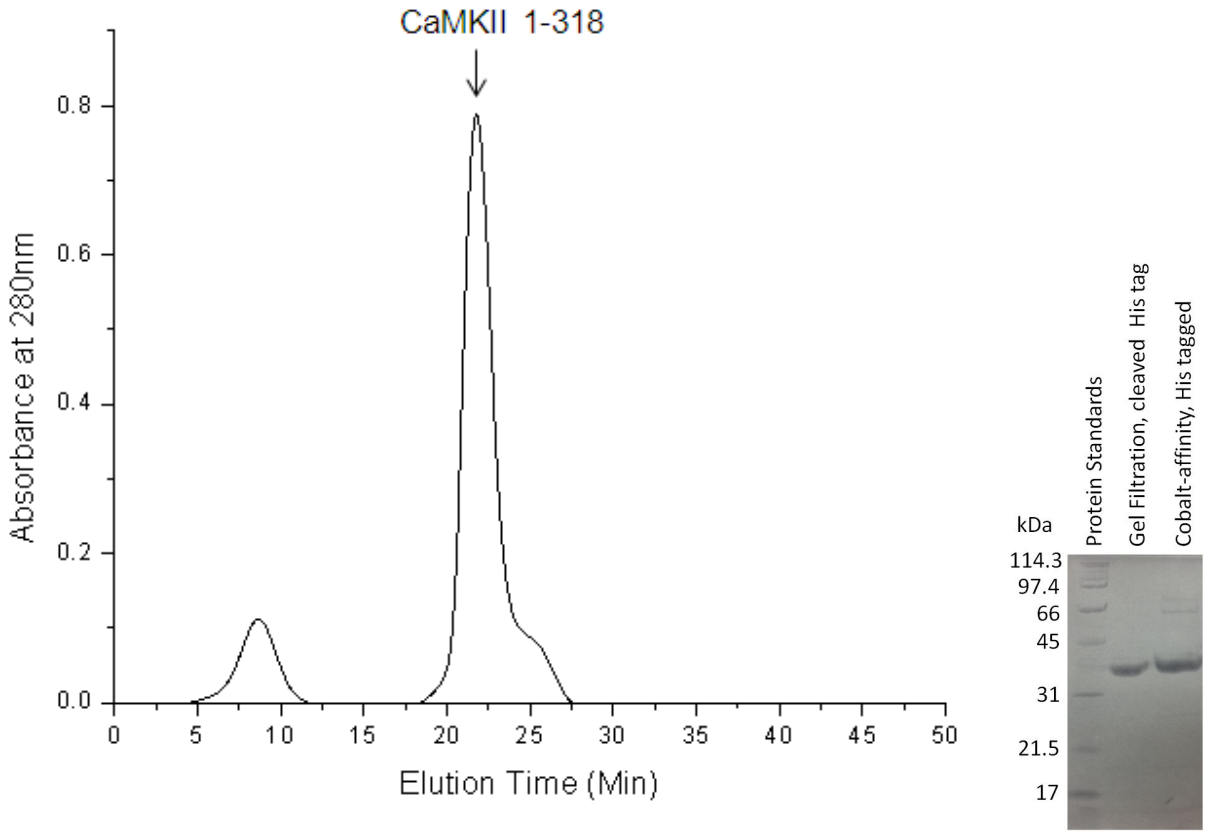

Figure 3.11: Purification data for CaMKII 1-318 construct. The final buffer was changed to 50mM KH_2PO_4, 50mM KCl, 0.02% NaN_3, 2.5mM EDTA, pH 7.4. Flow rate was 0.5mL/min on a Superdex-75 column (25mL column volume).

$^{13}CH_3$-Methionine labeling of 1-318 construct

Once sample conditions and choice of construct were satisfactory, a pilot experiment was carried out to test the applicability of selective labeling to study the R3 region. The construct contains seven Met residues, one of which is in R3 (307). The other Met residues were not expected to undergo major changes with ATP based on their location. Additionally, Met labeling was chosen because its side chain does not degrade into precursors for other amino acids in *E.coli*, its chemical shift appears within a narrow range of 1.5-2.5ppm (^{1}H), and methyl groups can be used as reporters for dynamics experiments.

The culture is grown in minimal medium containing 100% D_2O and ^{12}C-glucose to ensure that the only ^{13}C and ^{1}H come from the labeled methyl group on the Met supplemented.

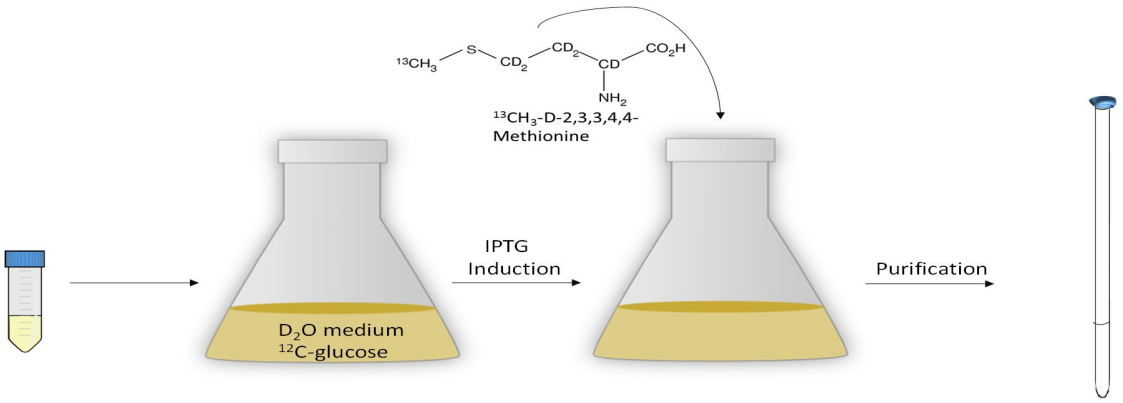

Figure 3.12: Schematic for the production of 13CH3-Methionine labeled CaMKII 1-318.

It was thought that the need to assign the entirety of R3 residues on the protein could be circumvented by this kind of approach, facilitating the study of the region of interest. ^{1}H-^{13}C spectra were collected at 37°C and 800MHz. There was a change in the spectrum as a function of ATP concentration for one peak, as expected, which was assumed to be reflective of a shift in a dynamic equilibrium of the R3 region. The chemical shift difference as a function of ATP equivalents was used to derive a K_D of 920μM, however, more data points are required since the error of the fit was about 25%. The large error is likely due to insufficient data points at the beginning of the curve, as an ATP titration on 15N-labeled protein yielded a value of 185uM (Appendix II, Figure AII.1), closer to the reported Km value of 145μM (Colbran, 1993). The experiment should be repeated on a single mutant of residue 307, e.g. M307A, where the signal from the mutated residue would be missing, to verify that the peak that shifts in the ATP titration is in M307.

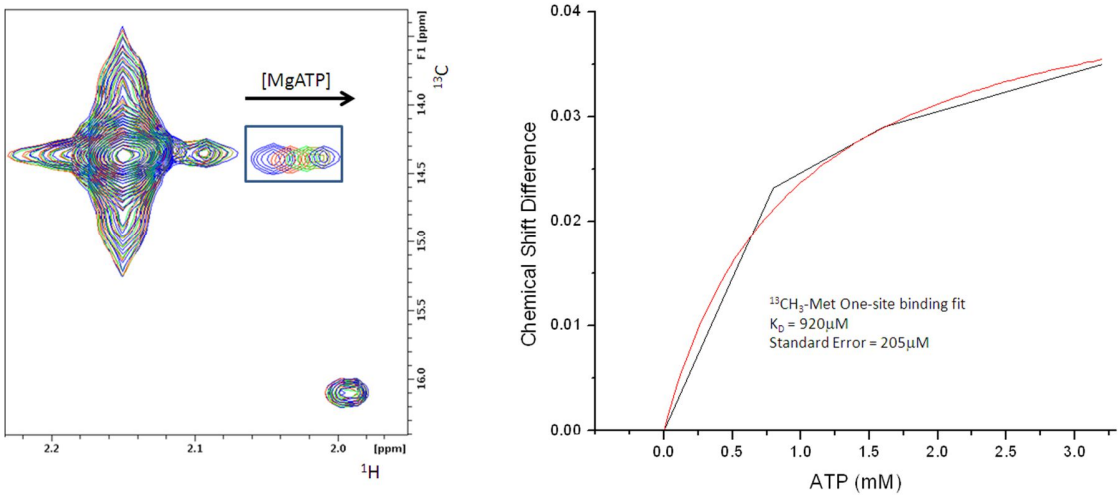

Figure 3.13: ^{1}H-^{13}C Methyl-TROSY spectrum of $^{13}CH_3$-Methionine labeled CaMKII 1-318 at 37°C, showing ATP-dependent change in chemical shift and fit of chemical shift difference as a function of MgATP.

Effect of ATP on the ^{1}H-^{15}N Spectrum of the 1-318 construct

Even though the results of the Met labeling experiment appeared promising, it was still necessary to perform the ATP titration of CaMKII 1-318 with a ^{1}H-^{15}N backbone amide spectrum since it would be needed for assigning R3 residues, and to ensure ATP-induced changes could be trackable globally. The experiment was performed at 25°C (Figure 3.14) and 37°C (not shown) with 100µM protein and 600MHz field strength at apo, 8X, and 32X MgATP. A peak count revealed about 280 resonances or >85% of the sequence. From this point on, it was decided to carry out all experiments with CaMKII 1-318 at 25°C due to stability concerns.

Various clusters of high intensity signals shift between apo and +ATP between 7.2 and 9ppm (^{1}H dimension), 117 and 130 ppm (^{15}N dimension), which falls into the region where the majority of backbone resonances appear. Most of the perturbed signals are of high intensity, suggestive of a

highly mobile or disordered region. This is in agreement with our expectation of a shift in the R3 equilibrium towards an undocked state.

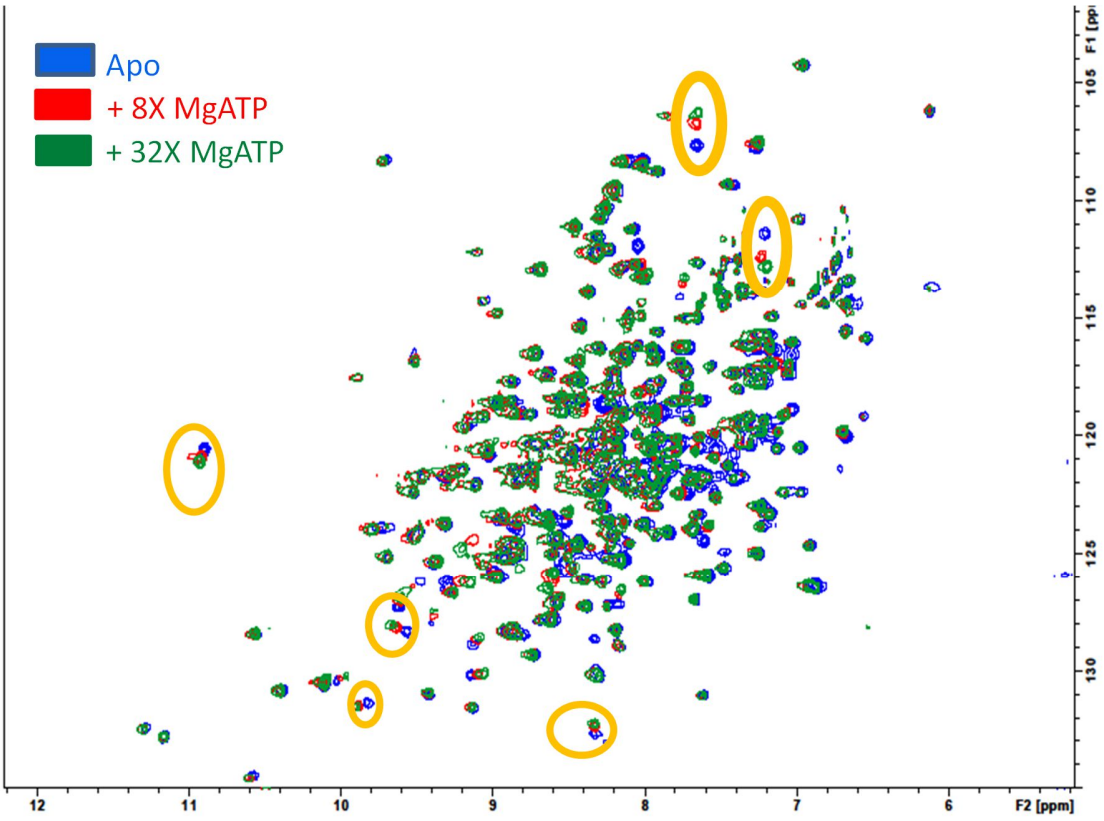

Figure 3.14: ^{1}H-^{15}N spectrum of 100μM CaMKII 1-318 at 25°C in apo (blue), 8X ATP (red), and 32X ATP (green). Chemical shift changes due to ATP can be easily observed (orange circles).

Assignment of Residues of the R3 Subdomain

Next, a set of triple resonance experiments employing ^{2}D, ^{13}C, ^{15}N were carried out in order to identify the peaks in the backbone amide spectrum as the residues in the protein sequence. The sample was concentrated to 200μM protein and the experiments were HNCA, HN(CO)CA, HNCACB, and HN(CO)CACB at 25°C and 900MHz field strength. HNCA is used to detect the Cα of the residue, which appears as a strong peak, and the Cα of the preceding residue, the weaker

peak. HN(CO)CA detects only the Cα of the preceding residue. In this way both experiments are complementary and provide connectivity between residues adjacent in the primary sequence. The HNCACB and HN(CO)CACB set of experiments provide similar information, but they also allow detection of Cβ atoms (Kay et al., 1990). Unfortunately, the HN(CO)CA provided limited insight and the HN(CO)CACB was unusable because the experiments were of low signal quality. A second dataset was performed on non-deuterated sample for HNCA, HN(CO)CA and HNCO, which identifies the carbonyl carbon, to complement the 3D assignment experiments (data not shown).

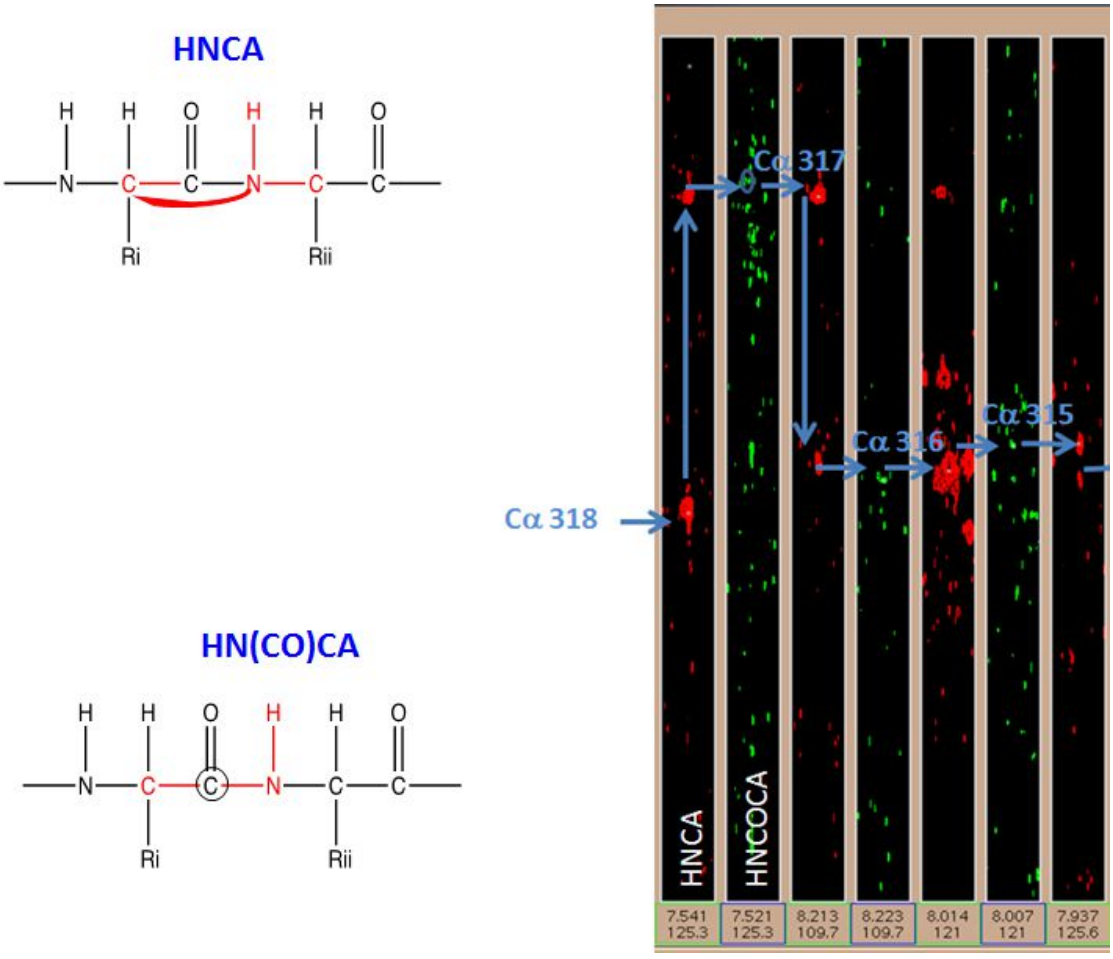

Figure 3.15: Assignment of R3 Tail Residues. Connections between Ca carbons arising from successive residues in the primary sequence can be made based on the 3D (^{2}H, ^{13}C, ^{15}N) experiments HNCA and HN(CO)CA. The peaks can then be traced back onto the ^{1}H-^{15}N (backbone) spectrum.

Spectra of Constructs Truncated at the R3 Subdomain

The C-terminus end of the 1-318 construct contains the R3 region (298-318). It was decided to make C-terminal truncations and superimpose spectra to identify missing resonances, which would then be assigned based on the connections of the aforementioned experiments. The truncations made were as follows: 1-313; 1-308, and 1-303.

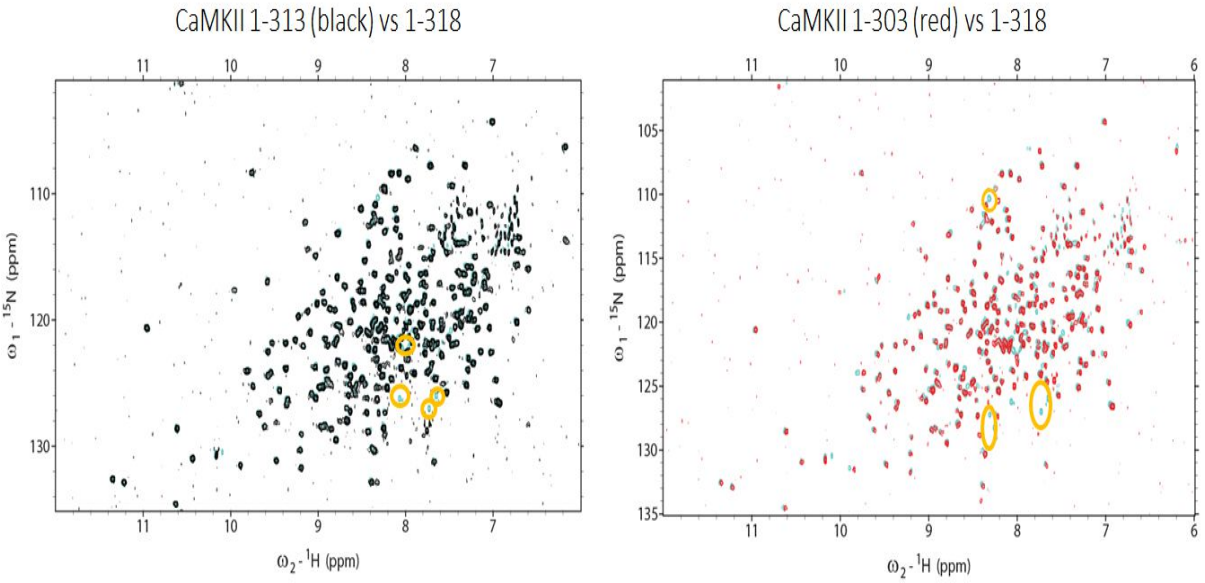

Figure 3.16: ^{1}H-^{15}N spectra of constructs truncated at the R3 region superimposed onto 1-318. The resonances missing in the truncations are highlighted with orange ovals.

From the truncated spectra and the 3D experiments, it was possible to identify residues 301-303 and 313-318. The missing portion includes the segment 304-310, which based on EPR data is suspected to experience the dynamic equilibrium most prominently (Hoffman et al., 2011 and Chapter II). If such is the case, it is possible that the exchange between equilibrium states is causing broadening of the peaks belonging to these residues.

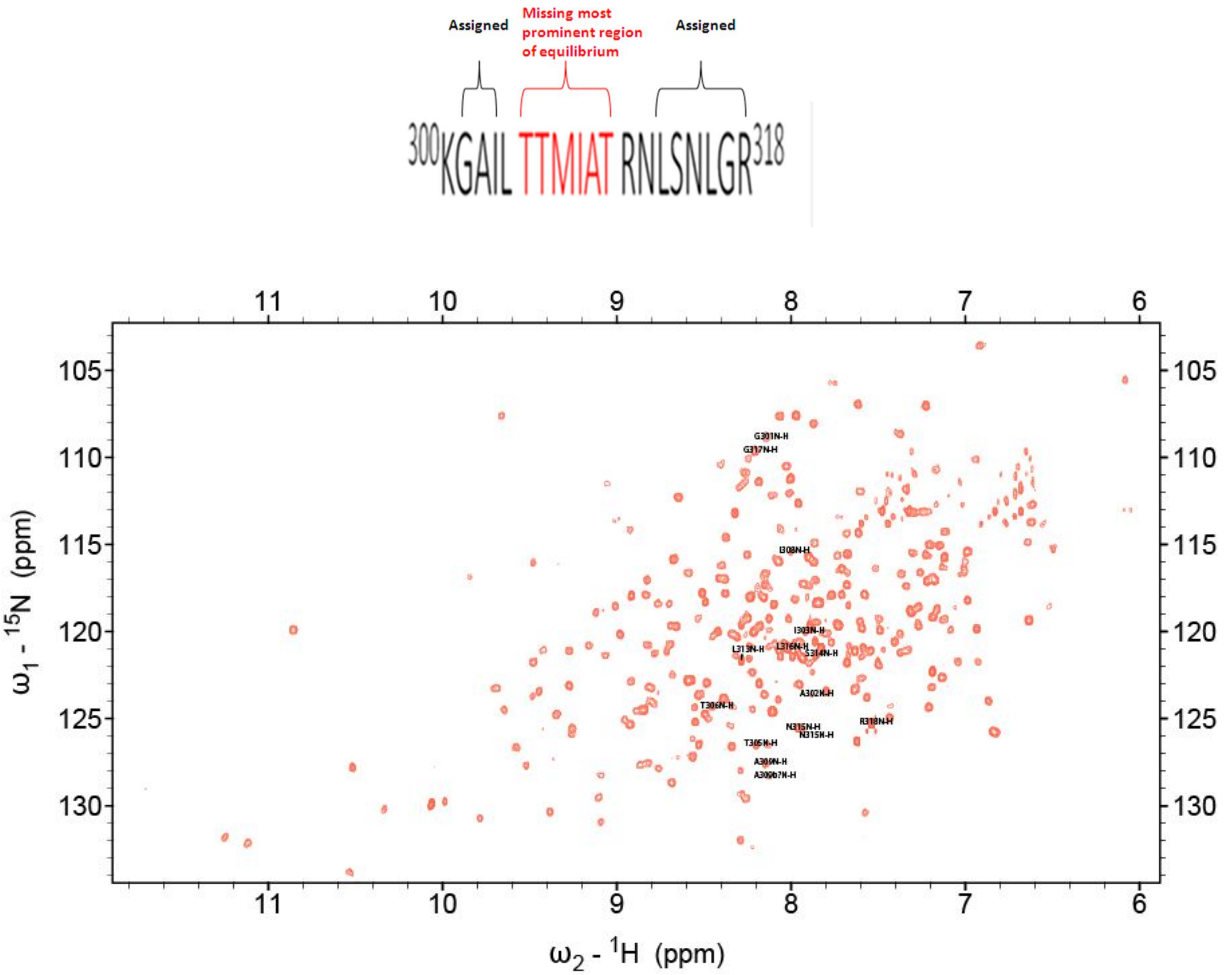

Figure 3.17: Schematic of residues in the R3 region that were assigned from the triple resonance experiments and spectra truncated at R3. The residues are labeled on the H-N spectrum of apo CaMKII 1-318. The segment 305-310 could not be identified from the backbone assignment experiments, so a different strategy involving mutation of the residues was employed (see text).

Glycine Single Mutants for Complementing Assignment

Single Gly mutants were made for residues 305-309 in order to aid in their identification. Gly was chosen because it generally appears in a narrow chemical shift window 8-9ppm, 105-115ppm (^{1}H, ^{15}N) separate from most of the resonances observed in the spectrum of 1-318. An example is shown for the spectrum of CaMKII 1-318 T305G.

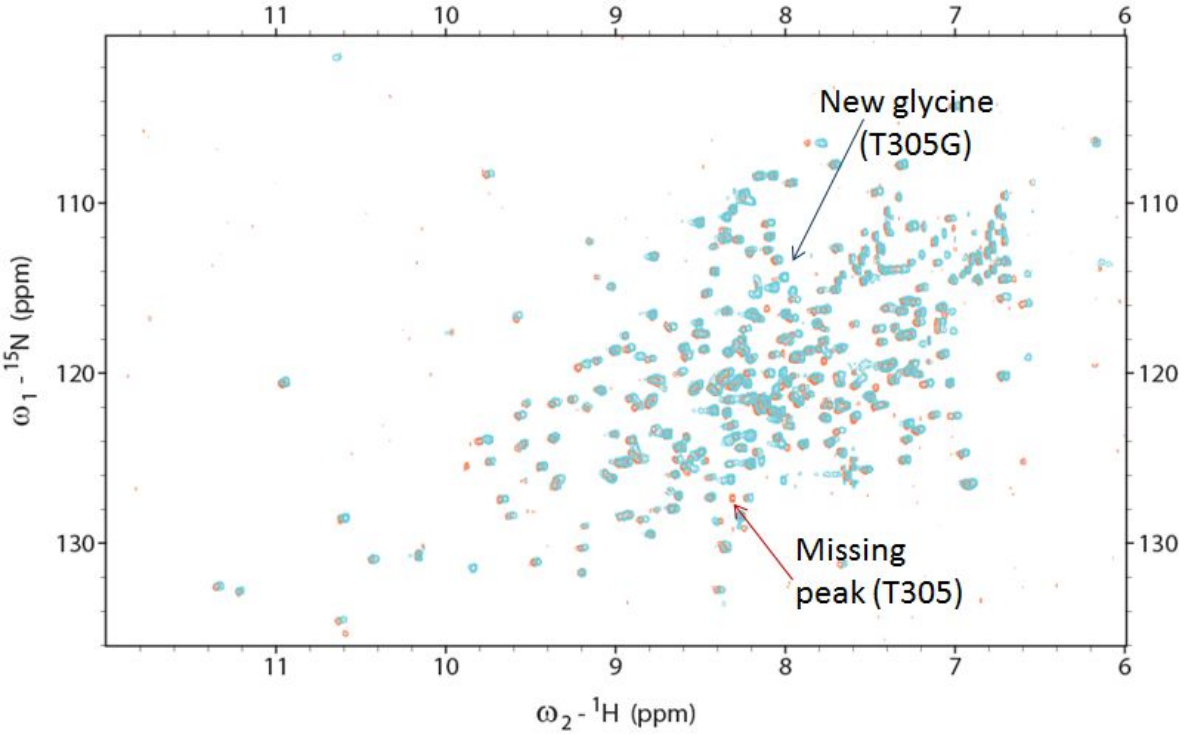

Figure 3.18: ^{1}H-^{15}N spectrum of CaMKII 1-318 T305G (turquoise) superimposed onto 1-318 wild-type T305 (red). *Both constructs bear a D135N inactivating mutation.

The Gly mutant strategy worked for identifying all but one residue (307), in which case the mutated glycine was easily identified, but superimposition onto wild-type did not reveal a missing resonance. An additional attempt at identifying residue 307 was to supplement the medium with unlabeled (^{14}N) Met prior to induction, in order to dilute the Met signals in the spectrum. While the spectrum did show a few signals that were weaker in intensity, it turned out that none of them could be 307 due to them being present in the spectrum of the 1-303 truncation. It is possible that the peak is so weak that it cannot be seen at the concentrations used. It was decided to move forward without identifying residue 307.

Of interest, two resonances were assigned to residue 301 at the N-terminus of R3. There is a peak at ~ 8.25ppm, 109.5ppm (^{1}H, ^{15}N) and a smaller peak at 8.17, 110.0ppm. This is interpreted as a

residue undergoing slow chemical exchange (greater than or on the order of μs, in order to resolve the two signals). The chemical shift and of the smaller peak changes downfield with MgATP. Based on the hypothesis of a dynamic equilibrium of R3, this peak is thought to arise from the undocked conformation, whereas the major peak would reflect the docked state.

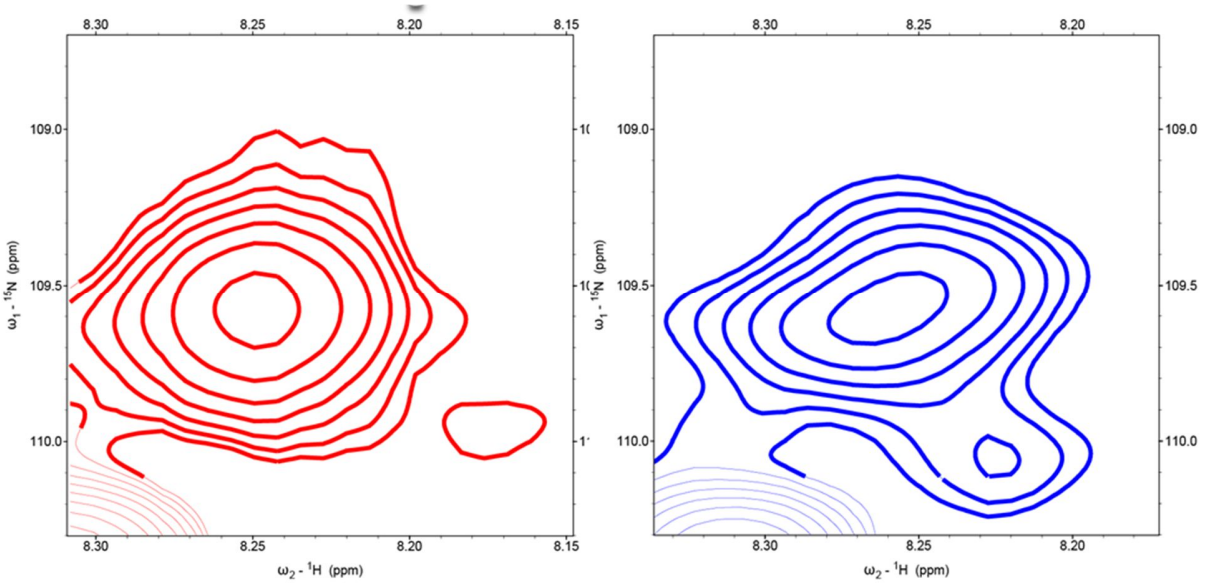

Figure 3.19: Close-up of 1H-15N spectrum of CaMKII 1-318 showing residue G301, at the base of R3, in apo (red) and ATP conditions. CaMKII was 120uM, MgATP 3.84mM or 32X over protein.

This interpretation is further strengthened by the finding shown in Figure 3.20: the smaller G301 peak, denoted B in the figure, becomes more intense in the constructs where the C-terminus of R3 is truncated (1-313 and 1-308), until the major peak is no longer visible (1-303).

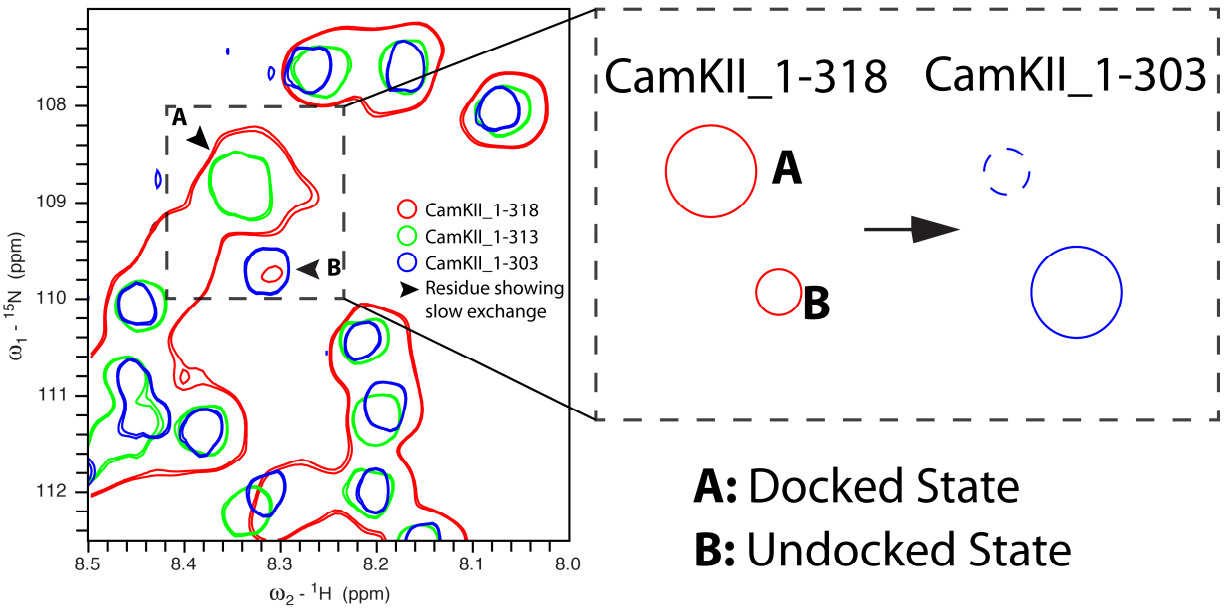

Figure 3.20: Populations of R3 Residue are Altered Across Truncations. The two resonances arising from residue G301 shift in proportion as the R3 tail is truncated at the C-terminus, with the minor component, interpreted to arise from an R3 region that is undocked from the kinase, becoming the major component in the shorter (1-303) construct.

T1 and T2 Relaxation Data of Assigned R3 Residues

After identifying R3 residues, a set of experiments that measure T1 and T2 relaxation across the H-N bond were set up in apo and 100X MgATP for CaMKII 1-318 at 150μM. Because the working hypothesis is that ATP favors increased exposure of R3 to the solvent, it was thought that T1 would be shorter and T2 would be longer with ATP for the R3 residues. It appears that residues 305, 306 and 308 show the most changes in relaxation with ATP, whereas the segment from 313-318 does not change between the two conditions.

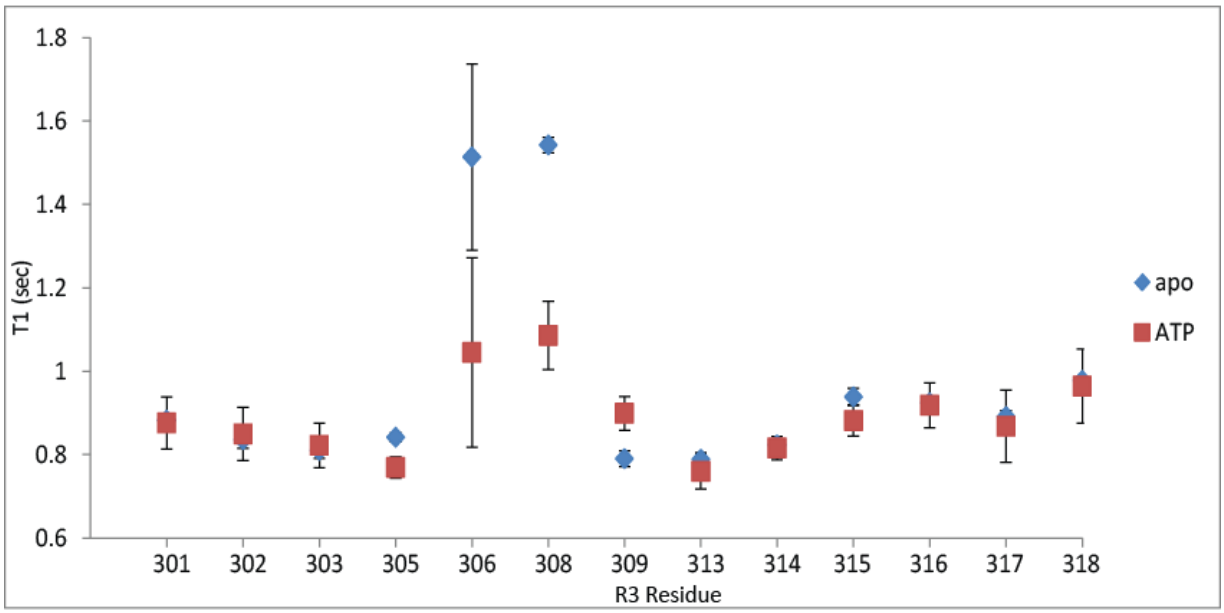

Figure 3.21: T1 values from assigned R3 region peaks in apo and 100X MgATP conditions show a change in flexibility across the N-H bond for residues T305, T306 and I308 between the two conditions. These residues are in the segment of R3 thought to undergo conformational motions mediated by ATP.

T2 (Apo)			T2 (100X MgATP)		
Assignmen	T-decay (msec)	Std Dev	Assignmen	T-decay (msec)	Std Dev
G301N-H	**168,8**	**9,22**	**G301N-H**	**195,6**	**10**
G301bN-H	**95,46**	**5,11**	**G301bN-H**	**121,1**	**9,82**
A302N-H	**155,2**	**15**	**A302N-H**	**164,2**	**12,2**
I303N-H	**150,2**	**5,59**	**I303N-H**	**175,9**	**4,89**
T305N-H	**142,6**	**2,05**	**T305N-H**	**189,8**	**12,8**
I308N-H	**44,56**	**0,617**	**I308N-H**	**49,45**	**1,89**
A309N-H	70,48	1,41	A309N-H	66,87	2,76
L313N-H	288,3	16,7	L313N-H	292,7	55,7
N315N-H	278,4	3,77	N315N-H	289,7	21,3
G317N-H	198,9	1,75	G317N-H	207,6	12,3
R318N-H	399,1	8,46	R318N-H	362,6	19,7

Table 3.1: T2 values obtained from assigned R3 region peaks in apo and 100X MgATP conditions. Residues with altered flexibility between the conditions are highlighted in red.

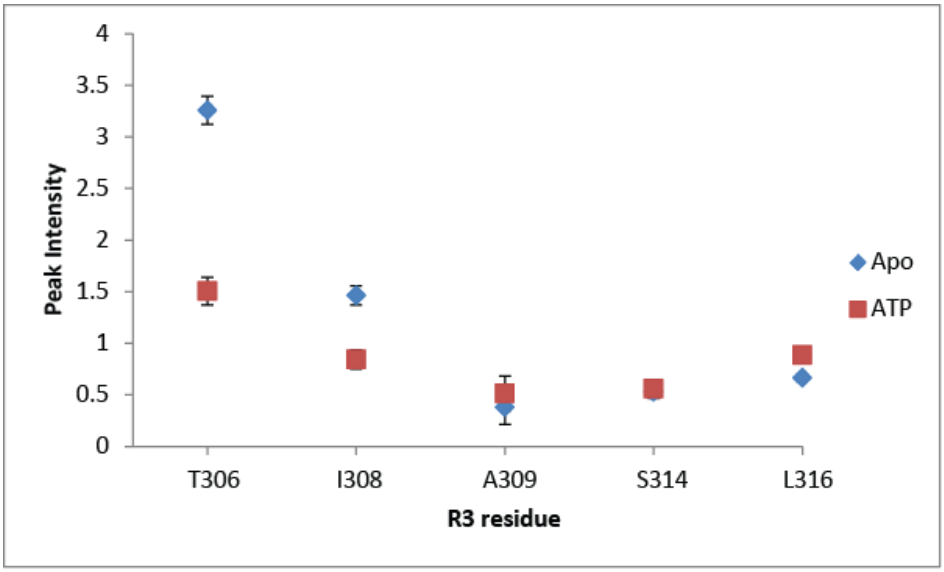

Figure 3.22: Peak height data from NOE experiment for assigned R3 region peaks in apo and 100X MgATP conditions. Results show a change in flexibility across the N-H bond for residues T306 and I308 between the two conditions.

Since the timescale of interdomain movement between docked and undocked conformations was not known, it was decided to also perform ZZ-exchange experiments that measure dynamics in the slow chemical exchange regime (ms-s) (Farrow et al., 1994). It was expected that if there were any peaks from the R3 region undergoing conformational dynamics in this timescale, crosspeaks arising from the interconversion between the docked and undocked states would be visible. However, no changes were observed after acquisition of the apo spectrum at three different mixing times (45ms, 60ms, 100ms) – which allow for the exchanging peaks to be resolved. In fact, the spectra remain unchanged from the reference sample (Figure 3.23), indicating that the dynamics of slowly exchanging residues of the R3 region (such as G301) may nonetheless occur on a faster regime than ZZ-exchange is able to detect. CPMG experiments that allow measuring dynamics on the μs-ms order may be used for probing slow-intermediate exchange in future experiments.

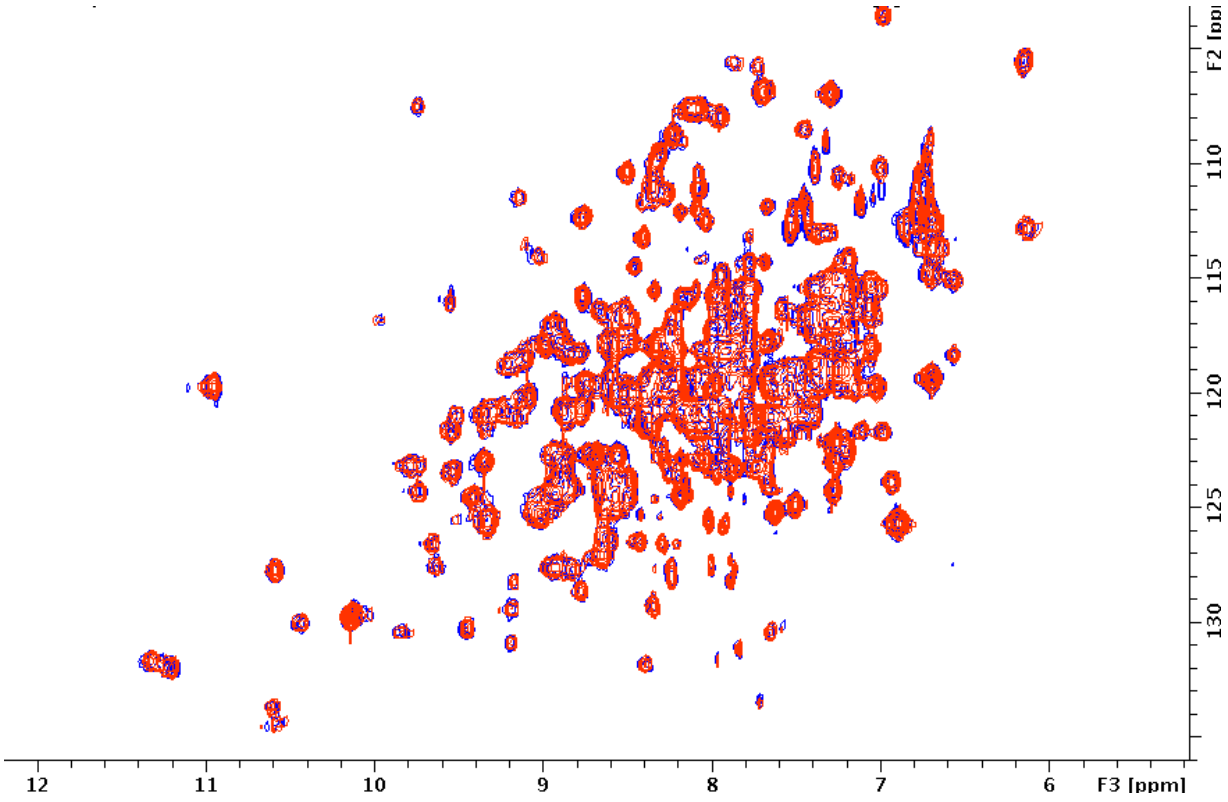

Figure 3.23: ZZ-Exchange Experiment on apo CaMKII 1-318. To discern whether R3 resiudes were undergoing chemical exchange in the slow (ms-s) timescale, the ZZ-exchange experiment, which includes mixing times that allow to resolve the crosspeaks between two exchanging states, was set up at three different mixing times (45ms, 60ms, 100ms (red). However, no differences were observed when the spectra are overlaid onto the reference without a mixing time (blue) indicating that the exchange process does not occur on this timescale.

Chapter IV: Integrated Interpretation of DEER and NMR Data and Future Directions

Summary of Findings Regarding the R3 Subdomain

EPR probing of the base, middle, and end of the R3 segment, represented by sites 300, 307, and 315, showed differing results with respect to the response to ATP. DEER measurements to site 300 showed only a small effect of nucleotide that does not change the average distance, whereas the CW EPR spectra show components of different mobilities that also do not vary between apo and ATP conditions. The NMR data for residue 301, also in this segment of R3, indicates slow exchange modulated by ATP. While this may seem contradictory, a possible explanation is that the change from docked to undocked conformations do not involve a major displacement of the base of the R3 region. By contrast, site 307 appears to be affected most by ATP, with DEER distributions either showing broad populations (17-307; 93-307) or distinct short and long distances affected by ATP (65-307: 79-307: 125-307), with nucleotide changing the distribution toward the longer components. Site 310 seems to be similarly affected by ATP (compare 287-310 and 287-307). Finally, the C-terminus of R3, represented by site 315 does not show distance changes with nucleotide (45-315, 65-315, 85-315), by contrast to site 307. However, the distributions are broader (width >30Å) and the CW spectra show more mobile (sharper) components than pairs to sites 300 or 307. This is consistent with T1 and T2 NMR measurements which show that the C-terminus of R3 (313-318) does not show changes in backbone mobility between the apo and ATP conditions, whereas residues T305,T306, and I308 are more flexible with ATP. A possible explanation for these results is that the different segments of R3 interact distinctly with the kinase, with the base (residues 298-303) being stably abutted to the catalytic

domain and exchanging slowly between conformations; the middle (305-310) experiencing the conformational dynamics more strongly between docked and undocked conformations, and being majorly affected by ATP; and the C-terminus of R3 (313-318) already being unstructured and not docked to the kinase, therefore is not largely affected by ATP.

It is necessary to generate more DEER pairs to the N- and C-terminus of R3 to discern whether the diminished effect of ATP to sites 300 and 315 is not particular to the mutants shown. Preferably, measurements between these two ends of R3 and the catalytic N- and C-lobes should be made to the sites on the catalytic domain studied previously. A table of predicted Cβ-Cβ distances for new DEER pairs to site 300 is shown – site 315 is not part of the crystal (Table 4.1).

Pair	PDB 2VN9 Cβ-Cβ (Å)
17-300	22.8
33-300	36.4
65-300	30.3
79-300	30.4
93-300	23.6
125-300	29.7

Table 4.1: Additional labeling sites for measuring distances to site 300 at the N-terminus of the R3 subdomain.

Future Directions and Open Questions

The studies presented in this document were performed on monomeric constructs where the association domain was removed. It has to be determined whether the observed conformational heterogeneity of the R3 region, which is proposed to encompass conformations of R3 bound to the catalytic domain, is not an artifact resulting from the absence of steric constraints that the CaMKII holoenzyme arrangement places on individual subunits. In the crystal structure of a full-length CaMKII holoenzyme, R3 is actually docked to the association domain at an interface that

had not been identified previously (Chao et al., 2011) . However, this structure was obtained from a splice variant that has an unusually short linker and is less responsive to Ca^{2+}/CaM (Wang et al., 2000), so the question remains whether the crystallographic findings can be generalized to other isoforms. Moreover, since the holoenzyme has been shown to undergo subunit exchange as a dimer upon phosphorylation of T286/T305/T306 in R3, it is possible that the R3 equilibrium that is part of the interpretation of the DEER data could be favored when the exchanging dimer is freed from the energetic and spatial limits arising from the holoenzyme structure. The ability to use DEER to study the holoenzyme is complicated by the number of spin labels that would be present if all subunits were labeled. A potential method to overcome this issue might be to take advantage of the subunit exchange phenomenon (Stratton et al., 2013) to minimize the number of spin labeled subunits per holoenzyme. The idea would be to generate His-tagged CaMKII spin labeled at R3 and the catalytic domain - ideally, the same sites used in the monomeric studies would be chosen, and incubate the enzyme with ATP, Ca^{2+}/CaM, and Camguk, a protein that promotes T305/T306 phosphorylation (Lu et al., 2003; Hodge et al., 2006). The spin labeled holoenzyme would then be mixed with an excess of Cysteine-less, untagged CaMKII holoenzyme and allowed to exchange subunits. The reaction would then be stopped by dephosphorylating T286/T305/T306 with a phosphatase such as PP1, and finally the holoenzyme would be purified from Cobalt-affinity chromatography (Figure 4.1). Conditions would have to be optimized in order to minimize the extent of subunit exchange. In this way, DEER measurements could be made on the holoenzyme and comparison with the distance data from monomeric CaMKII might help ascertain whether the R3 equilibrium is relevant in full-length CaMKII.

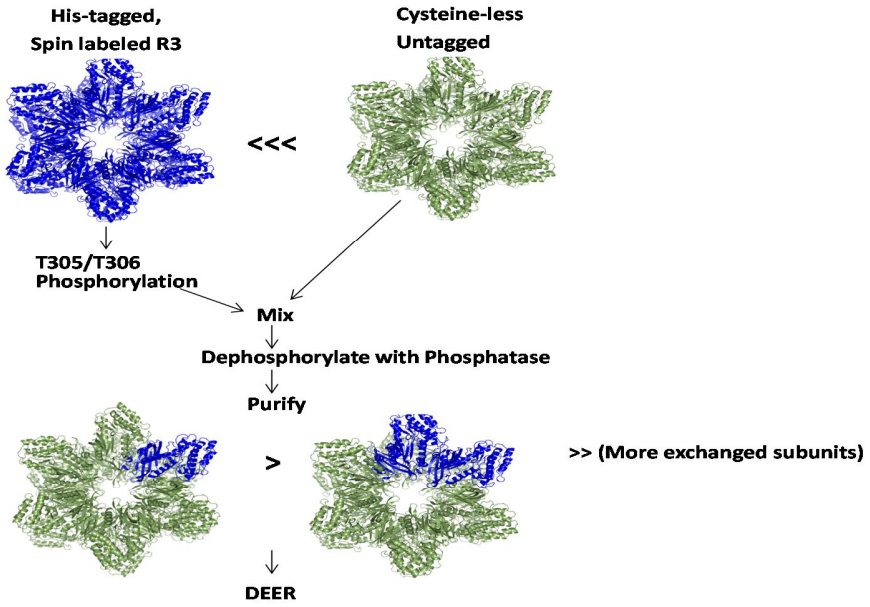

Figure 4.1: Use of subunit exchange for reducing spin labeled subunits in the holoenzyme. Mixing of Spin-labeled with Spin-free CaMKII in conditions that promote T305/T306 phosphorylation and subsequent subunit exchange may allow for the purification of hybrid holoenzymes with reduced number of labeled subunits to simplify DEER measurements.

A mutation (I205K) in the T-site, the pocket in the catalytic domain where the regulatory helix R1 is abutted , increases affinity of Ca^{2+}/CaM for CaMKII through an unknown mechanism (Yang and Schulman, 1999; Nguyen et al., 2015). It is hypothesized that the mutation perturbs the interaction of R1 with the kinase and makes both R1 and R3 accessible to the solvent. Distance measurements of previously generated pairs between the catalytic domain and the different subdomains of the regulatory region (R1 and R3) may provide a more complete picture of the effect of the mutation on the conformation of the enzyme. For instance, pair 17-288; 93-288; and 125-287 could be used to gauge whether there is an effect on R1, and pairs 287-307; 287-310; 17-307; 93-307 and 125-307 likewise for the R3 region.

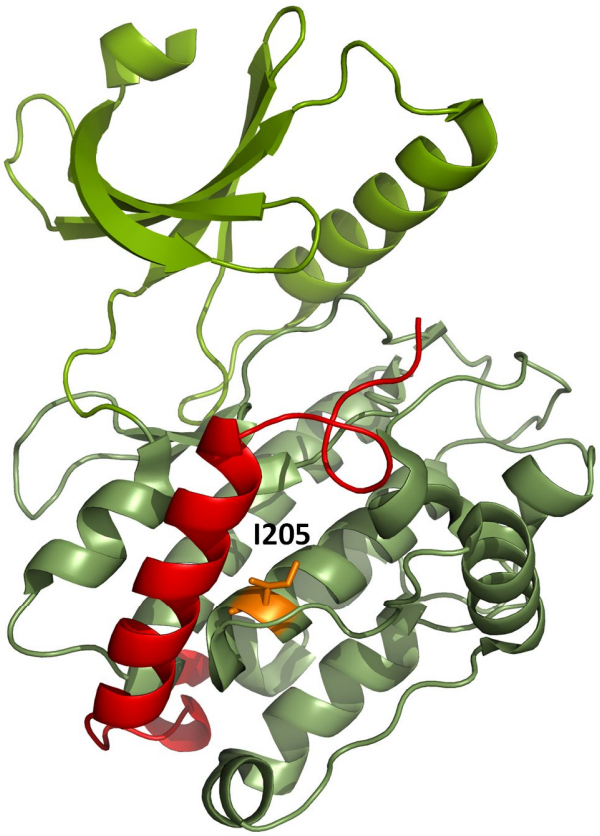

Figure 4.2: Location of I205 in the C-lobe. Background mutation I205K may be used to measure distances between the catalytic lobes (green) and the regulatory domain (red), to test the hypothesis that mutation of this residue disrupts the interaction between the catalytic C-lobe and R1, and possibly the R3 equilibrium as well.

Understanding the Conformational Changes of Novel CaMKII Activation Pathways

As mentioned in the introduction, novel mechanisms that maintain CaMKII in an autonomously active state after Ca^{2+} levels drop include oxidation of Met281/282, O-linked glycosylation of Ser280, and S-nitrosylation of Cys290. Because these residues are located in the R1 segment and the three mechanisms take place after initial Ca^{2+}/CaM activation, it is presumed they operate similarly to T286 autophosphorylation, by preventing the R1 segment to dock to the catalytic domain. However, local conformational changes at R1, and distance changes between R1 and

the catalytic domain following activation through these pathways have not been studied extensively. It remains an open question how the amplitude changes between these three novel pathways compare to one another and to T286 autophosphorylation. It is conceivable that NMR, SDSL-EPR or other probe-based method of similar nature to the one presented can be carried out to gain an understanding of the dynamics that result from these pathways by generating background mutants (Met281/282Gln, Ser279Cys reacted with GlcNAc-thiol, or Cys290Trp) that mimic these post-translational modifications.

Identifying Interaction Surface for R3 on the Catalytic Domain Side

Because the assignment experiments used to identify the R3 region in this study were performed on uniformly isotopically labeled protein, data is available to identify residues in the catalytic domain and of R1 as well. This assignment data can be used for future experiments where identification of domain interactions might be informative. A viable starting point may be to assign the interface on the catalytic domain where R3 is docking. Preliminary efforts in this direction have involved the acquisition of the backbone amide spectrum of the 1-303 construct in the presence of peptide derived from residues 298-320 of the R3 region (KLKGAILTTMIATRNLSNLGRNL). Overlaying the spectrum with that of the 1-318 construct in apo and ATP conditions reveals several residues that are affected by both the R3 peptide and ATP. The experiment in the presence of the peptide should be carried out with the 1-318 construct to ensure that the results are reproducible across the constructs. The resonances that are perturbed by both ATP and the R3 synthetic peptide may belong to the docking interface for R3 on the

catalytic N-lobe and assignment experiments already performed may prove useful in identifying such residues.

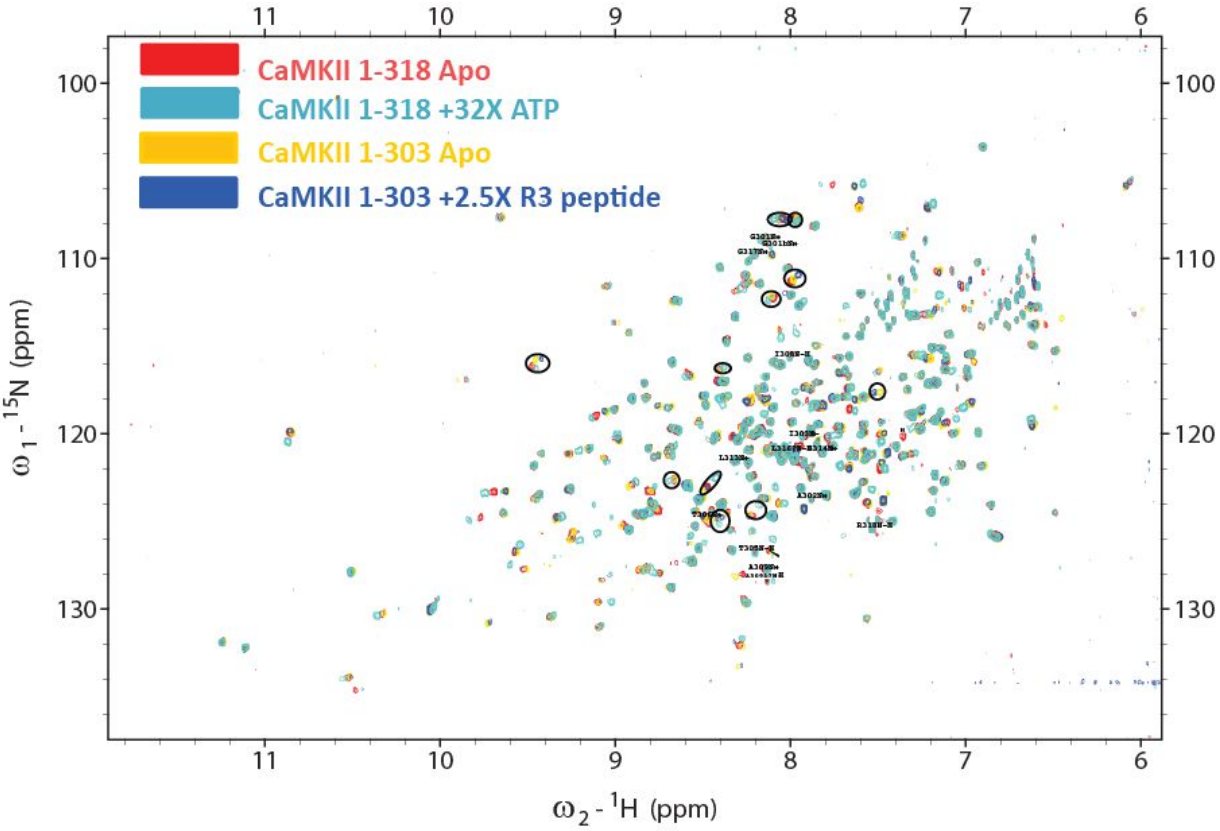

Figure 4.3: Unassigned CaMKII residues perturbed by both ATP and peptide derived from R3. Overlay of CaMKII 1-318 in apo (red) and in the presence of ATP (turquoise) with CaMKII 1-303 in apo (yellow) and in the presence of peptide corresponding to residues 298-320 of R3 (blue). Shown within black circles are unidentified resonances that are affected by both, ATP in the longer construct, and the R3 peptide in the construct with the truncated regulatory region. It is postulated that these resonances may belong to the docking interface for R3 on the catalytic domain side.

Conclusion

The DEER and NMR data presented in these studies shows a conformational resilience of the regulatory domain of CaMKII that is affected by MgATP, by altering the backbone flexibility of the R3 region that contains the Ca^{2+}/CaM binding element. From the perspective of the holoenzyme, this would facilitate CaM access to the R3 region, therefore contributing to enzyme activation.

DEER data also suggests that Ca^{2+}/CaM activates the kinase by rearranging the regulatory domain in a manner that abolishes interaction with the ATP and substrate binding sites on the catalytic domain, more specifically by setting the R3 region away from the main body of the kinase. These changes are coupled to a disruption of the interaction between the R1 helix and the C-lobe of the catalytic domain, which is a prerequisite for exposing T286 in R1 for phosphorylation by an adjacent subunit, a modification that endows CaMKII with Ca^{2+}-independent activity.

REFERENCES

Akamine P, Madhusudan, Wu J, Xuong NH, Ten Eyck LF, Taylor SS. Dynamic features of cAMP-dependent protein kinase revealed by apoenzyme crystal structure. J Mol Biol. 327(1):159-71 (2003).

Andersson DC, Fauconnier J, Yamada T, Lacampagne A, Zhang SJ, Katz A, Westerblad H. Mitochondrial production of reactive oxygen species contributes to the β-adrenergic stimulation of mouse cardiomycytes .J Physiol. 589(Pt 7):1791-801. (2011).

Aow J, Dore K, Malinow R. Conformational signaling required for synaptic plasticity by the NMDA receptor complex. Proc Natl Acad Sci U S A. 112(47):14711-6 (2015).

Bayer KU, De Koninck P, Leonard AS, Hell JW, Schulman H. Interaction with the NMDA receptor locks CaMKII in an active conformation. Nature. 411(6839):801-5 (2001).

Bayer KU, De Koninck P, Schulman H. Alternative splicing modulates the frequency-dependent response of CaMKII to Ca(2+) oscillations. EMBO J. 21(14):3590-7 (2002).

Bennett MK, Erondu NE, Kennedy MB. Purification and characterization of a calmodulin-dependent protein kinase that is highly concentrated in brain. J Biol Chem. 258:12735-44 (1983).

Berridge MJ, Lipp P, Bootman MD. Signal transduction. The calcium entry pas de deux. Science. 287:1604-5 (2000).

Bovo E, Lipsius SL, Zima AV. Reactive oxygen species contribute to the development of arrhythmogenic Ca^{2+} waves during β-adrenergic receptor stimulation in rabbit cardiomyocytes. J Physiol. 590(14):3291-30. (2012).

Brocke L, Chiang LW, Wagner PD, Schulman H. Functional implications of the subunit composition of neuronal CaM kinase II. J Biol Chem. 274(32):22713-22 (1999).

Burger D, Stein EA, Cox JA. Free energy coupling in the interactions between Ca^{2+}, calmodulin, and phosphorylase kinase. J Biol Chem. 258(23):14733-9 (1983).

Chao LH, Pellicena P, Deindl S, Barclay LA, Schulman H, Kuriyan J. Intersubunit capture of regulatory segments is a component of cooperative CaMKII activation. Nat Struct Mol Biol. 17(3):264-72 (2010).

Chao LH, Stratton MM, Lee IH, Rosenberg OS, Levitz J, Mandell DJ, Kortemme T, Groves JT, Schulman H, Kuriyan J. A mechanism for tunable autoinhibition in the structure of a human Ca2+/calmodulin- dependent kinase II holoenzyme. Cell. 146(5):732-45 (2011).

Chin D, Means AR. Calmodulin: a prototypical calcium sensor. Trends Cell Biol. 10:322-8 (2000).

Chin D, Means AR. Mechanisms for regulation of calmodulin kinase IIα by Ca^{2+}/calmodulin and autophosphorylation of threonine 286. Biochemistry.41:14001-9 (2002).

Clapham DE. Calcium signaling. Cell. 131:1047-58 (2007).

Colbran RJ, Smith MK, Schworer CM, Fong YL, Soderling TR. Regulatory domain of calcium/calmodulin-dependent protein kinase II. Mechanism of inhibition and regulation by phosphorylation. J Biol Chem. 264(9):4800-4 (1989).

Colbran RJ, Soderling Calcium/calmodulin-independent autophosphorylation sites of calcium/calmodulin-dependent protein kinase II J. Biol. Chem. 265:11213–11219 (1990).

Colbran, RJ Inactivation of Ca^{2+}/calmodulin-dependent protein kinase II by basal autophosphorylation. J Biol Chem, 268(10):7163-70 (1993).

Coultrap SJ, Freund RK, O'Leary H, Sanderson JL, Roche KW, Dell'Acqua ML, Bayer KU. Autonomous CaMKII mediates both LTP and LTD using a mechanism for differential substrate site selection. Cell Rep. 6(3):431-7 (2014).

Curran J, Tang L, Roof SR, Velmurugan S, Millard A, Shonts S, Wang H, Santiago D, Ahmad U, Perryman M, Bers DM, Mohler PJ, Ziolo MT, Shannon TR. Nitric oxide-dependent activation of CaMKII increases diastolic sarcoplasmic reticulum calcium release in cardiac myocytes in response to adrenergic stimulation. PLoS ONE 9, e87495. (2014).

De Koninck P, Schulman H. Sensitivity of CaM kinase II to the frequency of Ca^{2+} oscillations. Science. 279(5348):227-30 (1998).

Erickson JR, Joiner ML, Guan X, Kutschke W, Yang J, Oddis CV, Bartlett RK, Lowe JS, O'Donnell SE, Aykin-Burns N, Zimmerman MC, Zimmerman K, Ham AJ, Weiss RM, Spitz DR, Shea MA, Colbran RJ, Mohler PJ, Anderson ME. A dynamic pathway for calcium-independent activation of CaMKII by methionine oxidation. Cell. 133(3):462-74 (2008).

Erickson JR, Nichols CB, Uchinoumi H, Stein ML, Bossuyt J, Bers DM. S-Nitrosylation Induces Both Autonomous Activation and Inhibition of Calcium/Calmodulin-dependent Protein Kinase IIδ. J Biol Chem. 290(42):25646-56 (2015).

Erickson JR, Pereira L, Wang L, Han G, Ferguson A, Dao K, Copeland RJ, Despa F, Hart GW, Ripplinger CM, Bers DM. Diabetic hyperglycaemia activates CaMKII and arrhythmias by O-linked glycosylation. Nature. 502(7471):372-6 (2013).

Erickson JR. Mechanisms of CaMKII Activation in the Heart. Front Pharmacol. 5:59. (2014).

Farrow NA, Zhang O, Forman-Kay JD, Kay LE. A heteronuclear correlation experiment for simultaneous determination of 15N longitudinal decay and chemical exchange rates of systems in slow equilibrium. J Biomol NMR. 4(5):727-34 (1994).

Fujii H, Inoue M, Okuno H, Sano Y, Takemoto-Kimura S, Kitamura K, Kano M, Bito H. Nonlinear decoding and asymmetric representation of neuronal input information by CaMKIIα and calcineurin. Cell Rep. 3(4):978-87 (2013).

Fukunaga K, Kobayashi T, Tamura S, Miyamoto E. Dephosphorylation of autophosphorylated Ca^{2+}/calmodulin-dependent protein kinase II by protein phosphatase 2C. J Biol Chem. 268(1):133-7 (1993).

Giese KP, Fedorov NB, Filipkowski RK, Silva AJ. Autophosphorylation at Thr286 of the alpha calcium-calmodulin kinase II in LTP and learning. Science. 279(5352):870-3 (1998).

Grabarek Z. Insights into modulation of calcium signaling by magnesium in calmodulin, troponin C and related EF-hand proteins. Biochimica et Biophysica Acta (BBA) - Molecular Cell Research. 1813: 913–921 (2011).

Griffith LC, Lu CS, Sun XX. CaMKII, an enzyme on the move: regulation of temporospatial localization. Mol Interv 3:386-403 (2003).

Grimm M, Ling H, Willeford A, Pereira L, Gray CB, Erickson JR, Sarma S, Respress JL, Wehrens XH, Bers DM, Brown JH. CaMKIIδ mediates β-adrenergic effects on RyR2 phosphorylation and SR Ca(2+) leak and the pathophysiological response to chronic β-adrenergic stimulation. J Mol Cell Cardiol. 85:282-91. (2015).

Gutierrez DA, Fernandez-Tenorio M, Ogrodnik J, Niggli E. NO-dependent CaMKII activation during β-adrenergic stimulation of cardiac muscle. Cardiovasc. Res. 100, 392–401. (2013).

Hanks SK, Hunter T. Protein kinases 6. The eukaryotic protein kinase superfamily: kinase (catalytic) domain structure and classification. FASEB J. 9(8):576-96 (1995).

He BJ, Joiner ML, Singh MV, Luczak ED, Swaminathan PD, Koval OM, Kutschke W, Allamargot C, Yang J, Guan X, Zimmerman K, Grumbach IM, Weiss RM, Spitz DR, Sigmund CD, Blankesteijn WM, Heymans S, Mohler PJ, Anderson ME. Oxidation of CaMKII determines the cardiotoxic effects of aldosterone. Nat Med. 17(12):1610-8. (2011).

Hodge JJ, Mullasseril P, Griffith LC. Activity-dependent gating of CaMKII autonomous activity by Drosophila CASK. Neuron. 51(3):327-37 (2006).

Hoelz A, Nairn AC, Kuriyan J. Crystal structure of a tetradecameric assembly of the association domain of Ca2+/calmodulin-dependent kinase II. Mol Cell. 11(5):1241-51 (2003).

Hoffman L, Stein RA, Colbran RJ, Mchaourab HS. Conformational changes underlying calcium/calmodulin-dependent protein kinase II activation. EMBO J. 30(7):1251-62 (2011).

Hubbell WL, Mchaourab HS, Altenbach C, Lietzow MA. Watching proteins move using site-directed spin labeling. Structure. 4(7):779-83 (1996).

Hudmon A, Schulman H. Neuronal Ca^{2+}/calmodulin-dependent protein kinase II: the role of structure and autoregulation in cellular function. Annu Rev Biochem 71:473-51 (2002).

Hudmon A, Schulman H. Structure-function of the multifunctional Ca^{2+}/calmodulin-dependent protein kinase II. Biochem J.364(Pt 3):593-611 (2002).

Jarymowycz VA, Stone MJ. Fast time scale dynamics of protein backbones: NMR relaxation methods, applications, and functional consequences. Chem Rev. 106(5):1624-71 (2006).

Jeschke G. DEER distance measurements on proteins. Annu Rev Phys Chem. 63:419-46 (2012).

Johnson CK. Calmodulin, Conformational States, and Calcium Signaling. A Single-Molecule Perspective. Biochemistry. 45: 14233–14246 (2006).

Johnson DA, Akamine P, Radzio-Andzelm E, Madhusudan M, Taylor SS. Dynamics of cAMP-dependent protein kinase. Chem Rev 101(8):2243-70 (2001).

Kanaseki T, Ikeuchi Y, Sugiura H, Yamauchi T. Structural features of Ca^{2+}/calmodulin-dependent protein kinase II revealed by electron microscopy. J Cell Biol. 115(4):1049-60 (1991).

Kay LE, Ikura M, Tschudin R, Bax A. Three-dimensional triple-resonance NMR Spectroscopy of isotopically enriched proteins. J Magn Reson. 213(2):423-41 (1990).

Kay LE. Solution NMR spectroscopy of supra-molecular systems, why bother? A methyl-TROSY view. J Magn Reson. 210(2):159-70 (2011).

Kelly PT, Weinberger RP, Waxham MN. Active site-directed inhibition of Ca2+/calmodulin-dependent protein kinase type II by a bifunctional calmodulin-binding peptide. Proc Natl Acad Sci U S A. (14):4991-5 (1988).

King MM, Shell DJ, Kwiatkowski AP. Affinity labeling of the ATP-binding site of type II calmodulin-dependent protein kinase by 5'-p-fluorosulfonylbenzoyl adenosine. Arch Biochem Biophys. 267(2):467-73 (1988).

Kleckner IR, Foster MP. An introduction to NMR-based approaches for measuring protein dynamics. Biochim Biophys Acta. 1814(8):942-68 (2011).

Kolodziej SJ, Hudmon A, Waxham MN, Stoops JK. Three- dimensional reconstructions of calcium/calmodulin-dependent (CaM) kinase IIα and truncated CaM kinase II alpha reveal a unique organization for its structural core and functional domains. J Biol Chem 275:14354 –14359 (2000).

Kornev AP, Taylor SS, Ten Eyck LF. A helix scaffold for the assembly of active protein kinases. Proc Natl Acad Sci U S A. 105(38):14377-82 (2008).

Korzhnev DM, Kloiber K, Kanelis V, Tugarinov V, Kay LE. Probing slow dynamics in high molecular weight proteins by methyl-TROSY NMR spectroscopy: application to a 723-residue enzyme. J Am Chem Soc. 126(12):3964-73 (2004).

Kristensen AS, Jenkins MA, Banke TG, Schousboe A, Makino Y, Johnson RC, Huganir R, Traynelis SF. Mechanism of Ca2+/calmodulin-dependent kinase II regulation of AMPA receptor gating. Nat Neurosci. 14(6):727-35 (2011).

Lai Y, Nairn AC, Gorelick F, Greengard P. Ca^{2+}/calmodulin-dependent protein kinase II: identification of autophosphorylation sites responsible for generation of Ca2+/calmodulin-independence. Proc Natl Acad Sci U S A. 84(16):5710-4 (1987).

Lai Y, Nairn AC, Greengard P. Autophosphorylation reversibly regulates the Ca^{2+}/calmodulin-dependence of Ca2+/calmodulin-dependent protein kinase II. Proc Natl Acad Sci U S A. 83(12):4253-7 (1986).

Lee SJ, Escobedo-Lozoya Y, Szatmari EM, Yasuda R. Activation of CaMKII in single dendritic spines during long-term potentiation. Nature. 458(7236):299-304 (2009).

Lin CR, Kapiloff MS, Durgerian S, Tatemoto K, Russo AF, Hanson P, Schulman H, Rosenfeld MG. Molecular cloning of a brain-specific calcium/calmodulin-dependent protein kinase. Proc Natl Acad Sci USA 84:5962-6 (1987).

Lu CS, Hodge JJ, Mehren J, Sun XX, Griffith LC. Regulation of the Ca^{2+}/CaM-responsive pool of CaMKII by scaffold-dependent autophosphorylation Neuron, 40:1185–1197 (2003).

Luo M, Guan X, Luczak ED, Lang D, Kutschke W, Gao Z, Yang J, Glynn P, Sossalla S, Swaminathan PD, Weiss RM, Yang B, Rokita AG, Maier LS, Efimov IR, Hund TJ, Anderson ME. Diabetes increases mortality after myocardial infarction by oxidizing CaMKII. J Clin Invest. 123(3):1262-74. (2013).

Mchaourab HS, Lietzow MA, Hideg K, Hubbell WL. Motion of spin-labeled side chains in T4 lysozyme. Correlation with protein structure and dynamics. Biochemistry. 35(24):7692-704 (1996).

McHaourab HS, Steed PR, Kazmier K. Toward the fourth dimension of membrane protein structure: insight into dynamics from spin-labeling EPR spectroscopy. Structure. 19(11):1549-61 (2011).

Meador WE, Means AR, Quiocho FA. Modulation of calmodulin plasticity in molecular recognition on the basis of x-ray structures. Science. 262(5140):1718-21 (1993).

Meyer T, Hanson PI, Stryer L, Schulman H. Calmodulin trapping by calcium-calmodulin-dependent protein kinase. Science. 256(5060):1199-202 (1992).

Miller SG, Kennedy MB. Distinct forebrain and cerebellar isozymes of type II Ca^{2+}/calmodulin-dependent protein kinase associate differently with the postsynaptic density fraction. J Biol Chem. 260(15):9039-46 (1985).

Mukherji S, Soderling TR. Regulation of Ca^{2+}/calmodulin-dependent protein kinase II by inter- and intrasubunit-catalyzed autophosphorylations. J Biol Chem. 269(19):13744-7 (1994).

Nguyen TA, Sarkar P, Veetil JV, Davis KA, Puhl HL 3rd1, Vogel SS. Covert Changes in CaMKII Holoenzyme Structure Identified for Activation and Subsequent Interactions. Biophys J. 108(9):2158-70 (2015).

Ogawa Y, Tanokura M. Calcium binding to calmodulin: effects of ionic strength, Mg^{2+}, pH and temperature. J Biochem. 95(1):19-28 (1984).

Olwin BB, Edelman AM, Krebs EG, Storm DR. Quantitation of energy coupling between Ca^{2+}, calmodulin, skeletal muscle myosin light chain kinase, and kinase substrates. J Biol Chem. 259(17):10949-55 (1984).

Orrenius S, Zhivotovsky B, Nicotera P. Regulation of cell death: the calcium-apoptosis link. Nat Rev Mol Cell Biol. 4(7):552-65 (2003).

Payne ME, Fong YL, Ono T, Colbran RJ, Kemp BE, Soderling TR, Means AR. Calcium/calmodulin-dependent protein kinase II. Characterization of distinct calmodulin binding and inhibitory domains. J Biol Chem. 263(15):7190-5 (1988).

Pervushin K, Riek R, Wider G, Wüthrich K. Attenuated T2 relaxation by mutual cancellation of dipole-dipole coupling and chemical shift anisotropy indicates an avenue to NMR structures of very large biological macromolecules in solution. Proc Natl Acad Sci U S A. 94(23):12366-71 (1997).

Pi HJ, Otmakhov N, Lemelin D, De Koninck P, Lisman J. Autonomous CaMKII can promote either long-term potentiation or long-term depression, depending on the state of T305/T306 phosphorylation. J Neurosci. 30:8704-9 (2010).

Purohit A, Rokita AG, Guan X, Chen B, Koval OM, Voigt N, Neef S, Sowa T, Gao Z, Luczak ED, Stefansdottir H, Behunin AC, Li N, El-Accaoui RN, Yang B, Swaminathan PD, Weiss RM, Wehrens XH, Song LS, Dobrev D, Maier LS, Anderson ME. Oxidized Ca(2+)/calmodulin-dependent protein kinase II triggers atrial fibrillation. Circulation. 128(16):1748-57. (2013).

Rellos P, Pike AC, Niesen FH, Salah E, Lee WH, von Delft F, Knapp S. Structure of the CaMKIIdelta/calmodulin complex reveals the molecular mechanism of CaMKII kinase activation. PLoS Biol. 8(7):e1000426 (2010).

Rosenberg OS, Deindl S, Comolli LR, Hoelz A, Downing KH, Nairn AC, Kuriyan J. Oligomerization states of the association domain and the holoenyzme of Ca^{2+}/CaM kinase II. FEBSJ 273: 682-694 (2006).

Rosenberg OS, Deindl S, Sung RJ, Nairn AC, Kuriyan J. Structure of the Autoinhibited Kinase Domain of CaMKII and SAXS Analysis of the Holoenzyme Cell. 123(5):849-60 (2005).

Schwaller B. Cytosolic Ca^{2+} buffers. Cold Spring Harb Perspect Biol. 2(11):a004051 (2010).

Shields SM, Vernon PJ, Kelly PT. Autophosphorylation of calmodulin-kinase II in synaptic junctions modulates endogenous kinase activity. J Neurochem. 43(6):1599-609 (1984).

Shoju H, Sueyoshi N, Ishida A, Kameshita I. High level expression and preparation of autonomous Ca2+/calmodulin-dependent protein kinase II in Escherichia coli. J Biochem. 138(5):605-11 (2005).

Strack S, Choi S, Lovinger DM, Colbran RJ. Translocation of autophosphorylated calcium/calmodulin-dependent protein kinase II to the postsynaptic density. J Biol Chem. 272(21):13467-70 (1997).

Stratton M, Lee IH, Bhattacharyya M, Christensen SM, Chao LH, Schulman H, Groves JT, Kuriyan J. Activation-triggered subunit exchange between CaMKII holoenzymes facilitates the spread of kinase activity. Elife.3:e01610 (2013).

Swaminathan PD, Purohit A, Soni S, Voigt N, Singh MV, Glukhov AV, Gao Z, He BJ, Luczak ED, Joiner ML, Kutschke W, Yang J, Donahue JK, Weiss RM, Grumbach IM, Ogawa M, Chen PS, Efimov I, Dobrev D, Mohler PJ, Hund TJ, Anderson ME. Oxidized CaMKII causes cardiac sinus node dysfunction in mice. J Clin Invest. 121(8):3277-88. (2011).

Swedberg K, Eneroth P, Kjekshus J, Wilhelmsen L. Hormones regulating cardiovascular function in patients with severe congestive heart failure and their relation to mortality. CONSENSUS Trial Study Group. Circulation. 82(5):1730-6. (1990).

Thaler C, Koushik SV, Puhl HL 3rd, Blank PS, Vogel SS. Structural rearrangement of CaMKIIα catalytic domains encodes activation. Proc Natl Acad Sci U S A. 106(15):6369-74 (2009).

Tombes RM, Faison MO, Turbeville JM. Organization and evolution of multifunctional Ca^{2+}/CaM-dependent protein kinase genes. Gene. 322:17-31 (2003).

Török K, Tzortzopoulos A, Grabarek Z, Best SL, Thorogate R. Dual effect of ATP in the activation mechanism of brain Ca(2+)/calmodulin-dependent protein kinase II by Ca(2+)/calmodulin. Biochemistry 11;40(49):14878-90 (2001).

Tripathi S, Portman JJ. Inherent flexibility determines the transition mechanisms of the EF-hands of calmodulin. Proc Natl Acad Sci U S A. 106(7):2104-9 (2009).

Tsvetkov YD, Milov AD, Maryasov AG. Pulsed electron–electron double resonance (PELDOR) as EPR spectroscopy in nanometre range Russ. Chem. Rev. 77:487 (2008).

Tzortzopoulos A, Török K. Mechanism of the T286A-mutant alphaCaMKII interactions with Ca2+/calmodulin and ATP. Biochemistry. 43(21):6404-14 (2004).

Velez Rueda JO, Palomeque J, Mattiazzi A. Early apoptosis in different models of cardiac hypertrophy induced by high renin-angiotensin system activity involves CaMKII. J Appl Physiol. 112(12):2110-20.(2012).

Vetter SW, Leclerc E. Novel aspects of calmodulin target recognition and activation. Eur J Biochem. 270(3):404-14 (2003).

Wagner S, Ruff HM, Weber SL, Bellmann S, Sowa T, Schulte T, Anderson ME, Grandi E, Bers DM, Backs J, Belardinelli L, Maier LS. Reactive oxygen species-activated Ca/calmodulin kinase IIδ is required for late I(Na) augmentation leading to cellular Na and Ca overload. Circ Res. 108(5):555-65. (2011).

Wang P, Wu YL, Zhou TH, Sun Y, Pei G. Identification of alternative splicing variants of the beta subunit of human Ca(2+)/calmodulin-dependent protein kinase II with different activities. FEBS Lett. 475(2):107-10 (2000).

Waxham MN, Tsai A, Putkey JA. A Mechanism for Calmodulin (CaM) Trapping by CaM-kinase II Defined by a Family of CaM-binding Peptides. The Journal of Biological Chemistry. 273: 17579-17584 (1998).

Wayman GA, Tokumitsu H, Davare MA, Soderling TR. Analysis of CaM-kinase signaling in cells. Cell Calcium. 50:1-8 (2011).

Yang E, Schulman H. Structural examination of autoregulation of multifunctional calcium/calmodulin-dependent protein kinase II. J Biol Chem. 274(37):26199-208 (1999).

Zhang R, Khoo MS, Wu Y, Yang Y, Grueter CE, Ni G, Price EE Jr, Thiel W, Guatimosim S, Song LS, Madu EC, Shah AN, Vishnivetskaya TA, Atkinson JB, Gurevich VV, Salama G, Lederer WJ, Colbran RJ, Anderson ME. Calmodulin kinase II inhibition protects against structural heart disease. Nat Med. 11(4):409-17. (2005).

Zhang T, Miyamoto S, Brown J. Cardiomyocyte Calcium and Calcium/Calmodulin-dependent Protein Kinase II: Friends or Foes? Recent Progress in Hormone Research 59:141-168 (2004).

Zheng J, Knighton DR, ten Eyck LF, Karlsson R, Xuong N, Taylor SS, Sowadski JM. Crystal structure of the catalytic subunit of cAMP-dependent protein kinase complexed with MgATP and peptide inhibitor. Biochemistry.32(9):2154-61 (1993).

Zou DJ, Cline HT. Expression of constitutively active CaMKII in target tissue modifies presynaptic axon arbor growth. Neuron.16(3):529-39 (1996).

APPENDIX

Appendix I

His Tag	Residues	His Tag Cleavage Site	Vector	Native Cysteines?
***10His at N-terminus**	**1-340**	**Thrombin**	**pET-28b**	**No**
6His at N-terminus	1-340	3C Protease	pET-28b	Yes
6His at N-terminus	1-318	3C Protease	pET-28b	Yes
6His at N-terminus	1-313	3C Protease	pET-28b	Yes
6His at N-terminus	1-308	3C Protease	pET-28b	Yes
6His at N-terminus	1-303	3C Protease	pET-28b	Yes
6His at N-terminus	1-277	3C Protease	pET-28b	Yes

*** Background for double Cys mutants for DEER**

Table AI.1: CaMKII D135N Constructs.

*Mutants labeled at the R3 Subdomain	2VN9 Cβ-Cβ Distance(Å)
17-307	29.3
33-307	38.4
65-307	25.8
79-307	29.0
93-307	28.9
125-307	25.4
227-307	20.7
170-307	16.2
45-307	21.6
26-307	21.0
45-300	21.8
85-307	23.1
287-307	29
287-310	N/A
45-315	N/A
65-315	N/A
85-315	N/A

*Mutants labeled at the Catalytic Domain	2VN9 Cβ-Cβ Distance(Å)
12-125	27.7
33-125	31.1
51-125	30.6
51-170	21.6
93-125	22.5
143-170	34.9
143-227	34.8
170-227	21.7
111-170	37.9
125-287	29.6

*Mutants labeled at the R1 Helix	2VN9 Cβ-Cβ Distance(Å)
93-288	26.1
111-285	14.6
111-288	15.6
143-288	20.9

Table AI.2: List of double Cys mutants used for DEER and corresponding Cβ-Cβ distance from crystal 2VN9.

*Mouse CaMKIIα Numbering

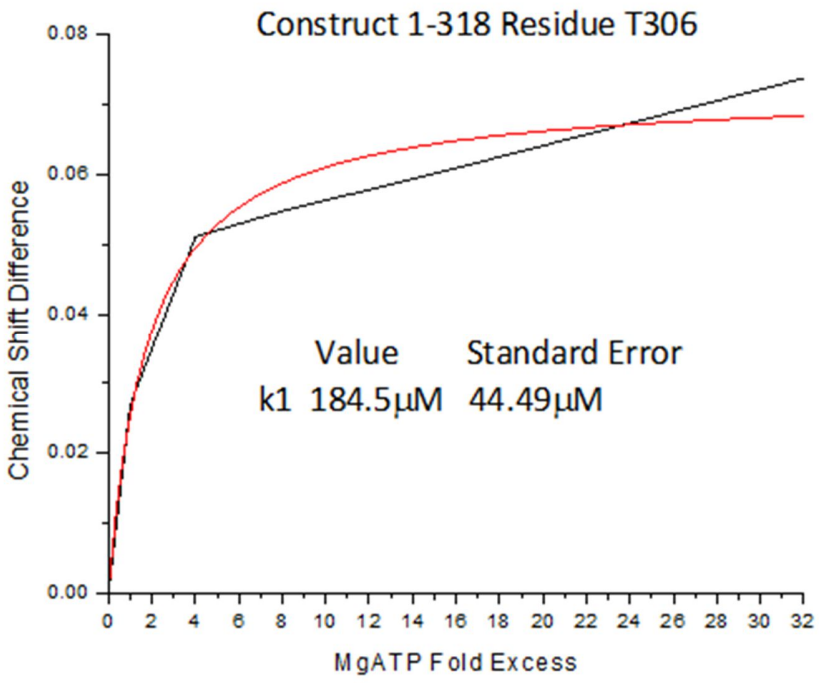

Figure AII.1: K_D determined from ^{1}H-^{15}N TROSY and ATP titration of CaMKII 1-318. The plot was obtained from the chemical shift difference of residue T306 as a function of MgATP.